TU Delft

BioMechanical Design

Master thesis report

from graduation internship at Bosch Transmission Technology B.V.

Investigation of the relation between grinding process parameters and created curvature and roughness of the pushbelt element saddle surface for optimizing the pushbelt element-ring contact in Continuously Variable Transmissions

---

Author:
A. Krämer - 4461339

TU Delft supervisor:
Jilt Sietsma
Company supervisors:
Sietske van Schagen
Theo Janssen

September 12, 2019

Preface

This graduation project report was written within the scope of the graduation internship at Bosch Transmission Technology B.V. in Tilburg. The project is part of the second year of the master's programme BioMechanical Design.
Bosch Transmission Technology produces the pushbelt used for torque transfer in a Continuously Variable Transmission (CVT). The graduation internship within the Technical Functions (TEF) department aims at reducing the friction losses of the CVT pushbelt by improving the contact between the pushbelt element saddles and the loop which holds the belt elements together. The literature study which preceded this graduation project revealed that belt grinding would be the most promising method to process the element saddle in order to achieve an optimally shaped and smoothed surface for friction reduction in the element-loop contact. Therefore, in this graduation project, a grinding machine was built and the relation between grinding process parameters and resulting curvature and roughness of the pushbelt element saddle surface was investigated.
Readers who are interested in the working principle of the Continuously Variable Transmission and its friction losses are advised to read chapter 1. Readers who are concerned with the requirements for an efficiency and durability improvement of the pushbelt are recommended to read chapter 2. Readers who are curious about the prototype grinding machine are advised to read chapter 3. Furthermore, I suggest reading chapters 4 to readers who are interested in the development of the experimental procedure. However, readers who are mainly interested in the results and evaluation of the experiments are advised to read chapters 5 and 6.
I would like to thank my company supervisors Sietske van Schagen and Theo Janssen for their helpful words of advice during my graduation internship.

Alexander Krämer
Tilburg, August 2019

Summary

In a Continuously Variable Transmission (CVT), the pushbelt is the torque transmitting part consisting of around 400 steel elements which are held together by steel ring packs. Relatively high friction losses of the operating pushbelt are associated with the element saddle surface on which the steel rings are lying. The pushbelt runs between two pulleys which are variable in diameter and, therefore, slip between the elements and the steel rings occurs, which leads to these friction losses.
In order to increase the efficiency and durability of the pushbelt, the shape and the surface roughness of the element saddle has to be adjusted such that the friction is reduced. The pushbelt element saddle surface is difficult to reach since it is situated in a small slot of the element, and in the production process, it is currently not specially treated after fine blanking.
The requirements in order to achieve a friction reduction in the pushbelt's element-ring contact were specified in terms of average surface roughness R_a along the long side of the element saddle, called the horizontal R_a, and the radius across the short side of the element saddle, called the short saddle radius (SSR). The surface roughness is required to be reduced from an initial average horizontal R_a of 0.786 µm to 0.150 µm or preferably lower, and for the SSR, a radius of 28.00 mm is targeted, which is a little bit smaller than the smallest running radius of the rings in the CVT pulley in order to optimize the contact between the element saddle and the rings in the operating pushbelt.
A grinding machine was specially built for testing the feasibility of belt grinding for this purpose and to be able to produce pushbelt elements with the required adjustments for pushbelt efficiency tests. The grinding machine uses two grinding belts to process the left and right saddle of the elements which are arranged in a row on a semi-circle in an element holder.

In this research the relation between grinding process parameters and created curvature and roughness of the pushbelt element saddle surface were examined. Furthermore, it was investigated which are feasible process conditions in order to achieve the required grinding result, and how accurately the saddle surface characteristics can be predicted in dependency of the machine parameters.
For this purpose, machine tests were executed and the ground element saddles were measured with the aid of a white light interferometer in order to evaluate the achieved response variables which are the surface roughness R_a and the SSR. The measurements were analyzed in order to describe the relationship between machine parameters and obtained grinding result. Furthermore, the measurements were used to fit an empirical model to the data, and the applicability of a polynomial and also an exponential model was investigated.

In preliminary machine tests, it was found that it is necessary to keep the elements in a certain distance in the element holder in order to achieve a stable grinding result. Furthermore, after the preliminary tests, a P600 grinding belt was chosen to be used and it was decided to hold the grinding speed constant during the final experimental design. The chosen predictor variables for the grinding result in the final experimental design were the grinding time and the pressure which is used in the pneumatic cylinder in the machine in order to bring the grinding belt to tension. A full factorial experimental design with nine duplication experiments was used, so in total 18 experiments, where the factors time and pressure were varied on three levels.

It was concluded that the applied pressure, so the tension force in the grinding belt, is the dominating factor for the achieved size of the SSR. An increased pressure decreases the size of the achieved SSR and also the variation of the response variables of the samples is decreased at higher pressures. The achieved horizontal R_a on the saddle is effected by both factors, time and pressure, however, the grinding time appears to have more influence. The empirical exponential model and also the polynomial model give a similar prediction for the grinding result within the experimental factor range, but beyond that range, it was found that the exponential model is able to make a better prediction. However, the predicted machine parameters from the exponential model, which would be necessary in order to achieve the desired grinding result according to the requirements, are not feasible. The needed pressure would be too low for the grinding belt to make sufficient contact with the saddle surface and the predicted grinding time would be very high. Within feasible machine conditions, the achieved SSR is always lower than the required 28.00 mm and decreases rapidly with increasing pressure. Additionally, the lowest roughness R_a which can be achieved according to the exponential model is 0.152 µm, which is slightly higher than the requirement. This is consistent with the performed experiments and it was concluded that with the current machine configuration, the requirements can not be achieved.

It is recommended to execute further experiments with an element holder having an increased diameter since with the current holder, although the element's saddle was positioned on a radius of 28 mm, the achieved SSR of the saddle was smaller after grinding. Furthermore, it is recommended to perform further experiments with different kinds of grinding belts having finer grain sizes for achieving a lower surface roughness or having structured abrasives for less variation and a better predictability in the grinding result.

Contents

List of Figures

List of Tables

1. Introduction

1.1 The Continuously Variable Transmission

In a Continuously Variable Transmission (CVT), a pushbelt transmits the engine output to the drive axle by transferring the torque from the primary variator pulley to the secondary variator pulley, as shown in figure 1.1. The pushbelt consists of around 400 steel elements which are held together by two high-alloy steel ring packs, as can be seen in figure 1.2. The steel ring packs are located between the ear and the leg on the left and right side of the pushbelt element, as depicted in figure 1.3. The elements have inclined flanks in order to make optimal contact with the conical sheaves of the variator pulleys.

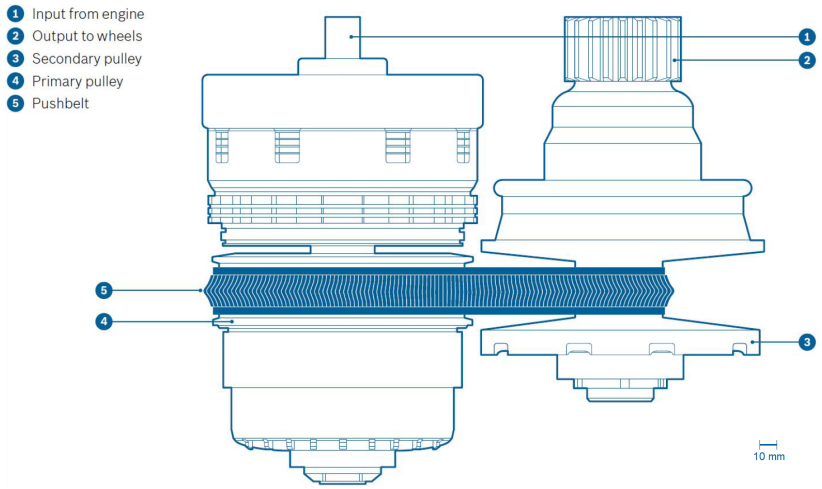

Figure 1.1: Continuously Variable Transmission

The transmission ratio is continuously variable since each pulley consists of a pair of conical sheaves which are able to adjust the running radius of the pushbelt. This can be seen in figure 1.4, where the variator pulleys are shown in the two most extreme transmission ratio configurations, LOW and OverDrive. The LOW gear ratio yields high torque transmission and low speed since the secondary pulley, due to its bigger running radius, rotates much slower than the primary pulley. On the contrary, in OverDrive, the running radius of the secondary pulley is smaller than the running radius of the primary pulley. This implies that

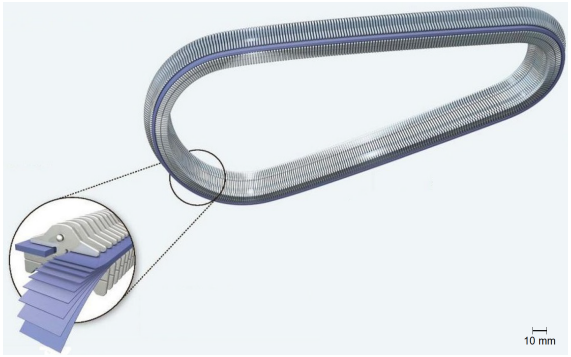

Figure 1.2: Bosch pushbelt

the secondary pulley rotates faster than the motor-driven primary pulley, resulting in higher speed and lower torque transmission. OverDrive can be seen as an economy gear since the engine can be run at relatively low speed compared to the wheel speed. Therefore, by constantly optimally adjusting the transmission ratio to the given conditions, the engine can be run more efficiently than with a stepped transmission. Furthermore, the torque transmission does not stop during shifting as it does in a stepped transmission, which enables smoother car driving.

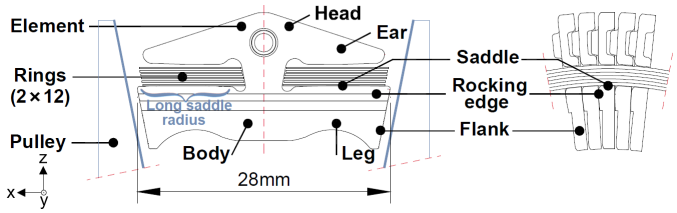

Figure 1.3: Steel ring packs lying on element saddles between ears and legs [4]

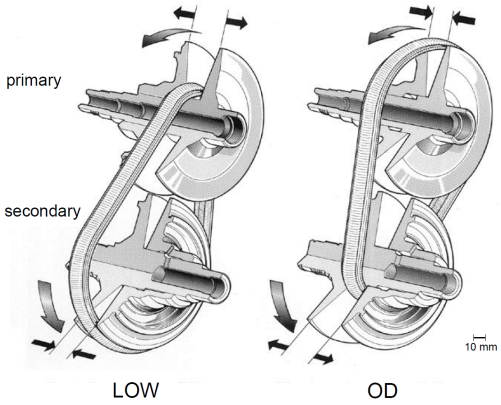

Figure 1.4: Extreme transmission ratios LOW and OD (OverDrive) [3]

1.2 Friction in the pushbelt

In operation, the pushbelt is clamped between the variator pulleys in order to transmit the engine torque. Figure 1.5 shows the forces working on the clamped elements with the steel ring packs. For a torque transfer with minimal slip, high friction is needed on the contact surfaces between the pushbelt and the pulleys. Therefore, the pushbelt elements are provided with rough grooved flanks to ensure that there is sufficient grip to drive or be driven by the pulleys. In contrast to that, friction on the other surfaces of the pushbelt components is undesirable for efficiency and durability reasons.

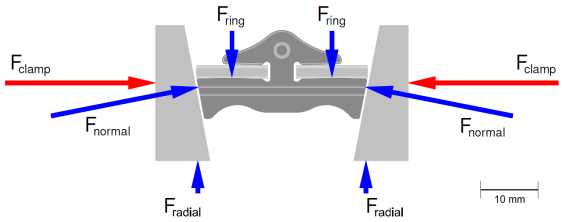

Figure 1.5: Forces working in the plane of the element on the elements and rings in the pushbelt [10]

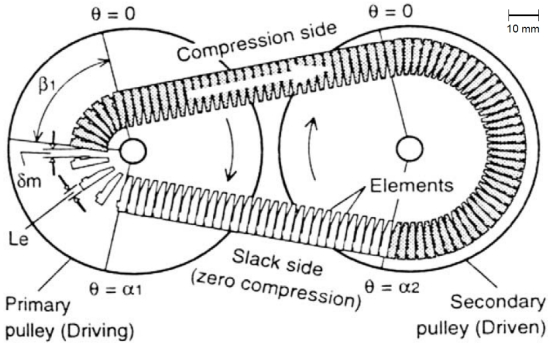

Figure 1.6: Torque transmission between CVT-pulleys [9]

An overview of the relative magnitude of the friction losses within the variator assembly is given in figure 1.7. There, it can be seen that the highest loss, 45%, is caused by the element-pulley contact due to the earlier mentioned needed clamping of the pushbelt elements between the variator pulleys. The clamped elements slip between the pulley, which causes friction losses. Figure 1.6 shows that the pushbelt elements located within the angle β_1 transmit the torque from the primary pulley to the secondary pulley by pushing the elements in between tightly against each other. The elements on the compression side actually act like a solid rod which drives the secondary pulley. In contrast, the elements running back from the secondary to the primary pulley on the slack side, are not tightly pushed against each other anymore and there are small gaps between the elements. These gaps are closed by slip between the element flanks and the pulley sheaves, causing friction losses.
However, there are also high friction losses of 32% caused by the element-ring contact. The left and right element saddle surfaces touch the inner rings of the two steel ring packs which hold the pushbelt together. But the elements and the inner rings do not always move at the same speed. The rotation of the elements and rings at different radii at the pulleys causes slip between the inner rings and the elements, leading to these internal belt losses [11].
The remaining losses of 33% are losses caused by the bearings, the element-element contact and the ring-ring contact.

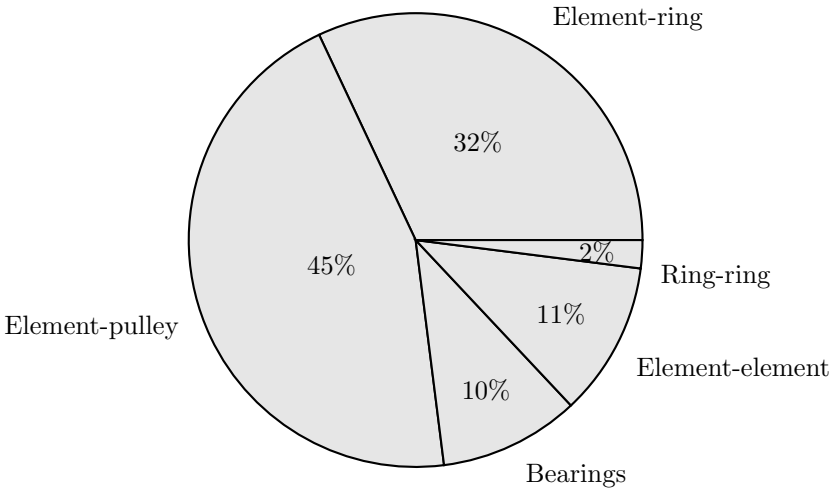

Figure 1.7: Variator loss distribution [4]

1.3 Purpose of research

The friction losses in the operating pushbelt should be reduced. As explained in the previous section, a very high proportion of the friction losses is caused by the element-ring contact. Therefore, optimizing this contact surface would increase the efficiency and durability of the pushbelt. Also, it makes the pushbelt more eligible for the use of high friction oils which is advantageous in the force transmission between the element flanks and the CVT pulley sheaves.

The literature study which preceded this graduation project investigated machining processes for mass production which are suitable for processing the element saddle in order to create a curvature and roughness on the saddle surface which improves the element-ring contact.

The current flow of the manufacturing process of the pushbelt elements can be seen in figure 1.8. The 75Cr1-steel coil material with an initial hardness of 175 HV is fine blanked and, subsequently, the steel elements are heat treated. After heat treatment, the hardness is increased to around 700 HV. Then, the elements are tumbled in order to remove burrs and to improve the surface roughness. Thereafter, elements from different batches are mixed, washed and go through the automatic optical inspection (AOI) which checks the elements automatically with the aid of cameras on damages like cracks, impressions or bending, and rejects elements if necessary. Then, the passed pushbelt elements are ready for assembly.

Figure 1.8: Process flow of pushbelt elements

Currently, the element saddle surface is not specially treated after fine blanking and its small distance of 2.3 mm to the element ear (see fig. 1.3) makes it difficult to access this area. Even the stones in the tumbling process are not small enough to fit in this gap. Therefore, an additional machining process must be implemented after fine blanking.

The literature study revealed that belt grinding would be the most promising process for mass production, since it is possible to achieve a very low surface roughness and good form accuracy in an economical and ecologically friendly way.
In order to examine the feasibility of belt grinding for the pushbelt element saddle treatment, a grinding machine was built, which was specially developed for this purpose. The goal of this graduation project is to investigate the effects of the grinding process parameters on the shape and roughness of the element saddle, and eventually find feasible process parameters. The obtained optimal machine settings can then be used to produce elements for building prototype pushbelts for further efficiency and durability testing.

2. Reduced friction in element-ring contact improves pushbelt features

2.1 Efficiency and durability improvement

The efficiency η of the CVT transmission is expressed by the ratio of outgoing power P_2 and incoming power P_1, where power is the product of torque and angular velocity:

$$\eta = \frac{P_2}{P_1} = \frac{T_2 \cdot \omega_2}{T_1 \cdot \omega_1}, \tag{2.1}$$

where P_1 = Input power,
P_2 = Output power,
T_1 = Input torque,
T_2 = Output torque,
ω_1 = Input angular velocity,
ω_2 = Output angular velocity.

Equation 2.1 can also be expressed in terms of power loss [13]:

$$\eta = 1 - \frac{\Delta P}{P_1} = 1 - \frac{\Delta T}{T_1} - \frac{\Delta \omega}{\omega_1}, \tag{2.2}$$

where $\Delta P = P_2 - P_1$ = Power loss,
$\Delta T = T_2 - T_1$ = Torque loss,
$\Delta \omega = \omega_2 - \omega_1$ = Loss in angular velocity.

As discussed in section 1.2, the main power losses are caused by friction in element-pulley and element-ring contact. It is difficult to reduce the friction between the elements and the pulleys since it is part of the working principle that friction is necessary to transmit the torque between the radii-changing pulleys. However, friction between the elements and the rings is not needed since the rings are mainly responsible for holding the elements together. Therefore, the efficiency of the CVT can be increased by reducing the friction losses due to slip in the element-ring contact.

A possible way to reduce those friction losses in the element-ring contact is to make the element saddle surface (see fig. 1.3) smoother and give a shape to the saddle which minimizes the Coefficient of Friction (CoF). This could increase the efficiency and also the durability of the pushbelt since reduced friction is associated with decreased wear of the pushbelt. Furthermore, it makes the pushbelt more eligible for high friction oils with low viscosity, which car manufacturers are aiming to use in CVT transmissions.

Figure 2.1 shows the typical efficiency curve dependent on the variator ratio for 50 Nm engine torque and 1500 rpm engine speed. The variator ratio r is the ratio of primary pulley speed v_1 and secondary pulley speed v_2:

$$r = \frac{v_1}{v_2} \tag{2.3}$$

The extreme variator ratios OverDrive and LOW, as shown in figure 1.4, can be found in the efficiency graph in figure 2.1 at $r = 0.4$ and $r = 2.6$, respectively. The graph shows schematically the typical efficiency curve obtained from pushbelt tests on the variator test bench. The red curve is the efficiency curve of the standard pushbelt and the blue curve is the efficiency curve of an improved pushbelt with adjusted element saddle curvature and surface smoothness, which was achieved by processing the elements with electrochemical machining. When the variator ratio equals 1, the efficiency is maximal and similar for both pushbelts, since the primary and secondary pulley have the same radius and rotate at the same speeds and, thus, the transmission is minimally affected by slip. Therefore, as can be seen in the graph, the efficiency can be considerably improved approximating OverDrive or also the LOW gear ratio.

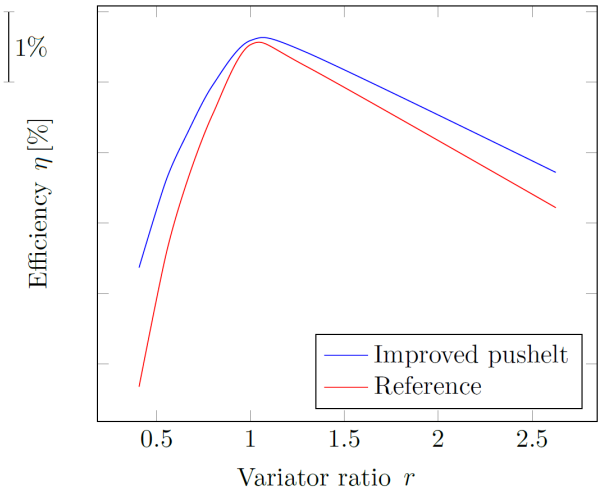

Figure 2.1: CVT-efficiency dependent on variator ratio

2.2 Requirements

Simulations and tests at Bosch have shown that the CoF can be reduced when the saddle surface has a low surface roughness in combination with a curvature across the saddle close to the running radius of the steel rings, which is dependent on the pulley radius. This radius across the short side of the elements saddle is called short saddle radius (SSR) and is visualized in figure 2.2. It was decided to target a SSR of 28.00 mm, which is a little bit smaller than the smallest running radius, in order to guarantee that the edges of the element saddles never prick the steel rings of the pushbelt.
Furthermore, the average surface roughness R_a which is the average absolute deviation of the roughness irregularities from the mean line of the surface profile [5], should preferably be as low as possible. R_a is a commonly used surface roughness parameter and, therefore, seems to be a suitable parameter for examining and comparing the results from surface measurements of the element saddles.
In earlier attempts to shape and smoothen the element saddles, electrochemical machining was used and a surface roughness R_a of around 0.150 µm was achieved. In the present work, it is aimed to achieve the same or an even lower saddle surface roughness with belt grinding.

Additionally, when the element saddle surface is processed in order to achieve the above mentioned requirements, the so called long saddle radius (LSR) should remain unchanged. The LSR is the curvature across the long side of the element saddle, perpendicular to the SSR (fig. 1.3). The LSR has an elliptical curvature as shown in figure 2.5 in order to keep the steel ring packs in place.

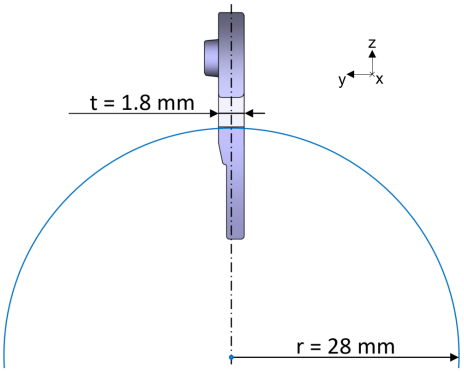

Figure 2.2: Definition of short saddle radius (SSR)

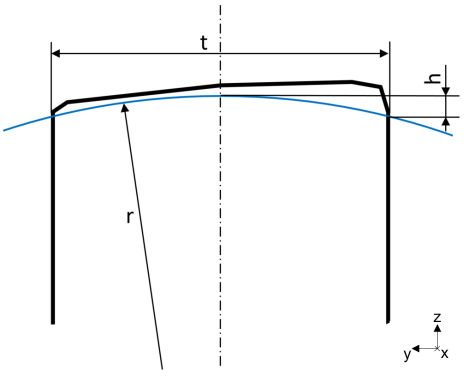

Figure 2.3: Enlarged element saddle with desired curvature (blue)

The common element saddle shape, defined by the SSR, after fine blanking, hardening and tumbling is shown in figure 2.4. It is depicted schematically again in figure 2.3 where can be seen that, due to the low element thickness $t = 1.80$ mm, the height of the arc h generated by a SSR equal to 28.00 mm is very small and has

a value of only 0.01 mm. This implies that the maximal material removal on the edges of the saddle in order to achieve a proper arc with radius 28.00 mm, is a little bit more than 0.01 mm, since the saddle surface is a little bit skewed (fig. 2.3, 2.4) after fine blanking.
The saddle roughness of the elements after tumbling is around $R_a = 0.8$ µm and, therefore, has to be made much smoother to achieve $R_a = 0.150$ µm or lower. Figure 2.6 shows an untreated element saddle and figure 2.7 shows the desired result after belt grinding, a smooth element saddle with the desired curvature.

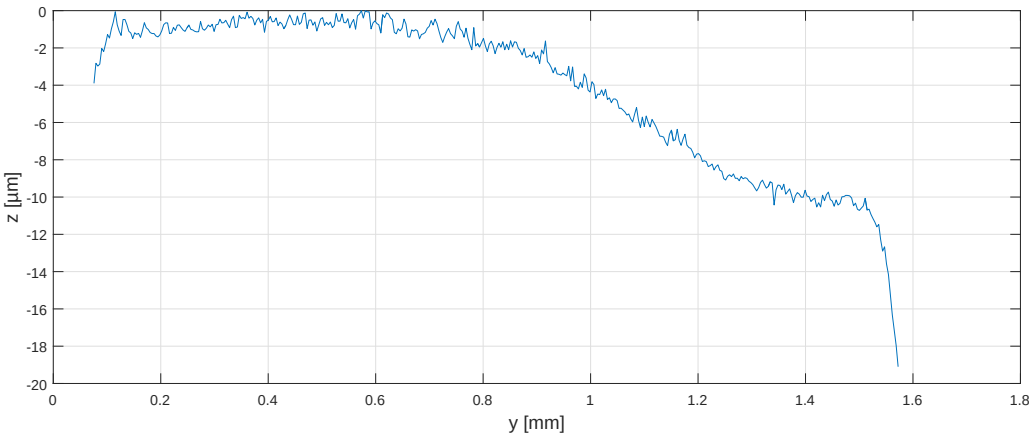

Figure 2.4: Profile of SSR of standard element (type 28/12) measured with white light interferometer

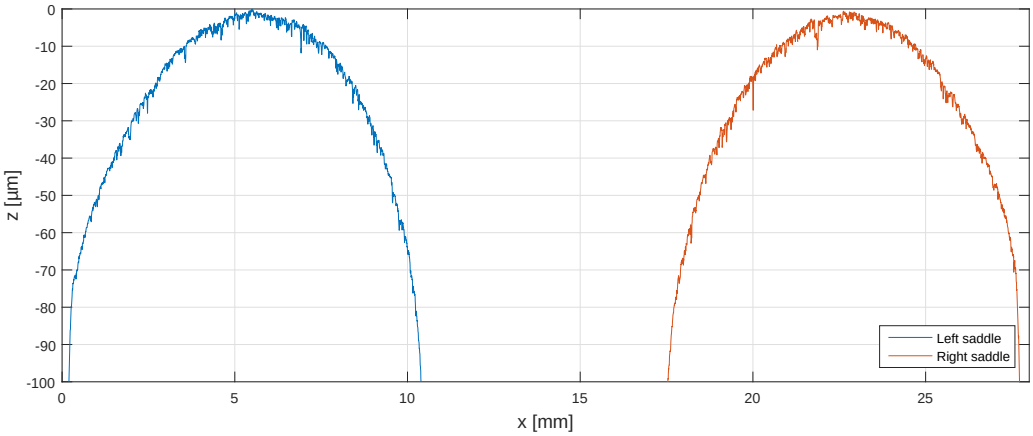

Figure 2.5: Profile of LSR of standard element (type 28/12) measured with white light interferometer

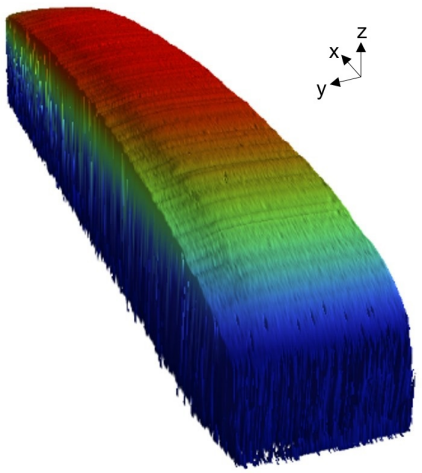

Figure 2.6: Untreated element saddle

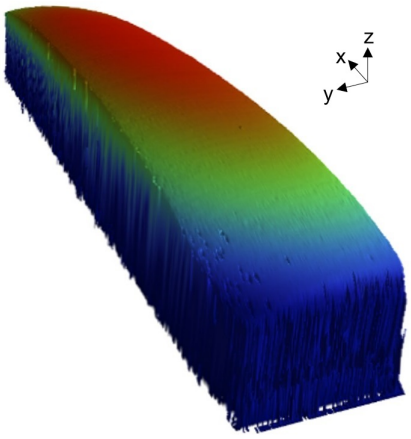

Figure 2.7: Smooth element saddle with desired curvature after grinding

3. Prototype grinding machine processes pushbelt element saddles

A prototype grinding machine, shown in figure 3.1, was built specially for the purpose of testing the feasibility of belt grinding for processing the pushbelt element saddle surface. There were no standard grinding machines available on the market, which could be used for this purpose due to the unusual requirements of grinding in such a small slot and, at the same time, smoothing the surface and creating a particular curvature over the surface. The built grinding machine is not appropriate to be used in mass production since the amount of elements which can be processed at the same time is limited and also the handling is not optimal. Replacing the grinding belts, and removing and refilling the elements is time consuming. However, the machine is suitable for testing purposes and also to produce small quantities of prototype pushbelt elements which can be used for pushbelt tests in order to investigate the effects on efficiency and durability.

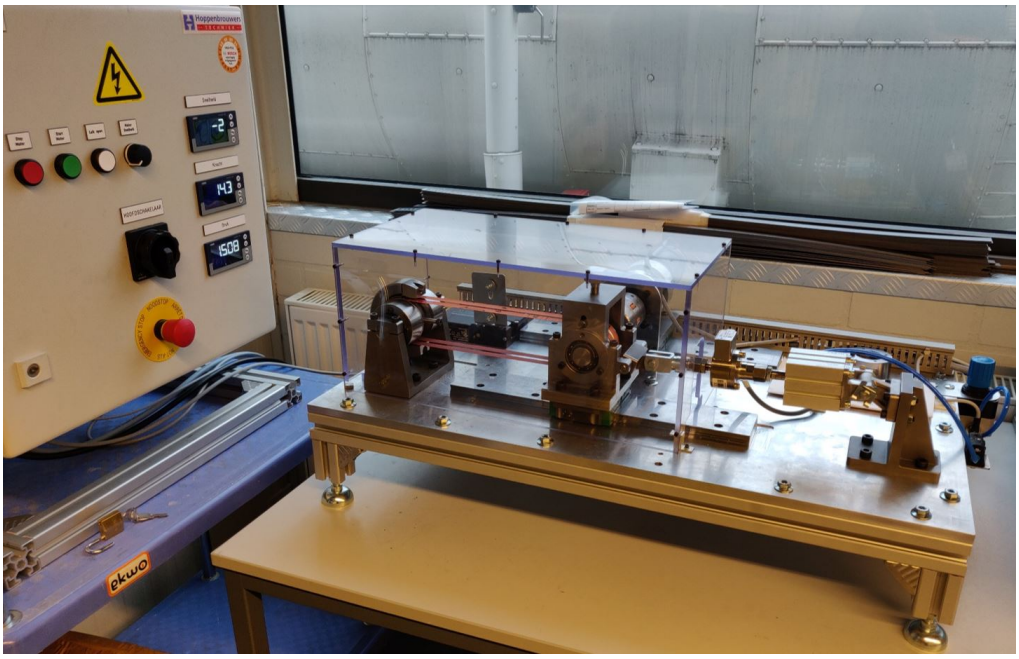

Figure 3.1: Grinding machine with control box

3.1 Grinding machine structure

In the grinding machine, grinding belts from the supplier Saint-Gobain Abrasives B.V. are used, as can be seen in figure 3.2. The belts consist of aluminium oxide (Al_2O_3) grains attached to a cloth backing, and have a length of 722.2 mm and are 12 mm wide in order to cover the length of the element saddle.
The elements are arranged on a semi-circle in the fixed element grinding cassette shown in figure 3.3. There are two different element holders for the positioning of the elements, which are explained in the following section. Two grinding belts process the left and right element saddle at the same time. In the first machine tests, the moving grinding belts fell of the saddles and therefore, guideways were made in order to prevent that.

Figure 3.2: Grinding belt

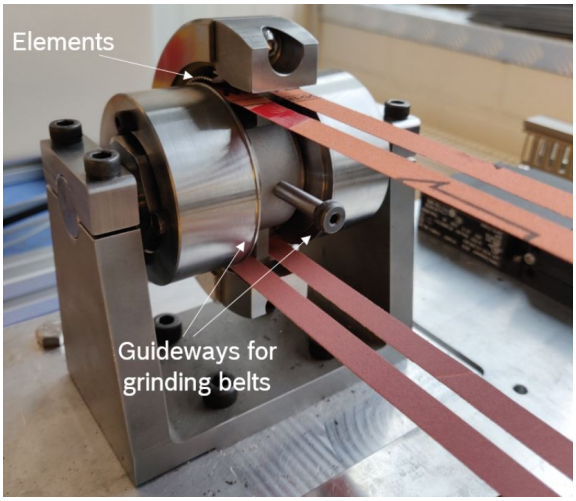

Figure 3.3: Element grinding cassette

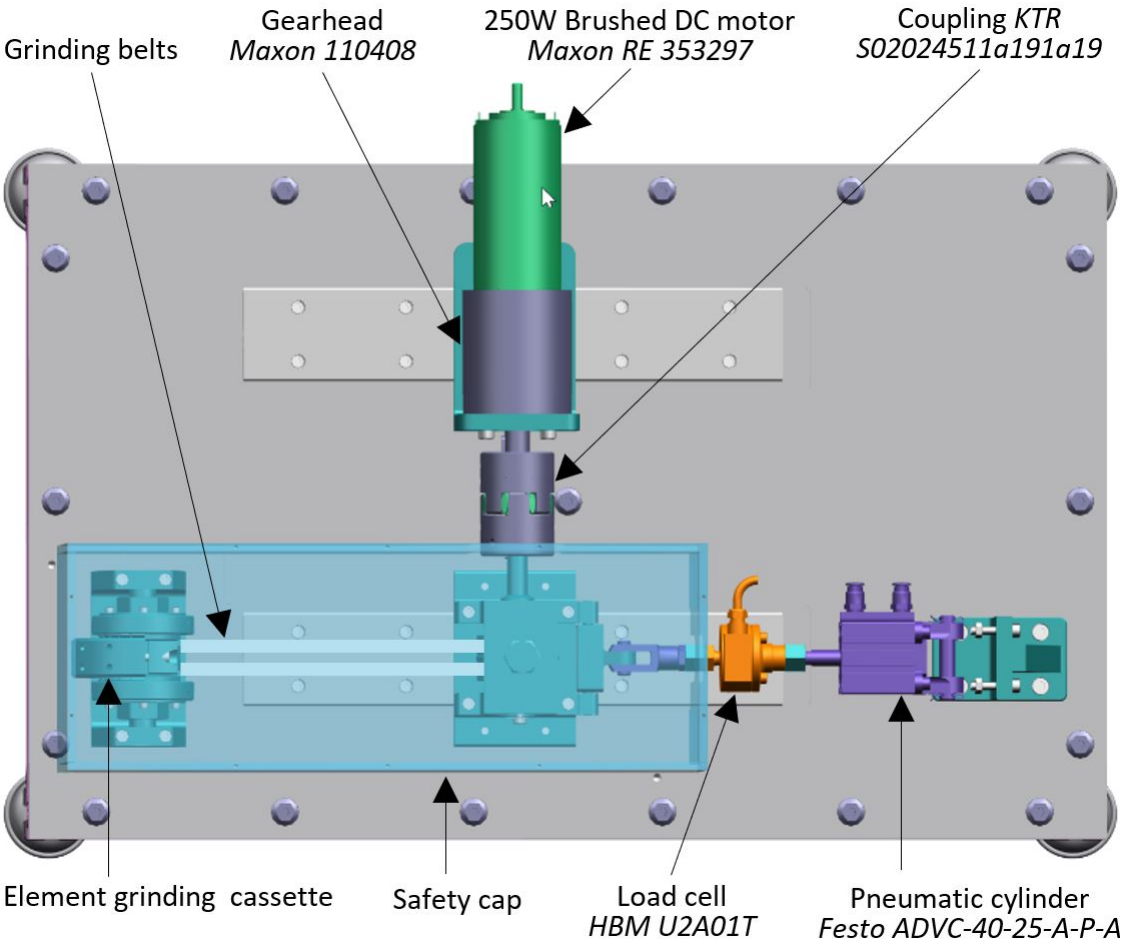

Figure 3.4: Topview of grinding machine

The grinding belt is held under tension with the aid of a short-stroke pneumatic cylinder, as can be seen in figure 3.4 which shows the top-view of the machine. The pneumatic cylinder exerts a tension force F_t on the suspension of the driving shaft, as depicted in figure 3.6. Pressurizing the pneumatic cylinder with 1 bar, for example, yields a force of 114.35 N according to the equation below. Figure 3.5 shows the linear relationship between pressure p and tension force F_t. The rod of the pneumatic cylinder is mounted to a load cell which measures this tension force F_t.

$$F_t = p \cdot \frac{1}{4} \cdot (d_p^2 - d_r^2) \cdot \pi, \tag{3.1}$$

where p = Pressure,
d_p = Piston diameter (40 mm),
d_r = Rod diameter (12 mm)

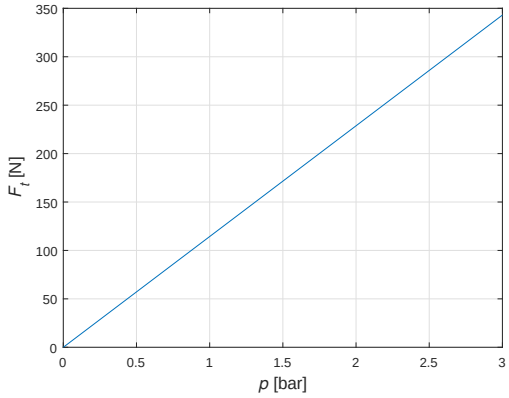

Figure 3.5: Tension force vs. pressure

The drivetrain of the machine consists of an electro motor combined with a planetary gearhead which has a reduction of 3.7. Therefore, the gearhead intensifies the 0.8 Nm torque of the electro motor to 3 Nm. The driven pulley with a radius of 0.03 m, as depicted in figure 3.6, moves the 722.2 mm long grinding belt. Due to the gearhead in between, a motor speed of 1000 rpm, for example, results in 270 rpm of the drive shaft, and 70 revolutions of the grinding belt according to the equations below. The resulting velocities and speeds are summarized in table 3.1.

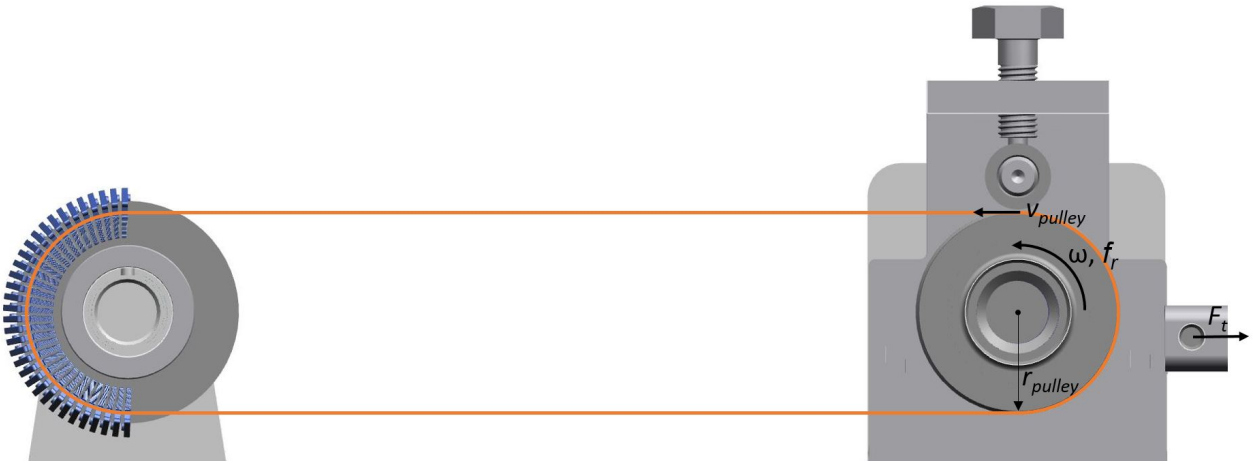

Figure 3.6: Side-view of grinding assembly

$$\omega = 2 \cdot \pi \cdot f_r \tag{3.2}$$

$$v_{pulley} = \omega \cdot r_{pulley} \tag{3.3}$$

$$f_{r,\,belt} = \frac{v_{pulley}}{l_{belt}}, \tag{3.4}$$

where ω = Angular velocity,
f_r = Rotational frequency,
v_{pulley} = Speed of pulley,
r_{pulley} = Radius of pulley,
l_{belt} = Length of grinding belt

Table 3.1: Gearhead and grinding belt speed at 1000 rpm motor speed

	f_r [1/min]	ω [rad/s]	v_{pulley} [m/s]	$f_{r,belt}$ [1/min]
250 W Brushed DC motor	1000.00	104.72	3.14	261.00
3.7 : 1 Planetary gearhead	269.84	28.26	0.85	70.43

The electrical installation of the grinding machine was done by Hoppenbrouwers, an external company. They built the control box shown in the left top corner of figure 3.1. It is used to unlock the safety cap, start and stop the electro motor, control and monitor the rotational speed of the electro motor, and to monitor the pressure and the tension force.

3.2 Element holders

Two element holders with different kinds of element positioning were made for testing. One holder without spacing and the other holder with spacing between the elements. In both holders, the elements are arranged on a semi-circle and the saddles of the placed elements lie on a radius of 28.00 mm which corresponds to the desired short saddle radius (SSR).

3.2.1 Holder without spacing between elements

The holder without spacing between the elements can be seen in figures 3.7 and 3.8. It can hold 52 elements and the elements are placed in a row on a semi-circle in direct contact with each other. The moveable sleeves, as shown in figure 3.9, clamp the elements on the flanks and hold them in position similar as the sheaves of the pulleys do in the CVT transmission. Additionally, an outer holder with a rubber layer inside prevents the elements from falling out.

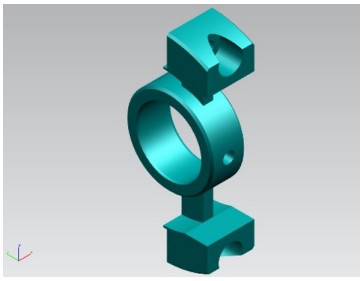

Figure 3.7: Holder without spacing between elements

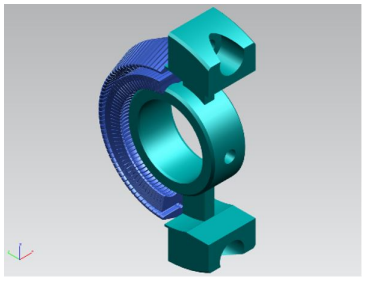

Figure 3.8: Filled holder without spacing between elements (52 elements)

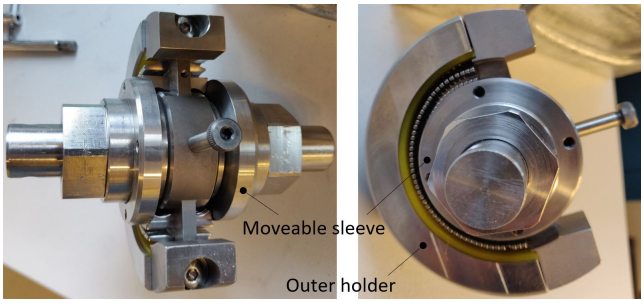

Figure 3.9: Complete holder without spacing between elements

3.2.2 Holder with spacing between elements

The holder with spacing between the elements can hold 34 elements and can be seen in figures 3.10 and 3.11. The elements are placed in slots where the saddles have a spacing of 0.84 mm in between. Figure 3.12 shows the completely assembled holder where the elements are clamped in the same way as in the holder without spacing as explained in the previous section.

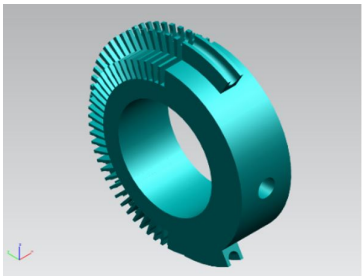

Figure 3.10: Holder with spacing between elements

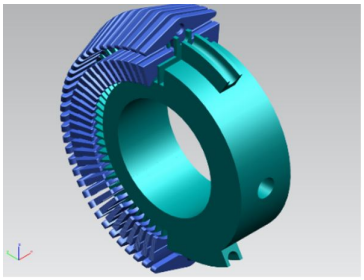

Figure 3.11: Filled holder with spacing between elements (34 elements)

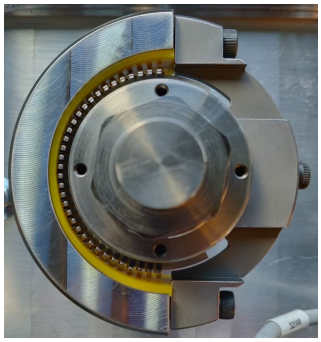

Figure 3.12: Complete holder with spacing between elements

4. Development of experimental procedure

The used grinding machine for processing the element saddles was newly developed specially for this purpose. The machine settings with which stable results could be achieved were completely unclear. Therefore, before a structured design of experiments could be established for investigating the relationship between the process parameters and resulting saddle surface roughness and curvature, the machine had to be initially tested. For this purpose, 74 experiments were executed and 193 elements were measured with the aid of the Bruker NPFLEX white light interferometer, which is an optical microscope for contactless, high precision 3D surface measurements based on optical interference. In white light interferometry, the surface height of a sample is determined from the interference signal of a reference beam and a measurement beam which is reflected from the surface [2]. Figure 4.1 shows an example of the resulting 3D representation of a ground element saddle measured with the white light interferometer. The roughness and curvature of the saddle surface is obtained by analyzing the measurement data and is used to examine the grinding result dependent on the grinding process parameters.

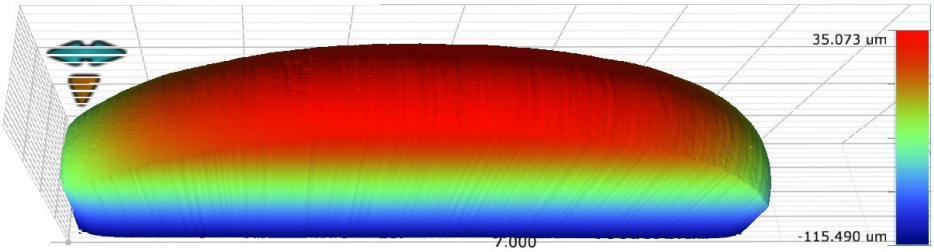

Figure 4.1: 3D surface measurement of element's left saddle in Bruker white light interferometer

4.1 Process parameters

The process variables which directly influence the grinding result of the element saddle are the grinding speed $f_{r,belt}$ and grinding time t, the belt tension force F_t which is dependent on the pressure p in the pneumatic cylinder, and the abrasive grit size of the grinding belt (P400, P600, P800). Furthermore, there are two different element holders where the elements are positioned with or without spacing, which also influences the grinding result which is characterized by the response variables: surface roughness R_a and short saddle radius r. Table 4.1 gives an overview over the involved process variables.

Table 4.1: Process variables

Predictor variables (Independent variables)	**Response variables** (Dependent variables)
- Grinding time t	- Surface roughness R_a
- Grinding speed $f_r, belt$	- Short saddle radius r
- Pressure p (tension force F_t)	
- Belt grit size	
- Element holder type	

4.2 Measurement procedure

The heads (fig. 1.3) of the elements from the test runs were removed with a pendulum hammer for the required measurement clearance. Then, the element saddles were scanned with the white light interferometer and, subsequently, the Bruker Vision64 program was used to analyze the saddles. Bruker's surface texture analysis is done according to ISO 4287. Figure 4.2 is an example screenshot of the program where the evaluated surface parameters over the x and y profile along the chosen range are displayed in the "Watch List" on the right.

4.2.1 Measurement of element curvature

The "PCurve" value in the "Watch List" gives the resulting radius of a circle fit over the measuring data in the chosen range. The "PCurve" value of the y profile is used as estimation of the SSR (fig. 2.2). The vertical length for the evaluation of this radius is chosen to be 1.1 mm within the nominal width of the element of 1.8 mm, so from 0.3 mm until 1.4 mm along the y-axis. In order to be able to reliably compare the radius values of all measured elements, the evaluation range is not along the whole 1.8 mm nominal element width since there are variations in the element dimensions and also variations in the positioning of the elements in the white light interferometer. Furthermore, the measurement data on the edges of the element would distort the circle fit of the Vision64 program because the slope abruptly changes there.
In this way, the radius is vertically measured eight times per element, so four times per element saddle with 2 mm horizontal distance between the measurements, as can be seen in appendix E where an example of a measurement of a ground element is illustrated. The measurements take place at x = 2 mm, x = 4 mm, x = 6 mm and x = 8 mm on the left saddle, and on x = 20 mm, x = 22 mm, x = 24 mm and x = 26 mm on the right saddle. The average of the four measured radii per element saddle is used to characterize the obtained SSR of an element saddle after a grinding experiment.

The long saddle radius (LSR), which describes the curvature over the x profile (fig. 4.2) is only examined qualitatively. As described in section 2.2, the LSR is elliptical and should not deviate much from its initial form after grinding. Therefore, it is only visually checked during the data analysis whether the LSR curvature is approximately retained after grinding.

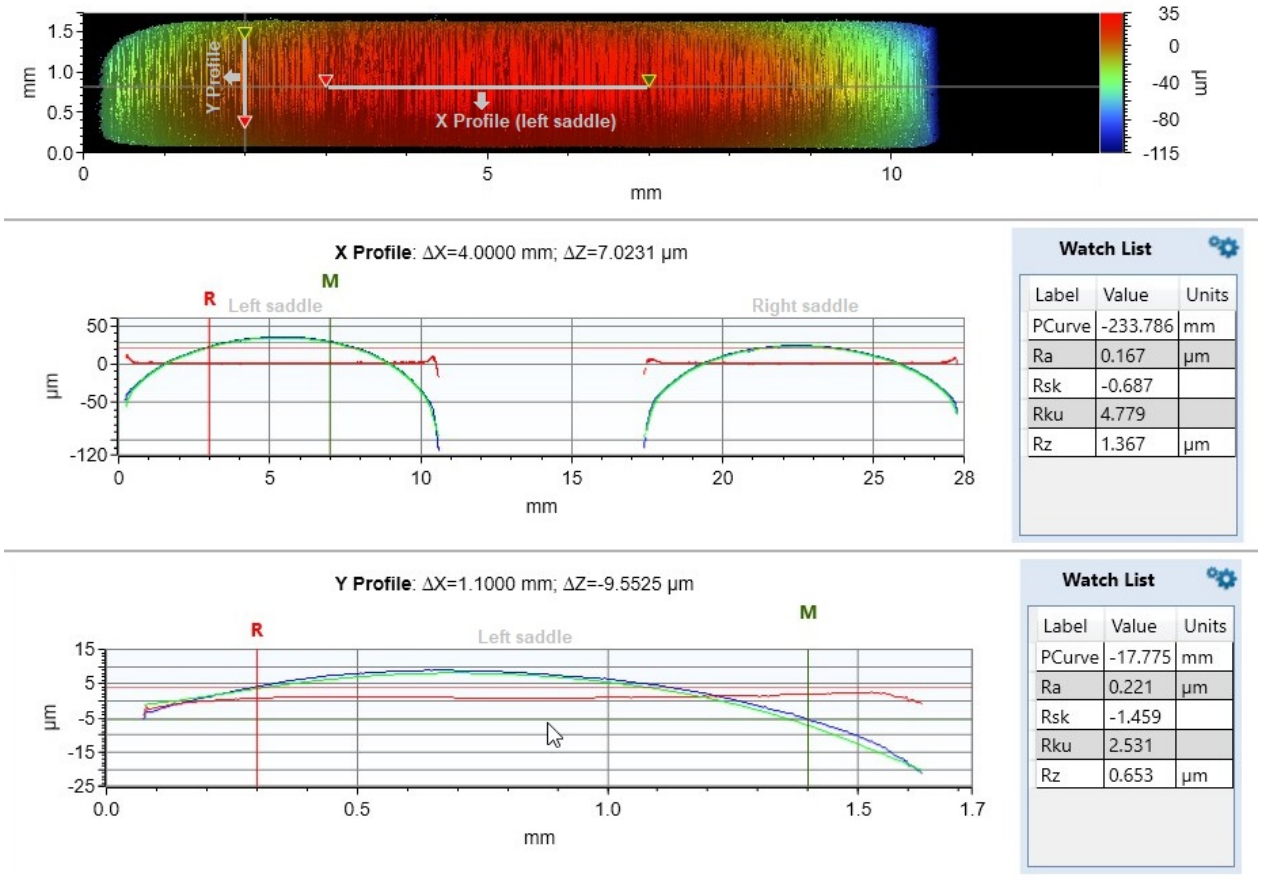

Figure 4.2: Measurement analysis in Bruker Vision64 program

4.2.2 Measurement of surface roughness

The arithmetic average surface height parameter R_a is the average absolute deviation of the roughness irregularities from the mean line of the surface profile [5], as can be seen in figure 4.3. The R_a parameter is calculated over the sampling length l as follows:

$$R_a = \frac{1}{l} \int_0^l |y(x)| dx \tag{4.1}$$

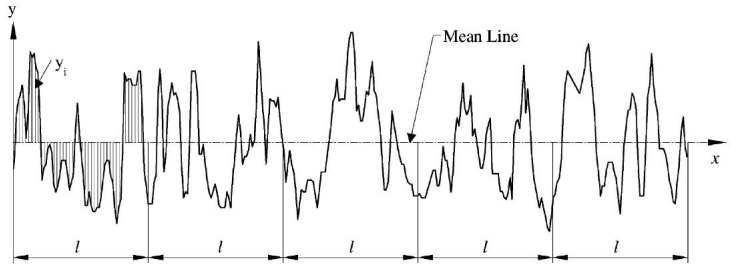

Figure 4.3: Definition of arithmetic average surface height R_a [5]

The roughness R_a of the element saddle is measured along the x and y profile, as shown in figure 4.2. In the following, the measured R_a in x and y-direction are also called the horizontal and vertical R_a, respectively. The Bruker Vision64 program displays the computed R_a value along the chosen range in the "Watch List" on the right (fig. 4.2). Figures 4.4 and 4.5 show again the used data for analysis within the chosen range, where the blue line is the raw measurement data. The red line is used for the calculation of the R_a value, which is obtained by subtracting the waviness data (green line) from the raw measurement data.

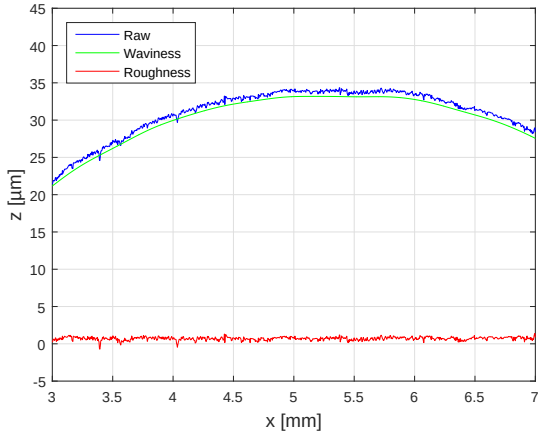

Figure 4.4: X profile of left saddle

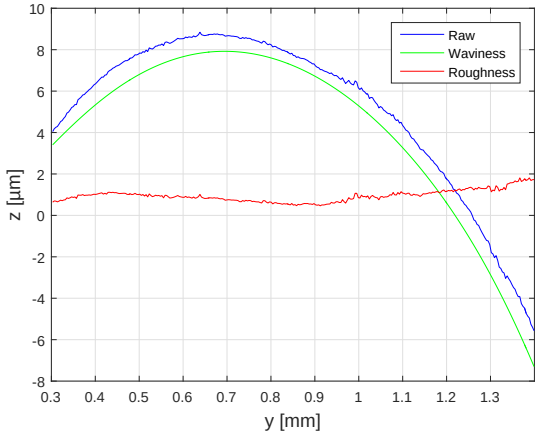

Figure 4.5: Y profile of left saddle

According to DIN EN ISO 4288, a surface roughness R_a which is expected to be within 0.1 µm and 2 µm has to be measured with a sampling length l (fig. 4.3) of 0.8 mm along an evaluation length of 4 mm. Therefore, the cut-off wavelength in the Vision 64 program is set to 0.8 mm and the used range for the evaluation of the horizontal R_a is set to a length of 4 mm in the x profile (fig. 4.4). The evaluation length is placed approximately in the middle of the element saddle starting at x = 3 mm until x = 7 mm (fig. 4.4) for the left saddle and at x = 21 mm until x = 25 mm for the right saddle. The R_a value is determined in this way horizontally three times per saddle with a distance of 0.5 mm in between, at y = 0.3 mm, y = 0.8 mm and y = 1.3 mm. as can be seen in appendix E. The average of these three R_a values is used to characterize the horizontal roughness of an element saddle after a grinding experiment.

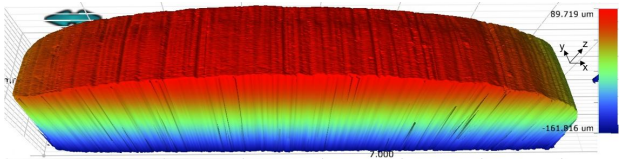

Figure 4.6: Vertical grooves (y-direction) on saddle surface after fine blanking

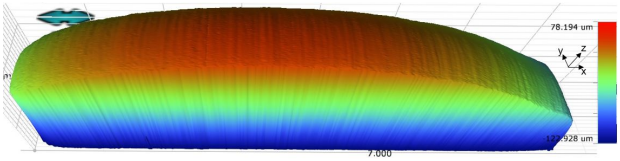

Figure 4.7: Vertical grooves (y-direction) on saddle surface after grinding

The vertical roughness R_a is measured in the Vision64 program simultaneously together with the curvature measurement of the SSR in the y profile (fig. 4.2) and, therefore, at the same eight places as the SSR. The cut-off wavelength is set as the same value as for the horizontal R_a measurement, however, the evaluation

length along the y-profile is only 1.1 mm (fig. 4.5). The vertical roughness R_a per measured element saddle is obtained by averaging the four evaluated R_a values per saddle.

The functional direction of the element saddles is the y direction, which means that there is slip between the pushbelt rings and element saddles in this direction causing friction losses. However, the vertical R_a is not considered to be as important and reliable for the surface characterization of the ground element saddles as the horizontal R_a because of several reasons, as explained in the following.

First of all, due to the thinness of the element, the evaluation length of only 1.1 mm for the vertical R_a is too short according to DIN EN ISO 4288. For a reliable and comparable surface roughness measurement, the evaluation length should have a length of 4 mm.
Additionally, DIN EN ISO 4288 states that the direction of the surface roughness measurement should be orthogonal to the direction of the grooves. Figure 4.6 shows the grooves on the element saddle which arise in y-direction during the fine blanking process. In figure 4.7 can be seen that also after the grinding process, grinding grooves remain in the y-direction since the grinding belt also runs across the saddle in this direction. Therefore, the measurement of the vertical R_a, thus the measurement along the y profile, would not be appropriate to characterize the roughness of the surface according to DIN EN ISO 4288 since the grooves on the saddles point in the same direction. So, in order to measure the surface roughness orthogonal to the grooves on the saddle, R_a has to be evaluated horizontally along the x-profile.

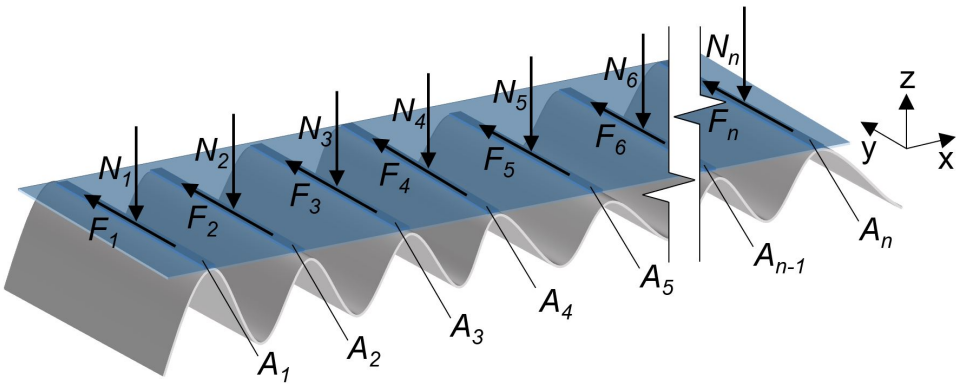

Figure 4.8: Force distribution between saddle surface and ring

Furthermore, the texture of the element saddle also plays a role during operation in the CVT, as there is load transfer between the element saddles and the (slipping) rings which hold the elements together. The rings bend across the element saddle and the load is distributed across the contact surface, as can be schematically seen in figure 4.8. There, the grooves on the saddle surface, caused from blanking or grinding, are shown in y direction as observed in figures 4.6 and 4.7. For simplicity, the first ring of the pushbelt ring-pack lying across the grooved surface is depicted ideally flat, however, in reality, the ring surface is provided with a fine crosshatch pattern. It can be seen how the normal force N is evenly distributed over the areas of contact A_1 to A_n, and the frictional force F acts in the y-direction due to the slip between the saddle and the ring. However, when the saddle surface would look like illustrated in figure 4.9 having a higher horizontal R_a, and the load would be carried only by a few high surface peaks, locally high load concentrations could occur in the ring leading to a ring failure.

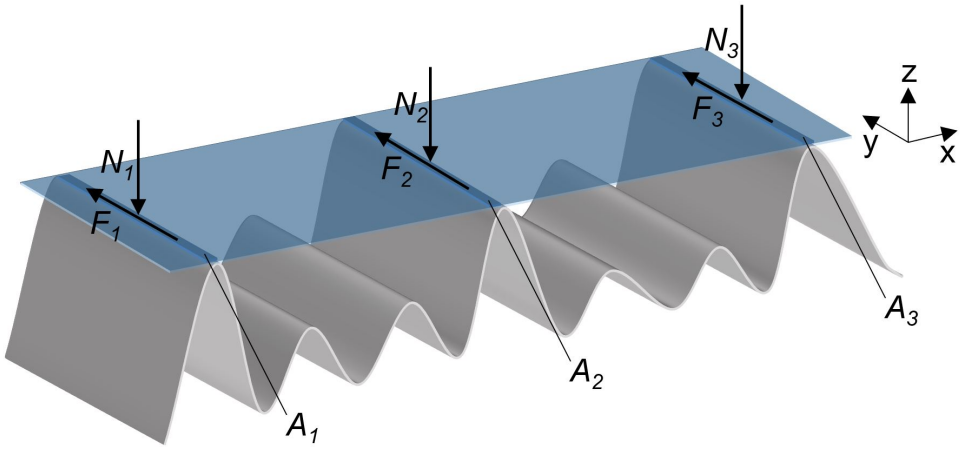

Figure 4.9: Load concentrations due to a few high surface peaks

In the illustrated example in figure 4.9, it can be seen that the roughness in x direction is mainly determining the kind of contact which is made between rings and saddle. So, the horizontal R_a would be the most appropriate parameter to characterize the saddle surface. By measuring the vertical R_a in groove direction along the y-profile, no differences between the surfaces from figures 4.8 and 4.9 would be observed. Furthermore, the vertical R_a measurement is also less reliable than the horizontal R_a measurement since the grooves are not perfectly straight and also not aligned with the y-axis in the Vision64 program, so, the line along which is measured can cross grooves several times distorting the evaluated R_a. Therefore, depending on the number of groove crossings, the vertical R_a changes and is less reliable to compare with other measurements.

4.3 Preliminary tests

For the development of a structured experimental design, broadly feasible machine settings which lead to stable outcomes had to be found first. Otherwise, the chance is high that a lot of experiments would be carried out within a structured experimental design, which eventually do not lead to results even close to the requirements, wasting time and resources. Furthermore, it had to be investigated whether some of the process variables, as described in section 4.1, could be held constant because it would be very time consuming to vary all the possible process variables in an experimental design. Therefore, orientating test had to be done in order to limit the amount and range of process parameters for the final experimental design. In every single test run within the preliminary tests, a new grinding belt was used in order to be able to compare the results properly.

Initially, ten reference elements were measured in order to determine the initial roughness and shape of the elements before grinding. The shape of the ten measured elements is illustrated in appendix A and an example of the measurement analysis of an element in the Vision64 program is shown in appendix B. There, it can be seen that, as for every measured element, the horizontal R_a was evaluated six times, and the vertical R_a and SSR was evaluated eight times, as described in section 4.2. In the y profile, it can be observed that the SSR of the unprocessed saddle has not a defined curvature and exhibits a kind of step (fig. 2.4) where the cutter enters the sheet metal in the fine blanking process. A circle is hardly possible to fit in the y profile for evaluating the SSR, however, the Vision64 program evaluated a radius of 35.44 mm on average for the ten measured reference elements. The surface roughness was evaluated with a cut-off wavelength of 0.80 mm which resulted on average to a horizontal $R_a = 0.786$ µm and to a vertical $R_a = 0.584$ µm, using the evaluation length of 4.00 mm and 1.10 mm, respectively.
Therefore, after implementing the grinding process, the saddle form should be fundamentally improved having a curvature where the circle fit results in a radius of 28.00 mm and, additionally, the saddle surface roughness should be extensively reduced to a horizontal $R_a = 0.150$ µm or preferably even lower.

Unfortunately, the data of the orientating tests were distorted by an afterwards detected fault in the machine's motor control and also by an incorrect measurement setting for the R_a evaluation in the Vision64 program, as explained below. However, the trends of the following data analysis and graphs in this chapter still give a valuable indication of the influence of the different process variables. In the execution and analysis of the final experimental design, these faults were corrected.

The first reason for the distorted data during the orientating tests was that the motor speed control was not working and, therefore, the motor speed display on the control box showed only the nominal motor speed based on the voltage which was regulated by a potentiometer. So, when the electro motor rotated freely without load, the displayed speed was correct, but when it was working under load, the speed reduced, however, this was not recognized since the speed display did not change and still showed the initial set speed. The external company Hoppenbrouwers which made the electrical installation, installed a motor controller, however, did not notice that the electro motor was not equipped with an encoder for measuring the actual speed and, therefore, the motor controller did not receive a speed signal. This meant for the orientating tests, for example, when the motor speed was set to 1000 rpm according to the display and a P800 grinding belt was used, which was brought to tension with 1 bar pressure, that the actual motor speed was 780 rpm which was determined by using a visible-light type non-contact handheld tachometer which measures rpm by means of a reflective mark on the driving shaft. This implied for the resulting grinding belt speed that the assumed 70 rpm (see table 3.1) were reduced to 55 rpm. Furthermore, using 2 bar pressure, the increased tension force in the belt further decelerated the motor speed to 566 rpm which corresponds to only 40 grinding belt revolutions and, therefore, the element saddles were always ground less than expected.

The second reason for distorted data in this chapter was that the cut-off wavelength in the Vision64 program was set to the, for this level of surface roughness, uncommon value of 0.08 mm by default which was unfortunately not recognized during the analysis of the measurements of the orientating tests. As described in section 4.2.2, the appropriate cut-off wavelength is 0.8 mm for this level of surface roughness according to the international standard. The application of a ten times smaller cut-off wavelength implies that the surface profile is filtered on 10 times shorter pieces. Therefore, a larger waviness of the profile might not be included in the R_a calculation which would lead to a lower obtained R_a.
Indeed, the unintended usage of the smaller unusual cut-off wavelength of 0.08 mm in the above described reference element measurement resulted in a horizontal $R_a = 0.381$ µm and a vertical $R_a = 0.280$ µm, so 0.406 µm and 0.204 µm smaller R_a values, respectively, than in the correct evaluation with 0.8 mm wavelength. Spot checks of the other measurement data where the R_a was incorrectly analysed also showed an off-set of the same order of magnitude, but, due to a lack of time, this data of the orientating tests which follows in this chapter was not again newly analyzed. However, conclusions can still be drawn from the trends of the R_a graphs and, fortunately, the analysis of the SSR was correct since the circle fit was not affected by this wrong setting in the Vision64 program.

4.3.1 Effects from element positioning in two different types of holders

First, the element holder without spacing between the elements, as described in section 3.2.1, was tested in the grinding machine in various test runs with different machine settings. However, no stable results could be achieved with this holder, as can be seen in figure 4.11 which shows the typical grinding result of two subsequent elements, in this case element 26 and 27 from the middle of the holder illustrated in figure 4.10.

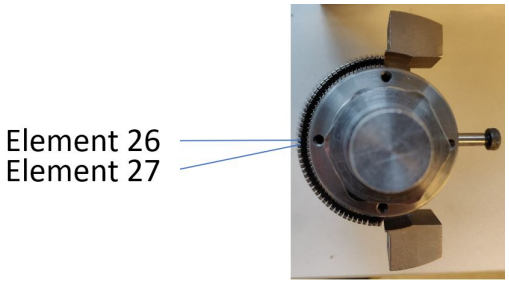

Figure 4.10: Elements 26 and 27 from element holder without spacing

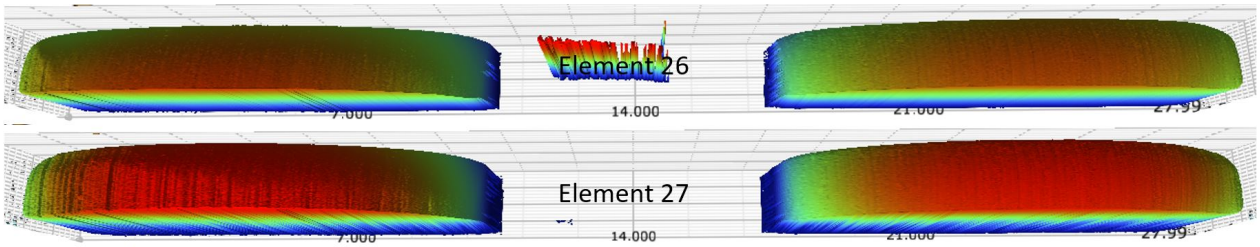

Figure 4.11: White light interferometer measurement of elements 26 and 27 from element holder without spacing

The white light interferometer scans in figure 4.11 show that the grinding result not only differs between left and right saddle, but also between subsequent elements. The left saddle of element 27 made apparently almost no contact with the the grinding belt. The right saddle of element 27 was seemingly ground better, but by carefully looking it can be seen that the frontal edge of the saddle, thus the upper edge in the picture, was also not touched sufficiently by the grinding belt. The left saddle of element 26 was not ground on the left outer end of the saddle, but the right saddle of element 26 made apparently very good contact with the grinding belt. It was smooth across the whole saddle surface and had also a nicely formed curvature with an SSR of close to the requirements.
These random results were observed throughout all elements in the holder caused by a poor positioning of the elements in this holder. Apparently, the elements are not sufficiently aligned in a row in the semi-circle and are clamped skew between the movable sleeves (fig. 3.9), as schematically illustrated in figure 4.13. Additionally, the heights of the element saddles are also lying between dimensional tolerances which implies that some of the element saddles protrude more than others in the element holder. In order to investigate this, the saddle heights of 40 not ground elements from the used element type were measured which revealed that there are differences in height of up to 50 µm between the element saddles. However, as described in section 2.2 and depicted in figure 2.3, the saddle height needs theoretically only reduced by a little bit more than 14 µm in order to create the desired SSR of 28.00 mm. Therefore, the grinding process is not likely to compensate saddle height differences of about 50 µm.
Due to these two described problems, skew positioning and saddle height differences, some element saddles stick out more than others and, as a consequence, adjacent element saddles are not sufficiently touched by the grinding belt leading to the random grinding results shown in figure 4.11.

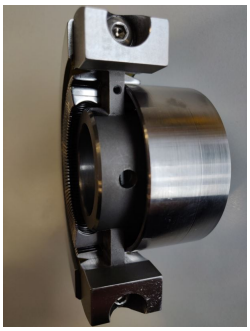

Figure 4.12: Holder with mounting aid on right side

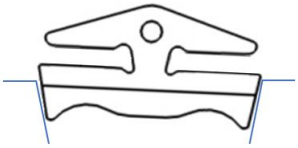

Figure 4.13: Schematic illustration of skew positioning of element between moveable sleeves

In order to solve this problem, two mounting aids for the left and right side of the holder, as shown in figure 4.12, were used in order to improve the alignment of the saddles. The mounting aids are metal rings which were pushed across the element saddles on the left and right side of the element holder in order to align all the element saddles on the same radius. In practice, this was more difficult to accomplish than expected because when the elements were clamped too tight in the mounted holder, the mounting aid could not be removed any more and when the elements were clamped more loose, they moved again when removing the mounting aid. Therefore, the grinding results did not improve by using these mounting aids.

The holder with spacing between the elements, as described in section 3.2.2 was expected to achieve better results due to the more accurate positioning of the elements in separate slots. This holder was also tested with different process parameters, however, the grinding results were varying, too, as can be seen in figure 4.15 where elements 17 and 18 are shown, which were taken from the middle of the element holder after grinding, as depicted in figure 4.14. This example measurement in figure 4.15 shows that in this holder

again, subsequent elements not always made the same contact with the grinding belt. Element 17 was not ground very well, but the saddles of element 18 were both completely smooth.

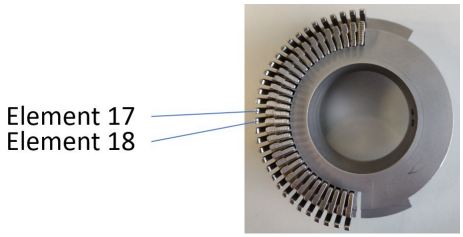

Figure 4.14: Elements 17 and 18 from element holder with spacing

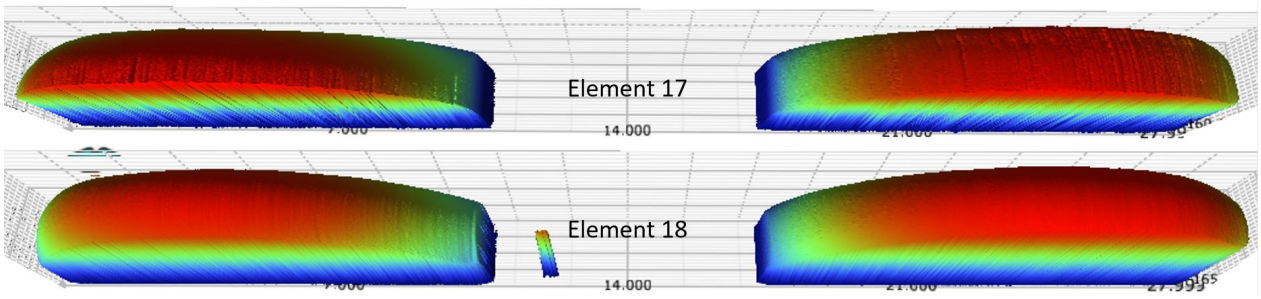

Figure 4.15: White light interferometer measurement of elements 17 and 18 from element holder with spacing

Additionally, in tests with this holder, it was observed, provided that the grinding belt made good contact with the element, as with the shown element 18 above, that the achieved SSR was usually much smaller than the desired 28.00 mm, but at least the SSR and also the surface roughness of left and right saddle were similar, opposed to the holder without spacing between the elements, where there were also differences in the grinding result between the left and right saddle. Apparently, the placement in separate slots in this holder helped for a better alignment between left and right saddle, however, the problem remained that some elements in between did not made sufficient contact with the grinding belt. By visual inspection of all the elements in this holder after grinding, it was observed that when an element had made good contact with the grinding belt, then the adjacent elements made usually no or very poor contact with it. Furthermore, it was observed that some elements sat tighter in the slots of this holder than others. Therefore, some elements possibly stuck out due to slight variations in the dimensions of the slots in combination with little thickness variations of the elements. Additionally, the saddle height variations, as described above, also probably contributed to the protrusion of some element saddles, which consequently impeded adjacent saddles from being ground properly.

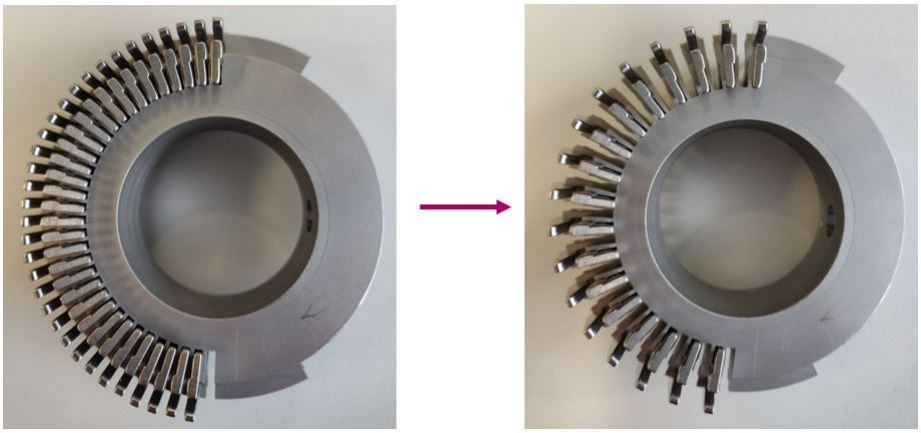

Figure 4.16: Increased spacing in element holder for stable grinding results

The solution to this problem was to increase the distance between the elements by omitting every second element, as shown in figure 4.16, which enables the grinding belt to make proper contact with all the elements in the holder except for the first and last element in the holder. The reason for this is that the grinding

belt enters and leaves the holder horizontally as depicted in figure 3.6 and, therefore, is not able to bend adequately across the saddle of the first and last element. Unfortunately, this was not taken into account in the design of the machine and, as a consequence, these two insufficiently ground elements have always to be rejected in this prototype machine.

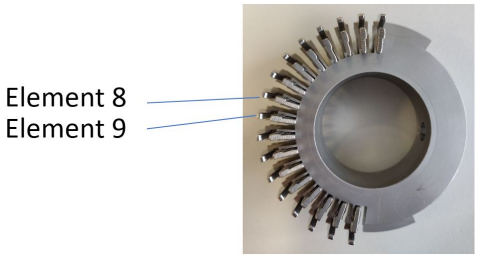

Figure 4.17: Elements 8 and 9 from element holder with extended spacing between the elements

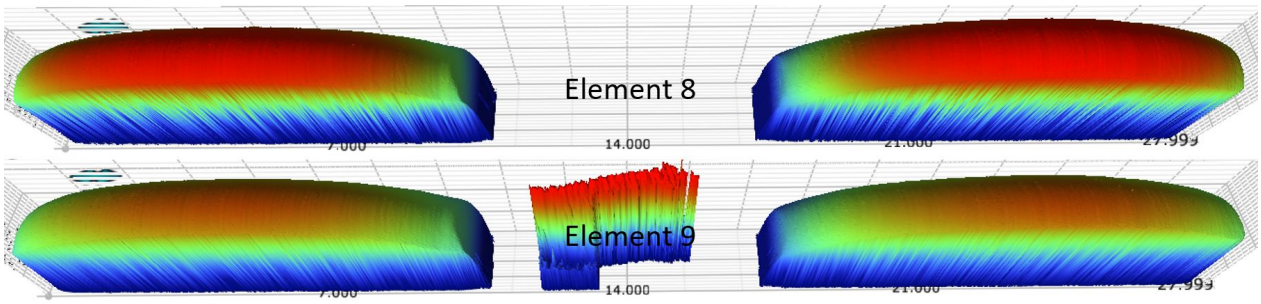

Figure 4.18: White light interferometer measurement of elements 8 and 9 from element holder with extended spacing between the elements

The distance between the element saddles in the holder with extended spacing was increased from initially 0.84 mm to 3.48 mm and, therefore, the amount of elements fitting in the holder was reduced to 17 elements. An example of the grinding results can be seen in the white light interferometer scan in figure 4.18 where the shown elements 8 and 9 were taken from the middle of the holder (fig. 4.17). It can be seen that for both elements, a similar grinding result was achieved with properly ground saddles. Also a similar curvature was created across the saddle surface, however the SSR was much smaller than the desired 28 mm. Nonetheless, the holder in this configuration with extended spacing between the elements was used from this moment on for the grinding tests which followed since, finally, stable grinding results were achieved with this holder.

4.3.2 Effect of belt grit size on surface roughness

The appropriate grit size of the grinding belt to be used in the grinding machine in order to achieve the surface roughness R_a according to the requirements had to be investigated. Grinding belts with the common grit sizes P400, P600 and P800 were tested. The FEPA P-grade indicates the grain size of the grinding belt, where the grain size becomes less coarse as the P-grade increases. According to the FEPA standard 43-1:2006, the P400, P600 and P800 grinding belts have grains with average particle sizes of 35.0 µm, 25.8 µm and 21.8 µm, respectievely. A lower grain size was expected to achieve eventually a lower surface roughness, but the question was how big are the differences and how much time does it take, or in other words, how many grinding belt revolutions are needed.

Six tests per grinding belt type were carried out, where the element saddles were ground in the grinding machine with a duration of 30 s, 60 s, 90 s, 120 s, 180 s, 240 s at a constant grinding speed and tension force in the belt. The grinding belt was brought to tension with the pneumatic cylinder using a pressure of 2 bar. The motor speed was set to 1000 rpm according to the display, however, as described above, after the execution of orientating preliminary trials, it was noticed that the displayed speed was not true since, due to the absence of motor control, the speed was lower depending on the load. Therefore, the true motor speed was determined afterwards to be 566 rpm using a P800 grinding belt at 2 bar pressure. This implies

that the speed of the grinding belt was around 40 rpm during these tests, however, not exactly since the coarser-grained belts also increased the load a little bit which slightly reduced the grinding speed.

After every test run, the surface roughness R_a of both element saddles of two sample elements from the middle of the holder, element 8 and 9 (fig. 4.17), was measured according to the measurement procedure described in section 4.2, so in total four R_a values were evaluated per test run. The sample mean is used as point estimate of the test run's R_a value. Figure 4.19 shows the obtained R_a values of the test runs depending on the grinding time and used grinding belt grit size.

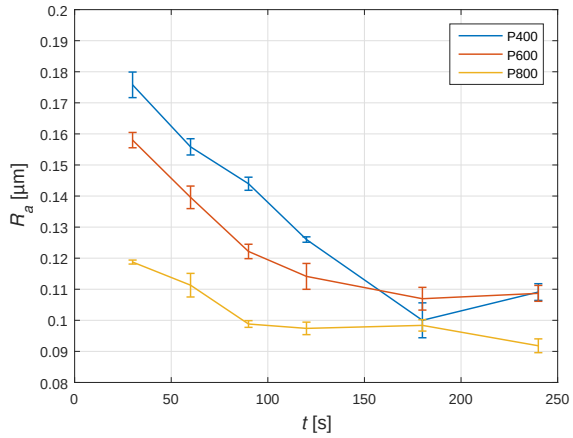

Figure 4.19: Horizontal surface roughness vs. grinding time with three different grain sizes of grinding belt (566 rpm, 2 bar)

In the graphs of this report, error bars are used as a measure of precision of the point estimates. The applied errorbars represent the standard errors of the mean. Assuming sampling from a normal distribution, the standard error $\hat{e}$ of the sample mean can be estimated as follows [7]:

$$\hat{e} = \frac{s}{\sqrt{n}}, \tag{4.2}$$

$$\begin{aligned} \text{where} \quad s &= \text{sample standard deviation}, \\ n &= \text{sample size} \end{aligned}$$

The standard error $\hat{e}$ is used for the errorbar since one can be reasonably confident that the true value of the parameter lies within two standard errors of the estimate [7].

In figure 4.19 can be seen that with the P800 grinding belt, a lower surface roughness is achieved much earlier than with the other grinding belts. The curve flattens already after about 90 s of grinding which corresponds to approximately 60 grinding belt revolutions, so the grinding belt is sliding about 60 times across the saddle of an element. The achieved R_a with the P600 grinding belt tends to be lower than with the P400 grinding belt, however where the curve flattens at 180 s, corresponding to approximately 120 grinding belt revolutions, the difference between P600 and P400 is unclear since the errorbars cross each other.
According to the test results, the P800 grinding belt seemed to perform the best within the three tested belt types, however, visual inspection of the saddles ground with the P800 grinding belt showed that the elliptical long saddle radius (LSR) was deformed during grinding and became wavy after approximately 120 s (80 grinding belt revolutions), as can be seen in figure 4.20. The P800 belt is denoted as ultra fine microgrit abrasive and the backing of the P800 belt differs from the other two belts which fall under the category of extra or super fine microgrit abrasives. Possibly, the belt backing of this ultra fine-grained P800 belt is too slack for these grinding conditions and, therefore, it was decided to exclude this grinding belt from further tests.

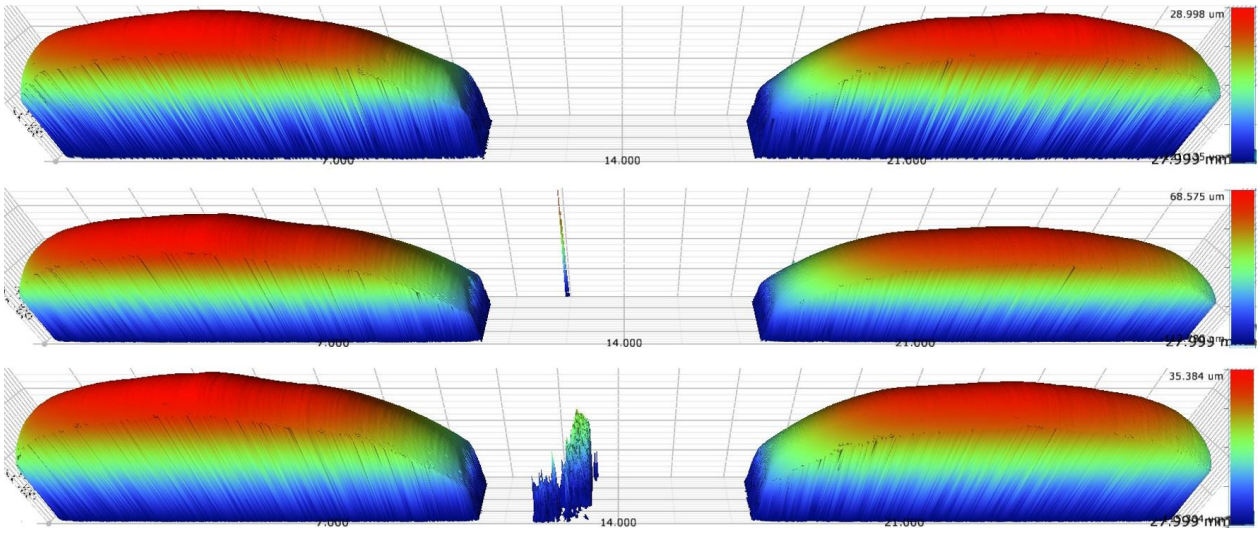

Figure 4.20: Examples of wavy LSR

4.3.3 Effect of belt tension on grinding result

A certain belt tension is necessary that the grinding belt is able to bend properly across the whole saddle surface which should reduce the overall saddle roughness and should help to achieve the desired curvature for an SSR of 28.00 mm.
In order to investigate the influence of the belt tension on the obtained surface roughness and SSR, seven tests were done where the belt is brought under tension by using pressures of 0.5 bar, 0.8 bar, 1 bar, 1.5 bar, 2 bar, 2.5 bar and 3 bar in the pneumatic cylinder. The trials had a duration of 60 seconds using P400 grinding belts and the motor speed was set to 1000 rpm according to the display.
The test results shown in figures 4.21, 4.22 and 4.23 were obtained in the same manner as described in the previous section, here, in every trial, three sample elements from the middle of the holder (fig. 4.17), elements 8, 9 and 10, were measured according to the measurement procedure described in section 4.2. The graphs show the mean roughness or SSR values with corresponding errorbars ($\pm\hat{e}$).

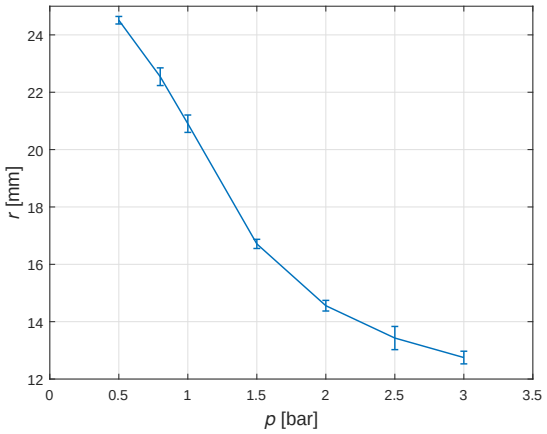

Figure 4.21: Short saddle radius vs. pressure (1000 rpm on display, 60 s, P400)

Figure 4.21 shows that the pressure in the pneumatic cylinder has a rather big influence on the obtained SSR. The obtained radius at 0.5 bar pressure is almost double as big as the obtained radius at 3 bar pressure. In these trials, the biggest achieved mean radius of 24.51 mm ± 0.13 mm at 0.5 bar pressure was still much smaller than the desired radius of 28.00 mm, however, it is not feasible to reduce the pressure further in order to increase the radius since a visual inspection revealed that the elements where 0.5 bar and 0.8 bar pressure was applied, were not sufficiently ground. Figure 4.24 shows images made with the white light interferometer, where can be seen that the surface at the outer ends of the saddle is still rough. Apparently, the tension force in the grinding belt was too low and, therefore, it could not bend over the elliptical LSR in order to grind the whole surface sufficiently.

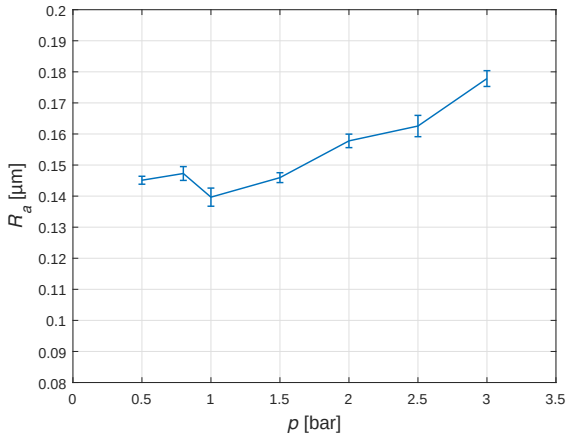

Figure 4.22: Horizontal surface roughness vs. pressure (1000 rpm on display, 60 s, P400)

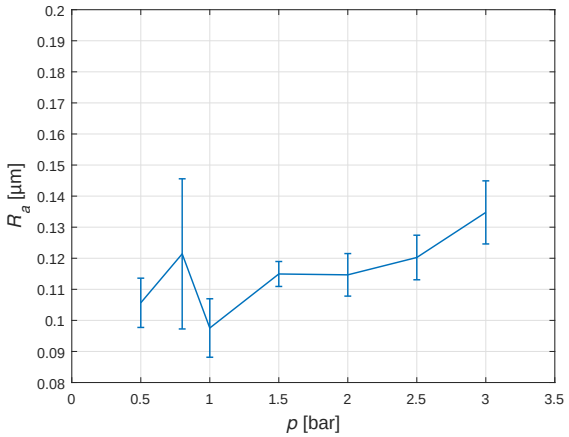

Figure 4.23: Vertical surface roughness vs. pressure (1000 rpm on display, 60 s, P400)

This can also be seen in figures 4.22 and 4.23 where the surface roughness at 0.5 bar and 0.8 bar appears to be higher than at 1 bar. However, from 1 bar on, the surface roughness increases again, which was not expected. Afterwards, it became clear that the reason for this was the not working motor control by which means the motor speed steadily decreased with increasing tension force in the belt, so with increasing pressure in the pneumatic cylinder. Therefore, the increase of surface roughness from 1 bar on, can be explained by the fact that the element saddles were ground less due to a decreasing number of grinding belt revolutions.

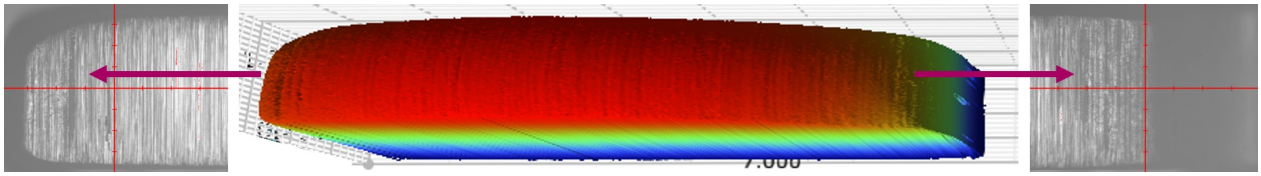

Figure 4.24: Not sufficiently ground outer ends of saddle (0.5 bar)

4.3.4 Influence of spacing between elements on grinding result

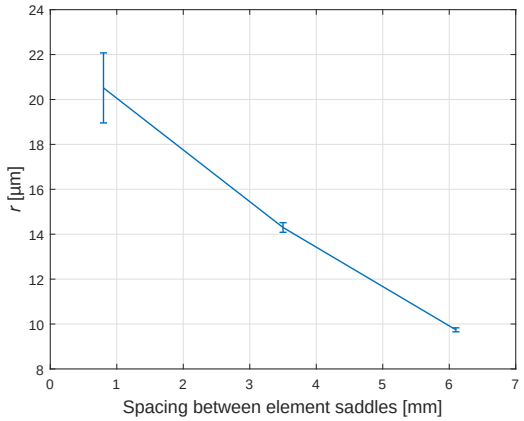

Figure 4.25: Short saddle radius vs. spacing between element saddles (511 rpm, 120s, 2 bar, P400)

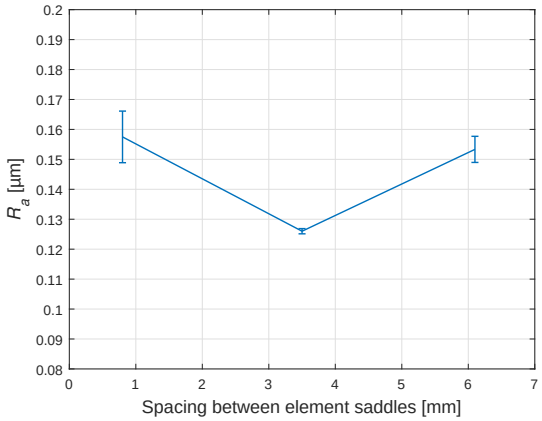

Figure 4.26: Horizontal surface roughness vs. spacing (511 rpm, 120s, 2 bar, P400)

When testing the different element holders described in section 4.3.1, it was noticed that using the holder with spacing between the elements, the obtained SSR after grinding was much smaller compared to the obtained SSR using the holder without spacing between the elements, although the element saddles lie on the same radius of 28.00 mm in both holders. Therefore, the influence of the spacing between the elements on the grinding result was also investigated. Three test runs were executed with a duration of 120 s using 2 bar pressure and P400 grinding belts.

In the first trial, the holder with spacing between the elements was completely filled (fig. 4.14) which implies that the element saddles have a distance of 0.84 mm between each other. In the second trial, the holder was filled as in the previous tests leaving every second slot free (fig. 4.17) which corresponds to 3.48 mm distance between the elements. In the last trial, two slots in the holder were left out between subsequent elements which corresponds to 6.12 mm distance between the elements. The motor speed was again set to 1000 rpm according to the display, however it was also checked this time with the handheld tachometer and the true motor speed was determined to be 511 rpm in this configuration, which implies that the grinding belt rotates 72 times during the test run duration of 120 s. Two sample elements from the middle of the holder were analyzed after every trial.

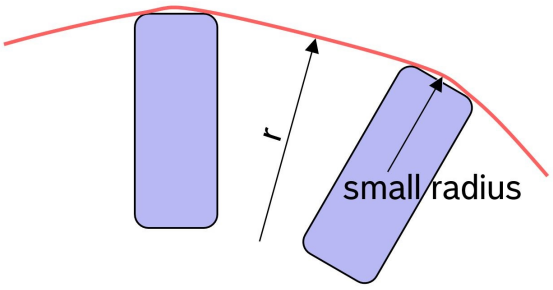

Figure 4.27: Short saddle radius is smaller than grinding belt running radius

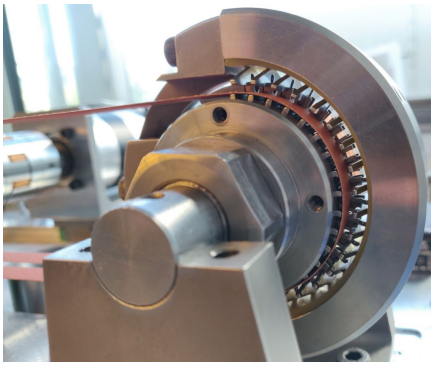

Figure 4.28: Element holder with inserted grinding belt

Figure 4.25 shows that the SSR nearly linearly decreases with increased spacing between the elements and becomes really small, only 9.74 mm at 6.12 mm spacing. The variance in the first trial is rather big since the contact between belt and saddle is not optimal as the distance between the elements is too narrow, as already described in section 4.3.1. This can also be seen in figure 4.26 where the horizontal R_a is also higher when the distance between the elements is narrow. The R_a is the lowest at 3.48 mm distance between the element saddles, which seems to be the optimal distance since at 6.12 mm, the R_a increases again, but the reason for this is unclear. However, the reason for the decrease of the SSR can be explained with the aid of figure 4.27 which depicts schematically a grinding belt lying across two element saddles, as also shown in the image in figure 4.28. It can be seen that the grinding belt takes the shortest path between two elements and forms a smaller radius across the element saddles than the grinding belt running radius, which is 28.00 mm.

4.3.5 Effect of grinding speed on grinding result

It was assumed that it makes no difference for the grinding result whether the grinding speed or the grinding time are adjusted as long as the total number of grinding belt revolutions stays the same. In order to check that assumption, three tests were executed where motor speed and grinding time were both varied but the product of time and speed remained constant resulting in 60 grinding belt revolutions. The following motor speed and time combinations were applied: 566 rpm and 90 s, 1132 rpm and 45 s and 1698 rpm and 30 s. P600 grinding belts were used which were brought under tension by pressurizing the pneumatic cylinder with 1.5 bar. After every trial, two sample elements from the middle of the holder (fig. 4.17) were measured.
In figure 4.29 can be seen that, as expected, the SSR remains approximately constant in the three grinding settings with a radius of around 16 mm. Figures 4.30 and 4.31 show that also the horizontal and vertical surface roughness stay relatively stable within the error margins. The variance of the measured vertical R_a values appears to be higher than of the horizontal R_a values, which is also as expected, since the measurement orthogonal to the main surface grooves is less accurate as described in section 4.2.2.
Therefore, the assumption is confirmed that grinding speed and time can be arbitrarily varied and only the resulting number of grinding revolutions determines the grinding result.

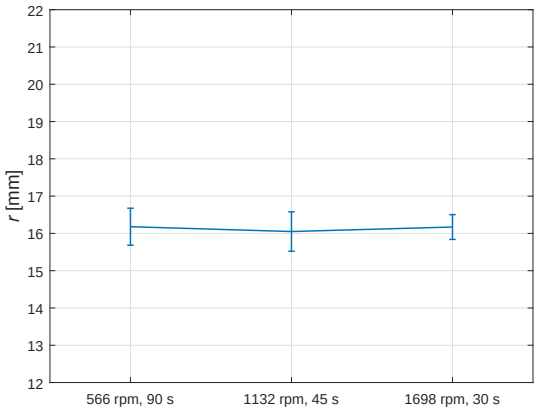

Figure 4.29: SSR at a constant product of time and speed (60 belt revolutions, 1.5 bar, P600)

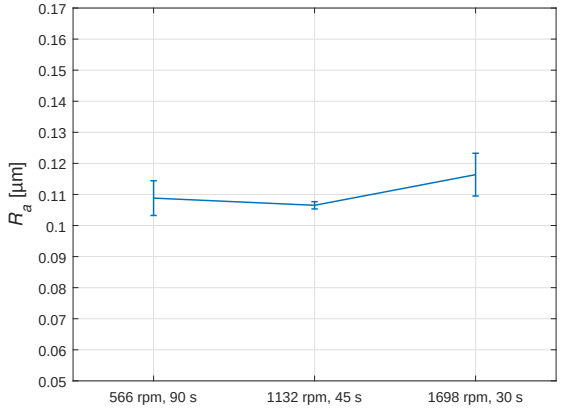

Figure 4.30: Horizontal surface roughness at a constant product of time and speed (60 belt revolutions, 1.5 bar, P600)

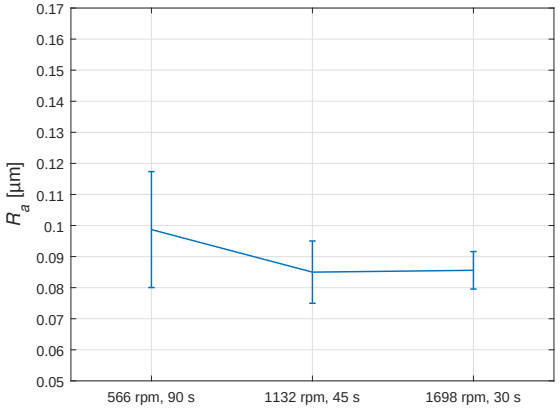

Figure 4.31: Vertical surface roughness at a constant product of time and speed (60 belt revolutions, 1.5 bar, P600)

4.4 Experimental Design

After completion of the orientating preliminary tests of the grinding machine, the obtained knowledge about the machine was used to establish a systematic experimental design in order to collect sufficient R_a and SSR data to be able to predict the grinding result, the response variables, depending on the machine process parameters, the predictor variables, and eventually find the optimal process parameters in order to achieve the required grinding result.
The values of the response variables, the surface roughness R_a and the short saddle radius r, were already defined in the requirements. After grinding of the element in the machine, the obtained roughness R_a of the saddle surface should be lower than 0.150 µm and the short saddle radius r should be 28.00 mm. However, the number and also the value range of predictor variables which should be used in an experimental design in order to be able to sufficiently investigate the effect on the grinding result was initially unclear. The outcomes of the orientating preliminary trials helped to decide which process variables should be considered as constants, and also helped to limit the value range of predictor variables in order to create a compact systematic experimental design which could be accomplished within limited resources and time.

During the orientating preliminary trials, it was found that only with the element holder with extended spacing between the elements stable grinding results could be achieved and, therefore, this holder was decided to be used in the final experimental design. Every second element slot is omitted in the holder (fig. 4.17), which implies that the distance between the element saddles is 3.48 mm and the capacity of the holder is 17 elements.
When testing the different available grit sizes of the grinding belts, it was observed that the belt backing of the P800 grinding belt was apparently too slack resulting in a deformation of the elliptical long saddle radius (LSR) during grinding. Although the lowest surface roughness was achieved using the P800 belt, it was rejected for this reason. Between the remaining P400 and P600 grinding belt, it was decided to choose for

the P600 belt since slightly lower surface roughness could be achieved within shorter grinding times compared with the P400 grinding belt.
The investigation of the relationship between grinding time and speed revealed that only the resulting number of grinding belt revolutions matters. Therefore, it was decided to hold the grinding speed constant and only vary the time in the final experimental design. The motor speed of the grinding machine was decided to be 566 rpm which corresponds to the grinding belt speed $f_{r,belt} = 40$ rpm. During the final experiments, the correct speed had to be checked by a handheld tachometer and manually corrected since, as mentioned earlier, the motor controller which should stabilize the speed, did not work due to a missing encoder in the electro motor.
The process parameters which were decided to be held constant, are summarized in table 4.2.

Table 4.2: Constant process parameters

Fixed factors	**Levels**
Grinding belt speed $f_{r,belt}$	40 rpm
Belt grit size	P600
Element holder	Extended spacing, 3.48 mm distance between saddles

The factors which exhibited a big influence on the grinding result during the orientating test were the grinding time and the tension force in the grinding belt, which depends on the pressure in the pneumatic cylinder of the grinding machine. Therefore, the pressure p and the grinding time t were decided to be used as predictor variables in the experiments. Furthermore, it was decided to use a full factorial experimental design where experiments of all possible combinations of the values of the two used factors are executed in order to be able to investigate all possible effects. It was decided to vary the predictor variables on three levels in order to detect non-linear behaviour of the response variables. The factor pressure p was decided to be varied in steps of 0.75 bar starting at 1 bar since below this pressure value, the saddle surface was observed to be not sufficiently ground during the orientating tests, and ending at 2.5 bar. The factor time t was decided to be varied in steps of 45 s from 45 s until 135 s. The chosen level values are summarized in table 4.3.

Table 4.3: Predictor variables with level values

				Levels:		
				1	**2**	**3**
Factors:	**1**	time	t [s]	45	90	135
	2	pressure	p [bar]	1	1.75	2.5

The full factorial design consists of 3^2 experiments and it was decided to execute one replication , so in total 18 experiments were performed. After every experiment, both saddles of three elements from the middle of the holder (fig. 4.17), elements 7, 8 and 9, were analyzed, which resulted in 6 measurement values per experiment, and together with the replication, in total 12 measurement values per machine setting.

5. Results

Nine duplication experiments, so in total 18 experiments, were performed in order to obtain measurement data of the response variables, surface roughness R_a and short saddle radius r, dependent on the machine parameters, grinding time t and pressure p of the machine's pneumatic cylinder which generates the tension force in the grinding belt.
The measurement data of the 18 experiments can be found in appendix C. The order of the first nine test runs and also of the last nine replication test runs was randomized in order to balance the effect of uncontrollable or unknown noise factors that could influence the test results.

5.1 Analysis of variance

Analysis of variance (ANOVA) is used to investigate the main and interaction effects of the predictor variables t and p on the response variables SSR, and horizontally and vertically measured R_a. The ANOVA gives an indication of the effect of the predictor variables on a certain response variable by determining the variation caused per predictor variable and the interaction of predictor variables. Therefore, a predictor variable which causes large variation within the response variable data is expected to have a strong effect on it. MATLAB is used to compute the ANOVAs from the experiment data (appendix C) for the SSR, horizontal R_a and vertical R_a, and the resultant ANOVA tables 5.1, 5.2 and 5.3, respectively, are shown below. In the ANOVA, the variation introduced on the data by a factor is indicated by the F statistic, also called variance ratio, named after the statistician Sir Ronald A. Fisher. The F statistic is the ratio of variance due to the effect of a factor and variance due to the error term [8]. The F value computed for a certain factor is used together with the F distribution to determine the P value which indicates the statistical significance of the effect caused by a factor. The P value is the area probability under the F distribution which is dependent on the degrees of freedom u associated with the examined factor and the degrees of freedom v associated with the error. The degrees of freedom (DoF) is the number of independent comparisons that can be made among the elements of a sample [7]. Therefore, the DoF of the executed experiments are, since there were 2 factors with each 3 levels and 12 samples per level, $3-1=2$ DoF per factor, $(3-1)\cdot(3-1)=4$ DoF for the interaction of the factors, $3\cdot3\cdot(12-1)=99$ DoF for the error term, and $(3\cdot3\cdot12)-1=107$ DoF in total. The $F_{2,99}$ distribution probability density function corresponding to degrees of freedom $u=2$ of the factor and $v=99$ of the error is illustrated in figure 5.1. The critical F value is evaluated to be 3.088 and corresponds to the significance level of $\alpha=0.05$ according to equation 5.1 which is the probability that this critical value is exceeded. A factor with a F value bigger than the critical value of 3.088 and, therefore, having a P value below this significance level, gives an indication of strong evidence that there is an effect caused by the factor in question and the null hypotheses (H_0), which assumes no effects, is rejected.

$$P(F_{2,99} > 3.088) = \int_{3.088}^{\infty} f(x)dx = 0.05 \tag{5.1}$$

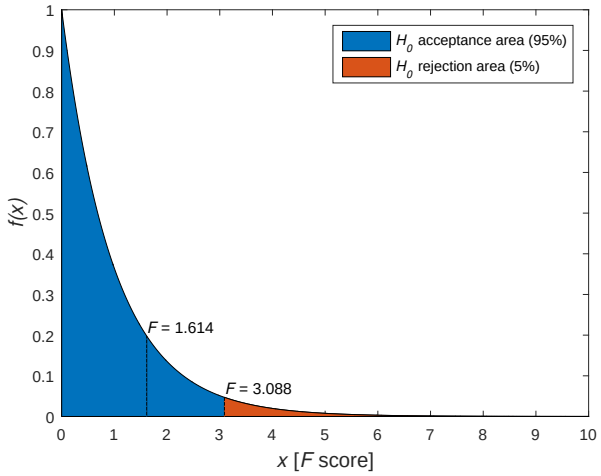

Figure 5.1: $F_{u,v}$ distribution probability density function ($u=2$, $v=99$)

The ANOVA for the SSR, shown in table 5.1, reveals by looking at the F values that the factor pressure p has clearly the largest contribution to the resulting SSR, hence is the cause for the largest variation. The factor time t has a relatievely small F value of 1.614 as depicted in figure 5.1, which is smaller than the critical F value and, therefore, no statistical significant influence on the SSR can be detected. Additionally, there are also no significant interaction effects.

Table 5.1: ANOVA for SSR

Source of Variation	**Sum of Squares**	**DoF**	**F-Value**	**P-Value**
Time	8.000	2	1.614	0.2043
Pressure	1066.378	2	215.138	$9.15 \cdot 10^{-37}$
Interaction	5.693	4	0.574	0.6819
Error	245.357	99		
Total	1325.428	107		

However, the ANOVAs for the horizontally (table 5.2) and vertically (table 5.3) measured R_a reveal effects of both factors, time t and pressure p, but also no significant interaction effects since the interaction P values are above the 0.05 significance level. The horizontal R_a's F value for the factor time t is bigger than for the factor pressure p , which indicates that the factor time t has a larger effect on the horizontal R_a than the factor pressure p , however, for the vertical R_a it is the other way around.

Table 5.2: ANOVA for horizontal R_a

Source of Variation	**Sum of Squares**	**DoF**	**F-Value**	**P-Value**
Time	0.124	2	29.595	$8.4 \cdot 10^{-11}$
Pressure	0.045	2	10.864	$5.4 \cdot 10^{-5}$
Interaction	0.018	4	2.155	0.0796
Error	0.207	99		
Total	0.395	107		

Table 5.3: ANOVA for vertical R_a

Source of Variation	**Sum of Squares**	**DoF**	**F-Value**	**P-Value**
Time	0.052	2	13.528	$6.4 \cdot 10^{-6}$
Pressure	0.132	2	34.165	$5.2 \cdot 10^{-12}$
Interaction	0.017	4	2.142	0.0812
Error	0.191	99		
Total	0.392	107		

5.2 Reproduceability

In order to get an indication of the variations between the experiments, the differences between the data in the first nine test runs and the nine replication test runs are examined before analyzing the relationship of the predictor and response variables, which is done in the following section. The results can be seen in the boxplots in figure 5.2 and 5.3, where the Δ-measurement values which are used in the boxplots, are computed by subtracting all the obtained data in the first nine test runs from the corresponding data at the same settings obtained in the nine replication test runs according to the equation below.

$$\Delta y_{n,s,t,p} = y_{1,n,s,t,p} - y_{2,n,s,t,p}\,, \tag{5.2}$$

where y_1 = Measurement value from the first series of experiments,
y_2 = Measurement value from the replication experiments,
n = Number of sample element,
s = Saddle side (left or right),
t = Machine setting for time,
p = Machine setting for pressure

In total, 54 Δ-measurement values are used per boxplot since the horizontal R_a, the vertical R_a and the short saddle radius r were measured at three sample elements on two saddles in nine duplication experiments.

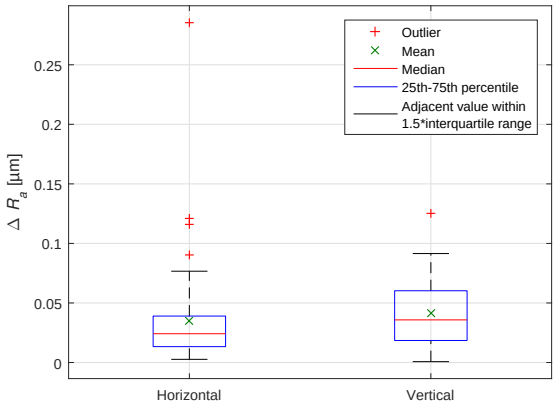

Figure 5.2: Boxplot: Differences in R_a between first experiments and replications

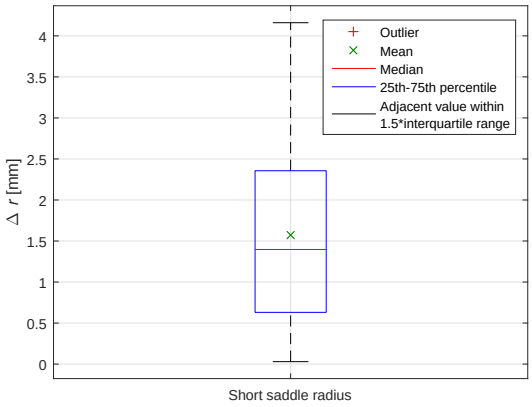

Figure 5.3: Boxplot: Differences in SSR between first experiments and replications

Between the experiments, the mean difference of the measured horizontal R_a, vertical R_a and SSR of an elements is 0.035 µm, 0.042 µm and 1.58 mm, respectively, which are indicated in the box plots with a green cross. The interquartile range (IQR) gives an indication of the variability within the differences between the duplication experiments, and the IQR for the horizontal ΔR_a, vertical ΔR_a and ΔSSR is 0.026 µm, 0.042 µm and 1.73 mm.

In order to investigate if there are significant differences in the obtained mean values of an experiment and its replication, a two sample t-test is conducted for the response variables of all test runs, which can be found in appendix D in tables D.1, D.2, D.3 for the horizontal R_a, the vertical R_a and the SSR, respectively. For the calculation of the mean value of a response variable of one test run, the measurement data of both saddles of the three sample elements, so 6 measurement values of a response variable, are considered. The computed standard deviation per trial setting, which can be found in the last column of the two sample t-test tables in appendix D, is therefore computed for 12 measurement values, the 6 values of an experiment and the 6 values of its replication, since equal variances are assumed in the two sample t-test. The two sample t-test reveals that at the trial setting $t = 90$ s and $p = 2.5$ bar, the mean values of the horizontal R_a are significantly different. The samples of one of the duplication experiments at this setting, show more variation in the R_a values than the other. Furthermore, at the trial setting $t = 45$ s and $p = 1.75$ bar, the mean values of the SSR are significantly different. Similar here, in one of the duplication experiments, more variation in the measured SSR is observed.
It is unknown what caused these variations, however, for the rest of the test runs, there is no difference found between the mean values of experiment and its replication.

5.3 Effect of process parameters on grinding result

The results of the test runs which are shown in appendix C, are illustrated in the graphs in figures 5.4, 5.6 and 5.8. In the graphs, the sample mean values of the response variables are depicted with the corresponding

errorbars ($\pm\hat{e}$). The sample mean at a trial setting is obtained from the measurement values of the two saddles of the six sample elements where three sample elements are from one test run and three sample elements from the replication test run, so 12 measurement values are used in total to compute the sample mean. For a better visualisation of the dependence of the response variables on the factors t and p, the results are also illustrated in 3D graphs, as shown in figures 5.5, 5.7 and 5.9.
In the surface roughness graphs, it can be observed that the R_a values are consistently higher than observed in the preliminary tests, which is caused by using a different cut-off wavelength for the evaluation of the surface roughness R_a in the Bruker Vision64 program. As explained in the beginning of section 4.3, the cut-off wavelength used in the preliminary trials was with 0.08 mm too low and now in the final experiments, it was adjusted to the more common value of 0.8 mm according to the international ISO standard.

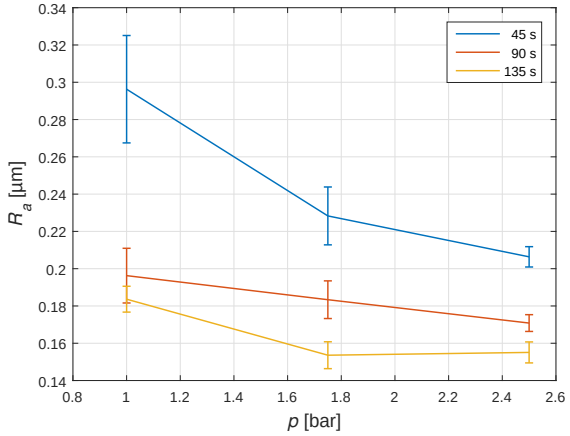

Figure 5.4: Horizontal R_a vs. pressure

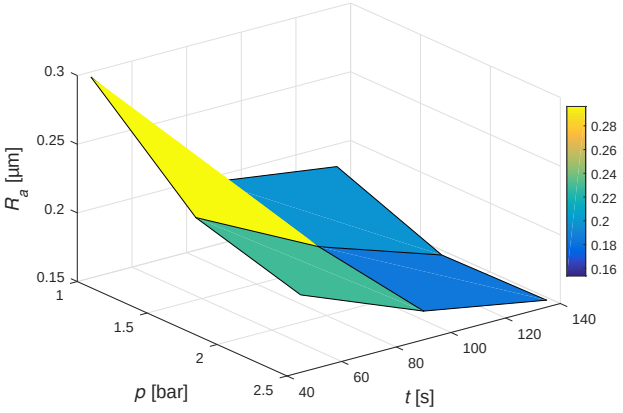

Figure 5.5: Horizontal R_a vs. time and pressure

Figure 5.4 and 5.5 show how the horizontal surface roughness R_a decreases with increasing grinding time t and pressure p. The unground saddle surface of an element has an R_a of about 0.8 µm, therefore, the saddle surface in the lowest setting $t = 45$ s and $p = 1$ bar is already reduced by a factor two. After 90 s of grinding, the roughness is again considerably reduced, however, by grinding longer, the rate of roughness improvement decreases. Furthermore, it catches one's eye that at 2.5 bar, the variance between the samples indicated by the errorbar, has become very small for all grinding times. Additionally, it appears that the pressure contributes most to lowering the surface roughness at shorter grinding times since at the longest grinding time, at $t = 135$ s, the evaluated surface roughness remains approximately the same between $p = 1.75$ bar and $p = 2.5$ bar with $R_a = 0.154$ µm $\pm$ 0.007 µm and $R_a = 0.155$ µm $\pm$ 0.006 µm, respectively, which are the lowest achieved horizontal R_a values in the experiments.

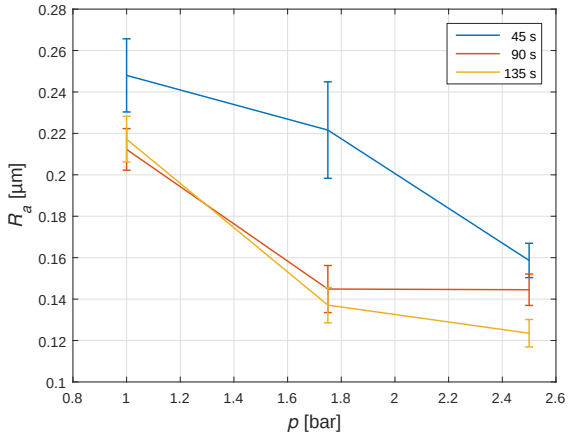

Figure 5.6: Vertical R_a vs. pressure

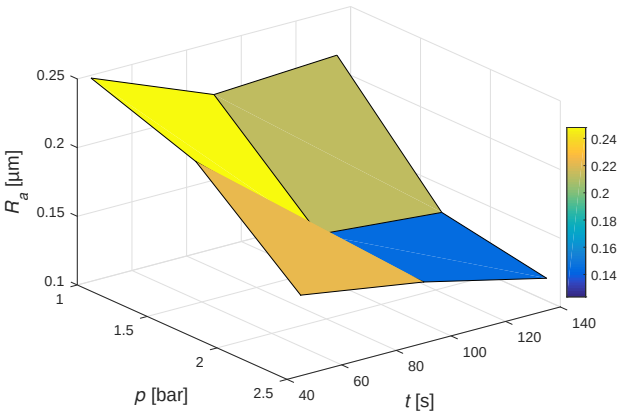

Figure 5.7: Vertical R_a vs. time and pressure

The trend of the measured vertical R_a is less clear observable and deviates from the trend of the horizontal R_a, as can be seen in figures 5.6 and 5.7. The variance in the measurements remains relatively high in the experiments with $t = 45$ s, and in the experiments with $t = 90$ s and $t = 135$ s, there is no clear difference observable in the achieved surface roughness at lower pressures between $p = 1$ bar and $p = 1.75$ bar.

However, the vertical surface roughness considerably improves there with increasing pressure with a higher rate compared to the horizontal surface roughness at $t = 90$ s and $t = 135$ s. Overall, the vertical surface roughness R_a is consistently lower than the horizontal surface roughness, however, the initial R_a before grinding was with around 0.6 µm also lower. At $p = 2.5$ bar, the variances of the vertical R_a samples at all grinding times are similarly low and are now clearly distinguishable having a lower surface roughness with increasing grinding time. The lowest vertical surface roughness was achieved at the setting $t = 135$ s and $p = 2.5$ bar with $R_a = 0.124$ µm $\pm$ 0.007 µm.

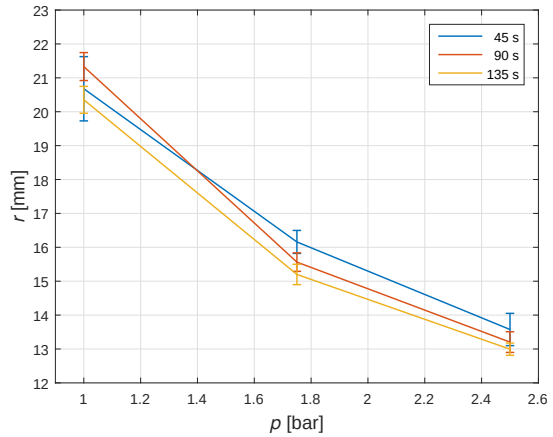

Figure 5.8: SSR vs. pressure

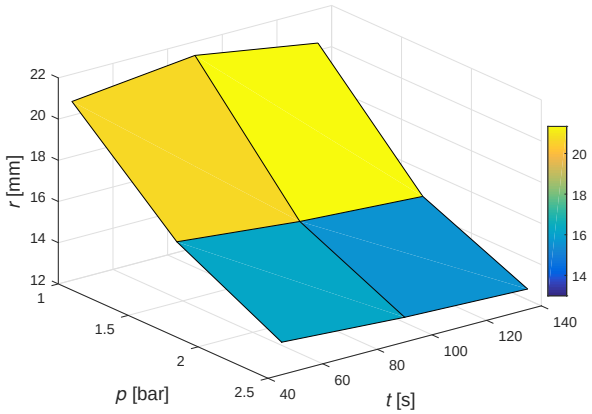

Figure 5.9: SSR vs. time and pressure

The results of the SSR are shown in figures 5.8 and 5.9, where can be seen that the SSR considerably decreases with increasing pressure, for example, in the experiments with $t = 90$ s, it decreases from $r = 21.33$ mm $\pm$ 0.41 mm to $r = 13.20$ mm $\pm$ 0.30 mm between $p = 1$ bar and $p = 2.5$ bar. Therefore, the SSR is in all used settings much lower than the desired 28.00 mm. Apparently, the grinding time has not much effect on the size of the SSR since the curves corresponding to the grinding times in the graph (fig. 5.8) lie closely together and, considering the errorbars, the results are hardly to distinguish from each other, certainly at $p = 1$ bar. However, looking at the results between $p = 1.75$ bar and $p = 2.5$ bar, it seems that higher grinding times tend to slightly decrease the SSR.

5.4 Polynomial data fit for prediction of grinding result

It is desirable to be able to select between a bigger number of parameter combinations than only the nine combinations from the experiments in order to find a machine configuration with which a certain feasible combination of SSR and surface roughness R_a can be achieved. This is not only beneficial for finding the optimal settings to obtain a R_a and SSR close to the current requirements, but also for choosing settings in the future for the case that at a later stage, the requirements for the elements would change.
Therefore, the measurement data consisting of the sample means from the experiments, is fitted to polynomials of second order in order to be able to predict the grinding result in terms of roughness R_a and short saddle radius r in a continuous way dependent on the machine settings. The data fit is accomplished with the aid of MATLAB which uses the method of least squares in order to estimate the model coefficients. The resulting polynomial equations 5.3, 5.4 and 5.5 for the horizontal R_a, vertical R_a and short saddle radius r, respectively, are shown below.

$$R_{a(h)}(t,p) = 0.5342\ \mu\text{m} - 0.003491\ \tfrac{\mu\text{m}}{\text{s}}\cdot t - 0.1537\ \tfrac{\mu\text{m}}{\text{bar}}\cdot p + 1.007\cdot 10^{-5}\ \tfrac{\mu\text{m}}{\text{s}^2}\cdot t^2 + 0.0004545\ \tfrac{\mu\text{m}}{\text{s}\cdot\text{bar}}\cdot t\cdot p + 0.0231\ \tfrac{\mu\text{m}}{\text{bar}^2}\cdot p^2 \quad (5.3)$$

$$R_{a(v)}(t,p) = 0.4557\ \mu\text{m} - 0.002024\ \tfrac{\mu\text{m}}{\text{s}}\cdot t - 0.1535\ \tfrac{\mu\text{m}}{\text{bar}}\cdot p + 8.463\cdot 10^{-6}\ \tfrac{\mu\text{m}}{\text{s}^2}\cdot t^2 - 3.229\cdot 10^{-5}\ \tfrac{\mu\text{m}}{\text{s}\cdot\text{bar}}\cdot t\cdot p + 0.02877\ \tfrac{\mu\text{m}}{\text{bar}^2}\cdot p^2 \quad (5.4)$$

$$r(t,p) = 31.58\ \text{mm} + 0.01479\ \tfrac{\text{mm}}{\text{s}}\cdot t - 13.45\ \tfrac{\text{mm}}{\text{bar}}\cdot p - 0.0001022\ \tfrac{\text{mm}}{\text{s}^2}\cdot t^2 - 0.001887\ \tfrac{\text{mm}}{\text{s}\cdot\text{bar}}\cdot t\cdot p + 2.457\ \tfrac{\text{mm}}{\text{bar}^2}\cdot p^2 \quad (5.5)$$

Figures 5.10, 5.11 and 5.12 illustrate the polynomial data fits based on equations 5.3, 5.4 and 5.5 for the horizontal R_a, vertical R_a and short saddle radius r, respectively, for time t and pressure p values within the experimental factor range. The root mean squared error (RMSE) is used to indicate the deviation of the response values from the fitted response values as a measure of accuracy. The RMSE is calculated as follows:

$$RMSE = \sqrt{\frac{\sum_{i=1}^{n}(y_i - \hat{y}_i)^2}{n-m}}, \tag{5.6}$$

where y_i = response value,
$\hat{y}_i$ = fitted response value,
n = Number of response values,
m = Number of fitted coefficients

The obtained RMSE for the horizontal R_a, vertical R_a and short saddle radius r are 0.01369 µm, 0.02141 µm and 0.3908 mm, respectievely.

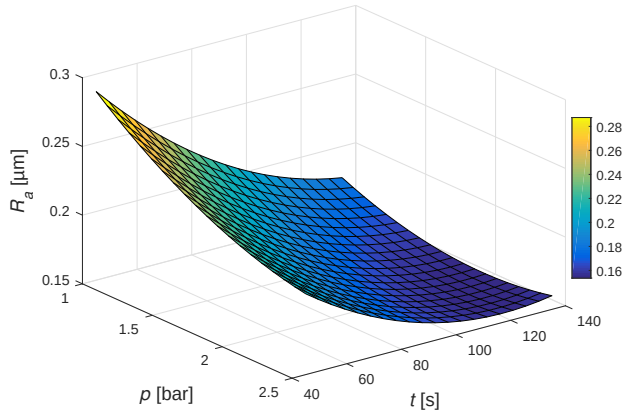

Figure 5.10: Polynomial fit: Horizontal R_a vs. time and pressure (RMSE = 0.01369 µm)

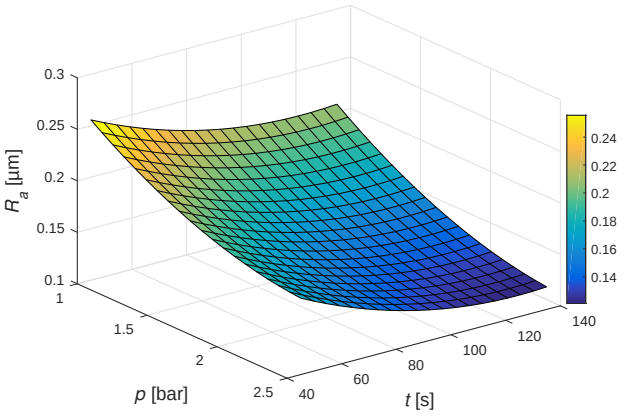

Figure 5.11: Polynomial fit: Vertical R_a vs. time and pressure (RMSE = 0.02141 µm)

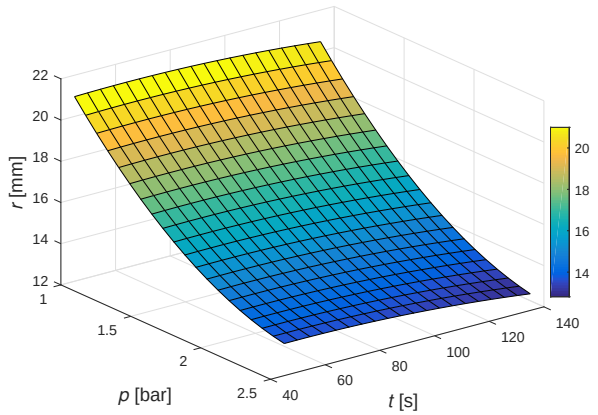

Figure 5.12: Polynomial fit: SSR vs. time and pressure (RMSE = 0.3908 mm)

The contour plot in figure 5.13 is obtained by combining the contour plots of the equation for the horizontal R_a (eq. 5.3) and the short saddle radius r (eq. 5.5) and, therefore, gives a good overview on the relationship of the two response variables. This way, the contour plot can be used to find the corresponding machine settings at a certain surface roughness R_a and SSR condition.

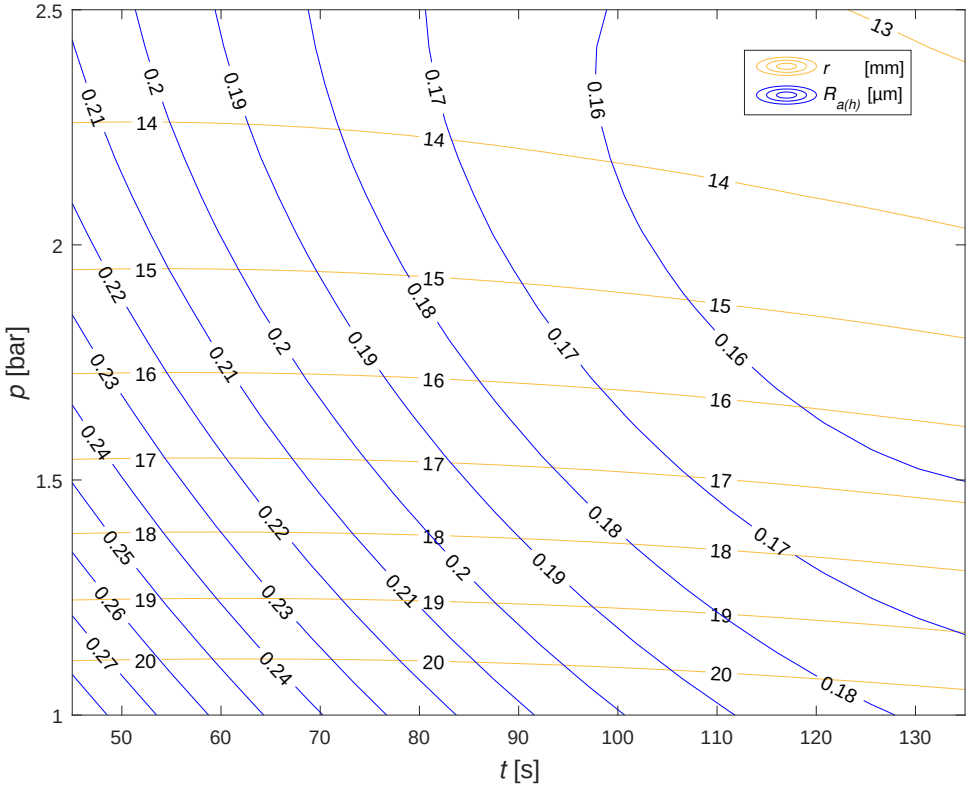

Figure 5.13: Time vs. pressure contour plot of polynomial fit for horizontal R_a and short saddle radius r

5.5 Exponential data fit for prediction of grinding result

The RMSEs of the polynomial data fits are low, however, it is still the question if the polynomials reflect the trends of the response values, especially in the proximity of borders of the experimental factor range. When looking at figure 5.10, for example, it can be observed that the slope of the curve along the t-axis first decreases, but increases again slightly when approximating the end of the factor range, which is not the expected trend of the surface roughness R_a. On the contrary, it would be expected that the surface roughness further decreases with increasing grinding time. Therefore, in order to find appropriate functions for predicting the grinding result, an exponential data fit is also applied. The resulting exponential equations 5.7, 5.8 and 5.9 for the horizontal R_a, vertical R_a and short saddle radius r, respectively, are shown below.

$$R_{a(h)}(t,p) = 0.1519\ \text{µm} + \exp(-0.02273\ \tfrac{1}{\text{s}}\ \cdot\ t) \cdot \exp(-0.7141\ \tfrac{1}{\text{bar}}\ \cdot\ p) \cdot 0.8049\ \text{µm} \tag{5.7}$$

$$R_{a(v)}(t,p) = -0.03104\ \text{µm} + \exp(-0.002635\ \tfrac{1}{\text{s}}\ \cdot\ t) \cdot \exp(-0.2688\ \tfrac{1}{\text{bar}}\ \cdot\ p) \cdot 0.4179\ \text{µm} \tag{5.8}$$

$$r(t,p) = 10.99\ \text{mm} + \exp(-0.0007982\ \tfrac{1}{\text{s}}\ \cdot\ t) \cdot \exp(-0.9818\ \tfrac{1}{\text{bar}}\ \cdot\ p) \cdot 28.06\ \text{mm} \tag{5.9}$$

The obtained RMSE for the horizontal R_a, vertical R_a and short saddle radius r are 0.008993 µm, 0.02157 µm and 0.4059 mm, respectively. Therefore, the accuracy of the exponential fit for the horizontal R_a appears to be higher than of the polynomial fit and the accuracy for the vertical R_a and short saddle radius r is slightly lower. The corresponding graphs to the exponential fits can be found in figures 5.14, 5.15 and 5.16. Although the RMSE of the vertical R_a from the exponential fit is only 0.00016 µm higher than the RMSE from the polynomial data fit, comparing the corresponding graphs in figures 5.11 and 5.16, differences can be observed. It can be seen that the shape of the exponential fit is more similar to a skew plane within the factor range. However, the graphs of the horizontal R_a (fig. 5.14) and short saddle radius r (fig. 5.16) closely resemble the graphs of the corresponding experimental sample data (fig. 5.5 and 5.9).

Figure 5.17 shows the combined contour plot of the exponential equations of the horizontal R_a and the vertical R_a in dependence of the factors t and p. It can be observed that the level lines of this contour plot are less curved and more straight compared to the contour plot of the polynomial fits (fig. 5.13).

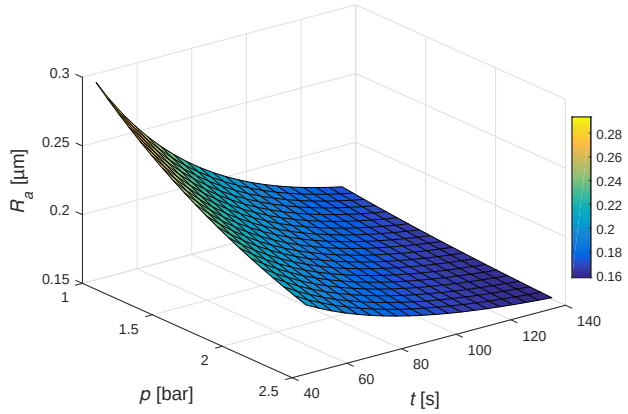

Figure 5.14: Exponential fit: Horizontal R_a vs. time and pressure (RMSE = 0.008993 µm)

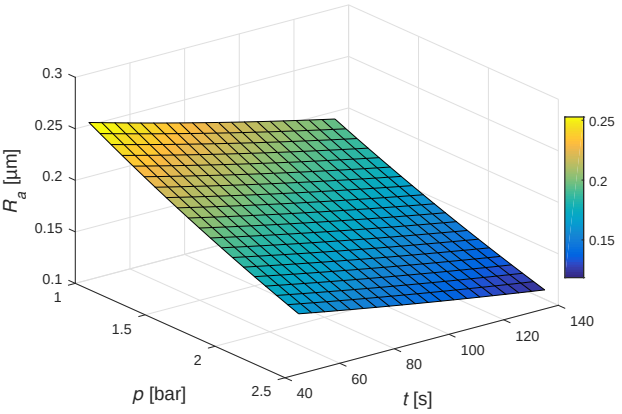

Figure 5.15: Exponential fit: Vertical R_a vs. time and pressure (RMSE = 0.02157 µm)

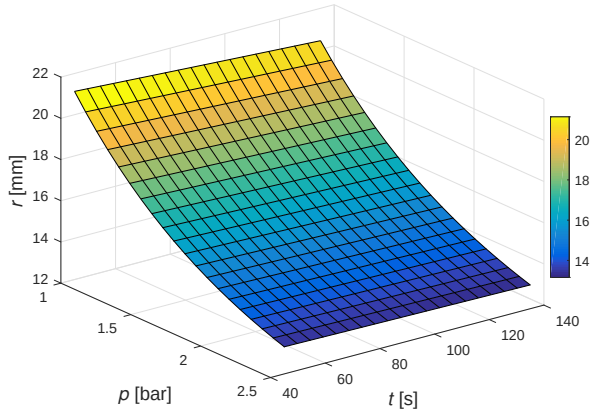

Figure 5.16: Exponential fit: SSR vs. time and pressure (RMSE = 0.4059 mm)

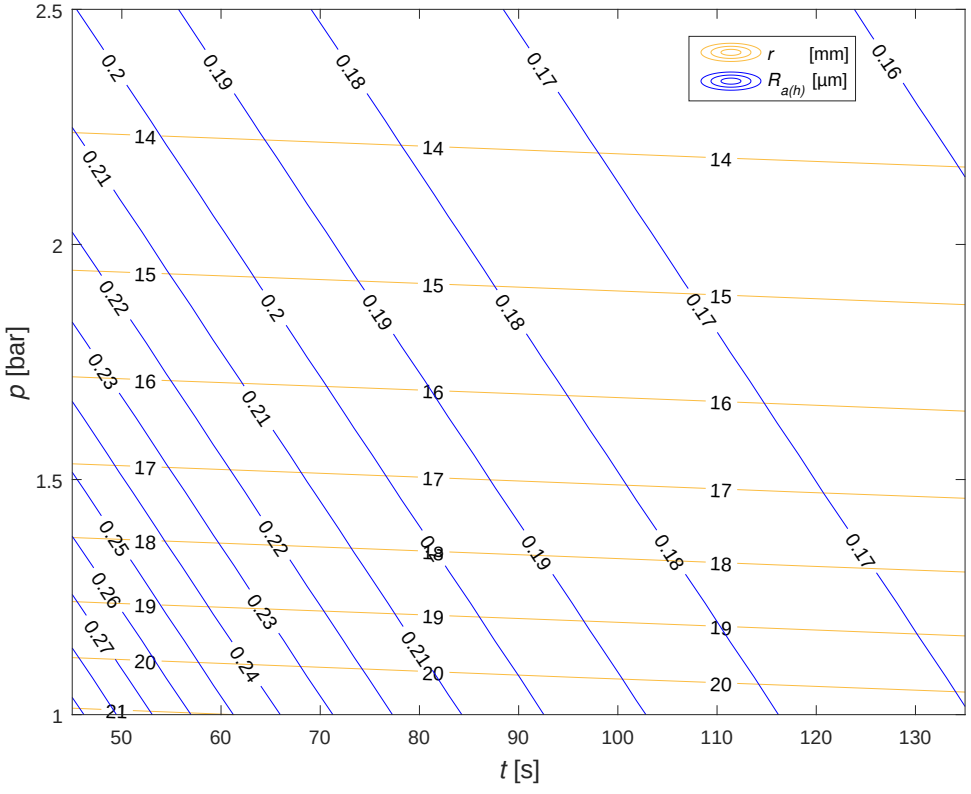

Figure 5.17: Time vs. pressure contour plot of exponential fit for horizontal R_a and short saddle radius r

The exponential model predicts a short saddle radius of $r = 28.00$ mm below pressures of $p = 0.5$ bar, as shown in figure 5.20 and in the contour plot in figure F.1 in appendix F, however a horizontal R_a value below 0.150 µm is not reached at all. The exponential model reaches eventually a plateau at high grinding times, as shown in figure 5.19, and the horizontal R_a becomes eventually not significantly lower than 0.152 µm. The machine settings which are required according to the exponential model in order to obtain the short saddle radius $r = 28$ mm together with the lowest achievable horizontal roughness $R_a = 0.152$ µm are $t = 390$ s and $p = 0.19$ bar. The red dot in the contour plot in the horizontal R_a graph and the SSR graph in figures 5.18, 5.19 and 5.20, respectively, represents the predicted grinding result at these settings.

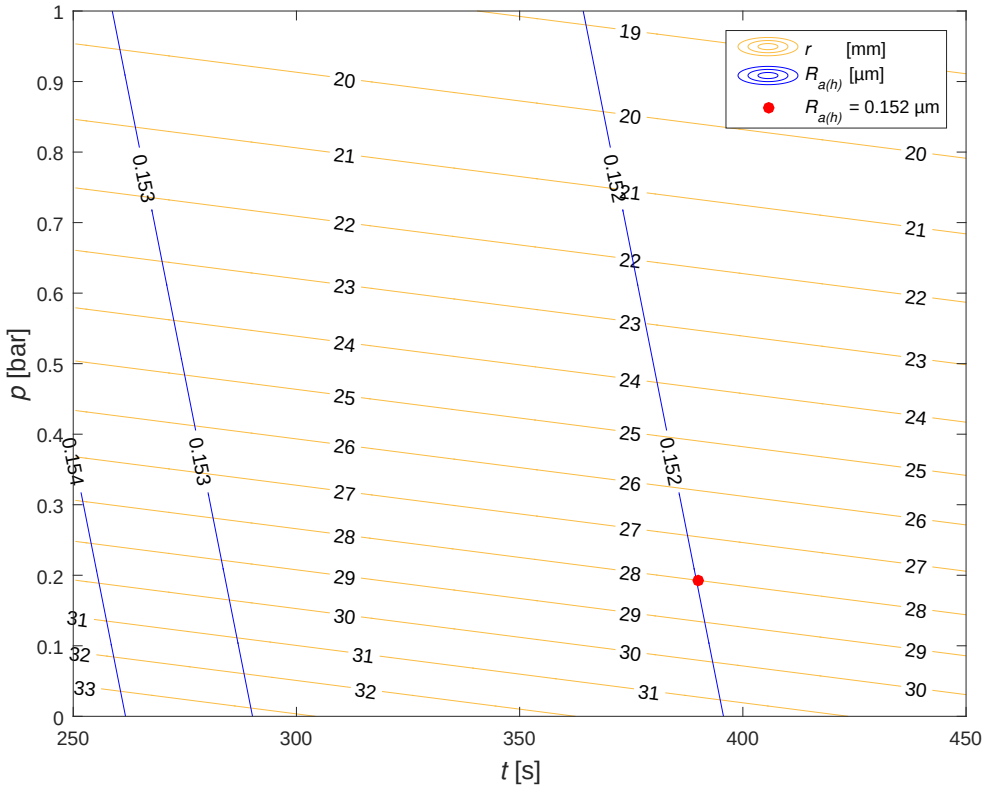

Figure 5.18: Time vs. pressure contour plot of exponential fit for horizontal R_a and short saddle radius r at low pressures and long grinding times

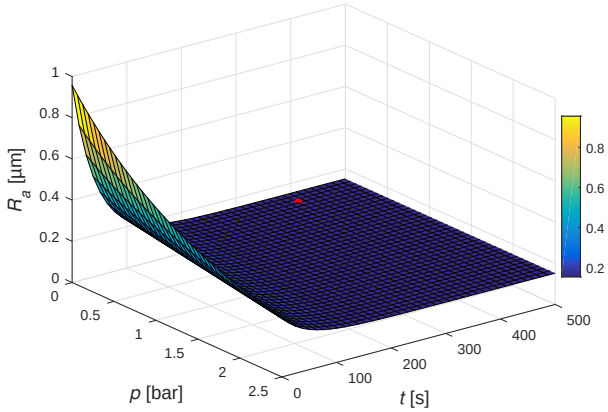

Figure 5.19: Horizontal R_a vs. time and pressure at long grinding times

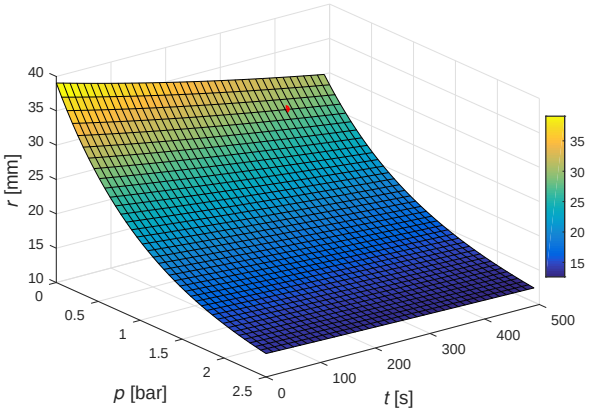

Figure 5.20: SSR vs. time and pressure at long grinding times

6. Discussion

In order to reduce friction in the CVT pushbelt's element-ring contact, the element saddle surface roughness along the x-profile (fig. 4.2), called horizontal R_a, is targeted to be reduced from about $R_a = 0.8$ µm to $R_a = 0.150$ µm or lower, and the curvature across the y-profile, the short saddle radius (fig. 2.2), is aimed to be adjusted to $r = 28.00$ mm. A specially for this purpose developed grinding machine was used to perform experiments based on a full factorial design in order to investigate the feasibility of belt grinding for processing the element saddle. The experiments were carried out with P600 grinding belts and 40 rpm grinding belt speed. The obtained measurement data of the response variables R_a and r dependent on the machine parameters grinding time t and pressure p, was analyzed in order to investigate the relationship between the machine parameters and the grinding result. Polynomial and exponential functions were fitted to the data in order to obtain a continuous representation of the interdependency of the process variables. The fitted functions give an estimation for the achievable horizontal R_a (measured along the x-profile, fig. 4.2), vertical R_a (measured along the y-profile, fig. 4.2), and short saddle radius r at the given machine settings in terms of time t and pressure p, and can be used to find feasible process variables.

The vertical R_a of the saddle was not defined in the requirements for the saddle surface improvement since the roughness along the x-profile is considered to characterize best the kind of contact that the elements make with the rings inside the pushbelt because the main surface grooves are perpendicular to it, as illustrated in figures 4.8 and 4.9. Furthermore, the DIN EN ISO standard for surface texture assessment also recommends measuring the roughness perpendicular to the surface grooves. Nevertheless, the vertical surface roughness R_a was measured and analyzed in order to capture the effect of grinding in this direction, too. However, the vertical R_a measurements appear to be indeed less adequate to characterize the grinding result since the trend of the vertical R_a related to time t and pressure p is not clearly interpretable due to the variance between the sample elements, as can be seen in figure 5.6. This made it also difficult to fit a polynomial or exponential function to the measurement data, as can be seen in figures 5.11 and 5.16, achieving a much lower accuracy of the fits according to the RMSE compared to the fits of the horizontal R_a. Therefore, the vertical R_a is not considered to reliably characterize the grinding result. However, it can be stated that the vertical R_a decreases with increasing grinding time t and pressure p from an initial R_a about 0.6 µm to 0.124 µm ± 0.007 µm at $t = 135$ s and $p = 2.5$ bar.

The specified requirements for the horizontal R_a and short saddle radius r could unfortunately not be achieved. The lowest achieved horizontal surface roughness R_a was 0.154 µm ± 0.007 µm after 135 s of grinding, as can be seen in figure 5.4, and since it was desired to achieve a horizontal R_a of 0.150 µm or lower, the obtained surface roughness was slightly higher. Furthermore, it can be observed that there is considerable variation between the samples. The differences between the samples of the duplication experiment are on average $\Delta R_a = 0.035$ µm, as shown in the boxplot in figure 5.2. However, these high average difference is most of all caused by samples ground at lower pressures or lower grinding times as can be observed in 5.4. There, it can be seen that the variation of the samples generally decreases with increasing pressures and grinding times considering the standard error of the mean $\hat{e}$ indicated by the error bars ($\pm\hat{e}$). At a pressure $p = 2.5$ bar, the standard error of the mean $\hat{e}$ has reached a relatively low value of around 0.005 µm at all grinding times. It is thought that, at higher pressures, the grinding belt bends closer across the whole elliptical saddle surface (fig. 4.4) and is able to make better contact with the saddle, resulting in more consistent grinding results.
However, the variations between the samples are also partly caused by the abrasive grits on the grinding belt which differ in grit size, shape, distribution and orientation [1]. Mezghani et al. [6] stated that this geometrical diversity of the cutting grit results in deviations of the cutting rate and the quality of the obtained surface under identical process conditions within the same batch. Therefore, the sample variations are only partly influenced by the machine parameters.
The achieved magnitude of the horizontal surface roughness R_a is according to the applied ANOVA (table 5.2) a bit more affected by the factor time t than by the factor pressure p since the F value evaluated for t is with 29.595 higher than the F value for p, which is 10.864.

The short saddle radius $r = 28.00$ mm according to the requirements was also not achieved. At all experimental settings, the resulting radius was much smaller, as shown in figure 5.8. During the preliminary tests, it was observed that it is necessary to increase the distance between subsequent elements in the element holder in order to achieve stable grinding results since at a too narrow distance, not all elements are able to

make contact with the grinding belt due to saddle height differences of the elements and inaccuracies in the positioning of the elements in the holder. However, although the elements saddles are still positioned on a radius of 28.00 mm in the holder, this increase in distance between the element saddles, which was specified to 3.48 mm, already decreases the achievable saddle radius. The reason for this is, as illustrated in figure 4.27, that the grinding belt lying between two elements takes the shortest path and therefore forms a slightly different radius across the saddle surface. Apparently, with increasing pressure p, so increasing tension force in the grinding belt, this effect is intensified. In figure 5.8, it can be seen that the highest achieved short saddle radius is $r = 21.33$ mm $\pm$ 0.41 mm at $p = 1$ bar and the lowest is $r = 12.99$ mm $\pm$ 0.18 mm at $p = 2.5$ bar. The factor time t has apparently only a small effect on the size of the SSR and it is decreased only a little bit with increasing grinding time t. This can be seen in figure 5.8 where the curves of the three different grinding times lie closely together, and it is actually not possible to clearly distinguish the curves since the corresponding error bars are overlapping. This is also confirmed by the ANOVA which reveals that only the factor pressure p shows a significant contribution to affect the SSR. The average differences between all evaluated SSR from the duplication experiments are $\Delta r = 1.58$ mm, however, inaccuracies in the estimation of the SSR might also play a role there, since the SSR is evaluated by trying to fit a circle to the measured surface y-profile in the Bruker Vision64 program.

Polynomial and exponential functions were fitted to the data in order to be able to estimate the surface roughness R_a and the short saddle radius r of the element saddle in dependency of the machine parameters p and t, and eventually find feasible machine settings achieving the desired grinding result. This empirical approach is used at this stage of process research since the complicated grinding mechanism is still not fully understood due to the randomness of abrasive grains' cutting behaviour [12]. The obtained contour plots of fitted polynomial and exponential functions, shown in figures 5.13 and 5.17, respectively, are convenient to find the machine settings corresponding to a certain combination of surface roughness R_a and short saddle radius r. Both contour plots basically show that when a surface roughness close to the requirements is wanted to be achieved, a long grinding time t and high pressure p have to be used in the machine. However, when a bigger SSR near the desired SSR of 28.00 mm is wanted to be achieved, the used pressure p has to be low and the grinding time t does not have much effect. Therefore, a trade-off has to be made between the surface roughness R_a and the short saddle radius r in order to be able to choose feasible corresponding machine parameters.
Within the experimental factor range, the accuracies of the polynomial and exponential fits are similar since the corresponding RMSEs do not differ much. However, the question is which of the two fits estimates the true grinding mechanism the best, and furthermore, which of the two fits might be feasible slightly beyond the factor range of the experiments in order to predict the grinding result and prevent additional time consuming machine tests and measurement work.
During grinding, the grinding belt slides across the surface of the element saddles and the grains which are attached to the belt backing, interact with the surface and remove material. In this abrasion process, the surface roughness becomes smoother dependent on the belt's grain size. With increasing grinding time, the grains sharpness reduces or the grains break away. When the grinding belt is worn out, the material removal stops and the belt just slides across the surface and does not change the surface roughness any more. So, the surface roughness continuously decreases during this process, and there is no reason to think that it would increase again at a certain point.
In figure 5.10, for example, it can be seen that towards the end of the range of the factor time t in the polynomial fit, the roughness R_a increases again, which is opposed to expected trend that the roughness should at least slightly further decrease.

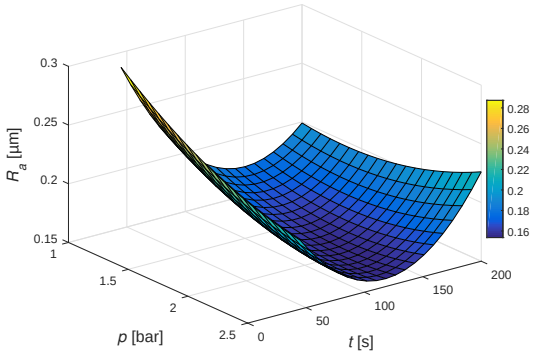

Figure 6.1: Polynomial fit: Horizontal R_a vs. time and pressure

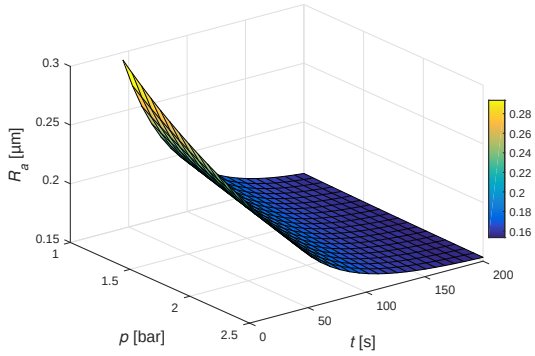

Figure 6.2: Exponential fit: Horizontal R_a vs. time and pressure

Figures 6.1, 6.3 and 6.5 show the polynomial fit for R_a, r and the combined contour plot, respectively, plotted until $t = 200$ s, so beyond the experimental factor range. It can be clearly observed that R_a increases very much with increasing time t which is definitely not an adequate trend, and the slope of the short saddle radius r also drops more with increasing t than would be expected. Considering the graphs in figures 6.2, 6.4 and 6.6 of the exponential fit for R_a, r and the combined contour plot, respectively, it can be seen that R_a and r follow more closely the expected trend and, therefore, it is chosen to use the fitted exponential functions for estimating the grinding result in dependency of the machine settings.

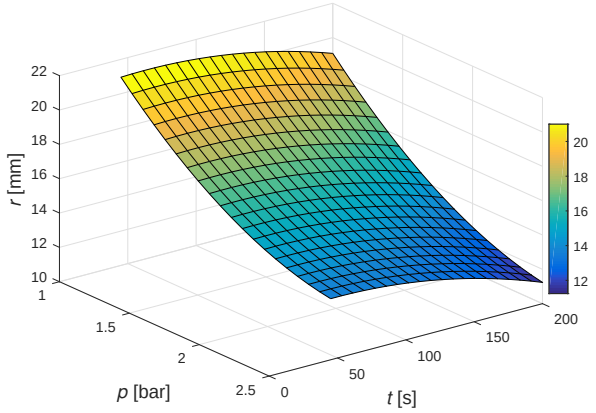

Figure 6.3: Polynomial fit: SSR vs. time and pressure

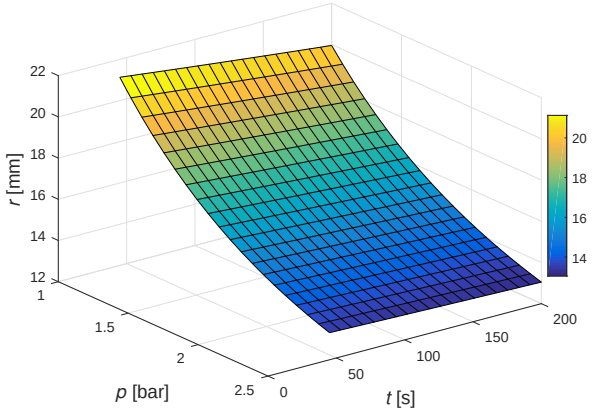

Figure 6.4: Exponential fit: SSR vs. time and pressure

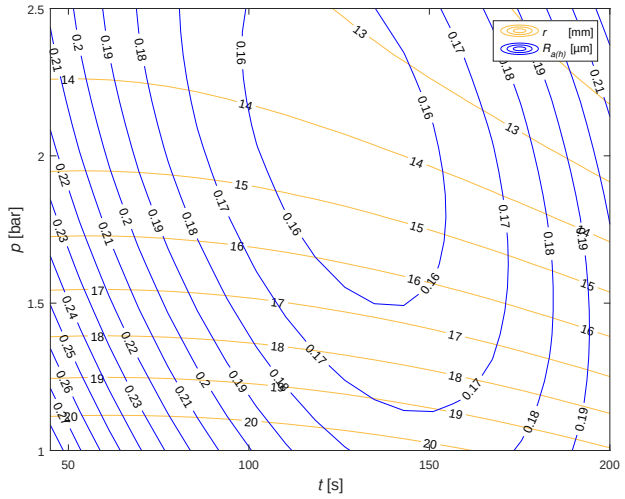

Figure 6.5: Polynomial fit: Time vs. pressure contour plot for horizontal R_a and SSR

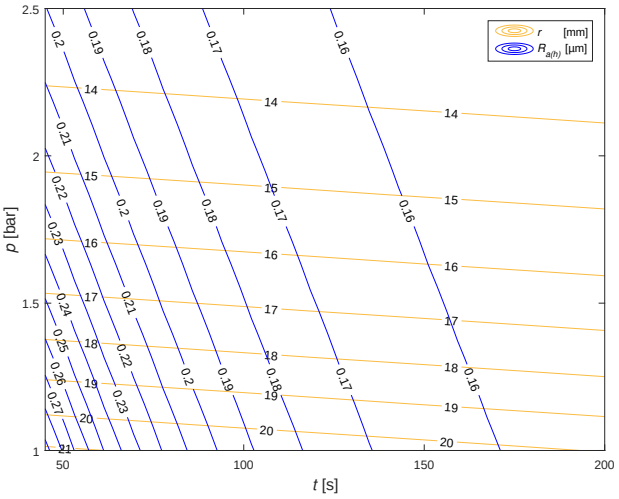

Figure 6.6: Exponential fit: Time vs. pressure contour plot for horizontal R_a and SSR

In order to find feasible machine settings where a grinding result at least close to the requirements can be achieved, the pressure p must be chosen low for a relatively large short saddle radius r, and a long grinding time t has to be chosen for a relatively low surface roughness R_a. Before choosing the machine settings which will be considered for producing prototype elements which will be used in pushbelt tests in order to test the friction improvement which is achieved from this grinding process, the grinding results from the experiments were again closely visually examined. It was found that at 1 bar pressure, the edge of the saddle is not sufficiently ground even at long grinding times, as shown in figure 6.7, which was not noticed in the evaluation of R_a since it was not measured close at the edge. It is thought that at $p = 1$ bar, the grinding belt apparently still has too small tension force in order to bend properly across the short saddle radius in order to sufficiently grind the surface. Therefore, the p setting for the machine has to be definitely higher than 1 bar which reduces the possible achievable short saddle radius r. Furthermore, at pressures of p =1.75 bar and p =2.5 bar in combination with longer grinding times, a kind of hump is observed, which is forming close to the inner edge of the saddles as can be seen in figure 6.8. The belt has a little bit horizontal play and at too high pressures, the material removal is increased, especially at long grinding times, and it is assumed that at a certain moment, the grinding belt just continues grinding in the most outer position causing these

humps at the inner side of the saddles.

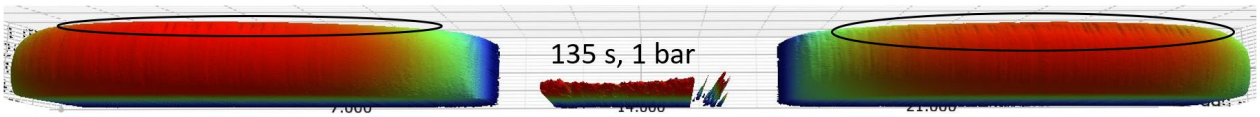

Figure 6.7: Insufficiently grinded saddle edge at $p = 1$ bar

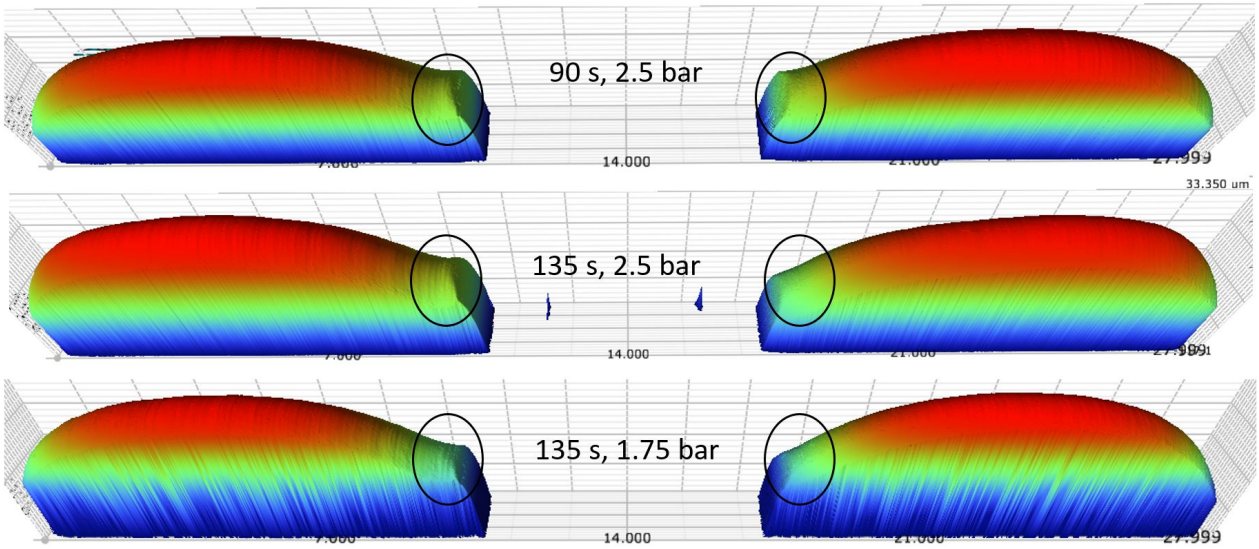

Figure 6.8: Examples of hump-forming on the saddle

It was decided to test whether the prediction of the empirical exponential model is indeed better than the prediction of the polynomial model by performing two validation experiments. Furthermore, at the same time, these experiments should also be used to finally find machine settings which could be used for producing prototype elements for pushbelt efficiency tests. The number of validation experiments was limited since only P600 grinding belts for two more experiments were still available. According to the exponential model, pressures below 0.5 bar and according to the polynomial model even lower pressures are required in order to achieve a short saddle radius of $r = 28.00$ mm, as can be seen in figures F.1 and F.2 in appendix F. However, pressures around 1 bar or below are not feasible as explained above. Therefore, the pressure setting was chosen to be p=1.3 bar for both validation experiments, so a little bit higher than 1 bar, but not too high in order to prevent hump forming and to not reduce the SSR too much in order to possibly achieve a SSR around 18 mm.
According to the exponential model, at $p = 1.3$ bar, a grinding time $t = 350$ s is required in order to obtain the lowest achievable horizontal roughness of 0.152 µm. The corresponding SSR according to the exponential model is r =16.91 mm which is considered as too low. Furthermore, such a long grinding time is expected to result in too much material removal and to distort the long saddle radius (LSR).
It was decided to execute one experiment within the experimental time factor range where the models are based on, and one beyond. The first validation experiment is chosen to be performed at $t = 120$ s in order to achieve at least an SSR of above 18 mm (fig. 6.6), however the expected surface roughness would be lower. In the second validation experiment, a trade-off has been made between r and R_a, and it was decided to accept a slightly lower short saddle radius r for a lower surface roughness R_a. Therefore, the second validation experiment was chosen to be performed at t =180 s in order to possibly achieve a surface roughness at least close to the requirements.

After each validation experiment, the two saddles of one sample element from the middle of the holder, element nine (fig. 4.17) were scanned with the white light interferometer and subsequently analyzed with the Bruker Vision64 program, which is illustrated for the element of the first validation experiment in appendix E. The results of the first validation experiment using the setting $p = 1.3$ bar and $t = 120$ s are shown in table 6.1 together with the predicted results from the exponential and polynomial models. The errors margins indicated next the predicted values in the table are estimated from the obtained standard errors of the mean ($\hat{e}$) within the experiments. However, the error margins indicated next to the validation experiment results are the errors within this experiment, so between left and right saddle of element nine. Comparing the results,

it can be seen that the prediction of both models is very good for the horizontal R_a and the short saddle radius r considering the error margins. The prediction of the vertical R_a deviates strongly in both models from the validation experiment result as expected, since the measurement of the vertical R_a was considered as less reliable, as explained in section 4.2.2.
Applying the machine setting $p = 1.3$ bar and $t = 180$ s results in the prediction and validation experiment results, as shown in table 6.2. It can be seen that the prediction of the exponential model beyond the experimental factor range is indeed closer to the measurement values than the polynomial model. The exponential model predicts the short saddle radius r very good and the predicted horizontal R_a is also very close to the obtained value in the validation experiment.

Table 6.1: Results of predictions and validation experiment at $t = 120$ s and $p = 1.3$ bar

	Horizontal R_a [µm]	**Vertical R_a [µm]**	**r [mm]**
Polynomial model	0.170 ± 0.010	0.178 ± 0.010	18.25 ± 0.35
Exponential model	0.173 ± 0.010	0.184 ± 0.010	18.11 ± 0.35
Validation experiment	0.171 ± 0.011	0.118 ± 0.004	18.15 ± 0.06

Table 6.2: Results of predictions and validation experiment at $t = 180$ s and $p = 1.3$ bar

	Horizontal R_a [µm]	**Vertical R_a [µm]**	**r [mm]**
Polynomial model	0.177 ± 0.007	0.214 ± 0.010	17.15 ± 0.35
Exponential model	0.157 ± 0.007	0.152 ± 0.010	17.77 ± 0.35
Validation experiment	0.149 ± 0.005	0.139 ± 0.044	17.68 ± 0.34

The horizontal R_a value achieved in the validation experiment is lower than in the prediction and would even meet the requirement for the R_a, however, the error margin of the measured element indicates that one saddle is higher and one saddle is lower than the R_a according to the requirements.
Comparing this error margin of one single element to the error margins from the full factorial experiments (fig. 5.4), which were derived from six whole elements, it can be observed that a relatively large proportion of the variations between the samples apparently originates from differences between the left and right saddle. Partly, this variations are assumed to come from variations in the texture of the used grinding belts, however, the deviations might also originate from other effects from the machine, for example, due to different slip of the left and right belts at the driving axle which implies that one belt would perform more revolutions than the other.

The results from the experiments and predictions show that it is not possible to produce elements which meet the requirements with the machine in the current configuration. However, the machine settings of the second validation experiment, using $t = 180$ s and $p = 1.3$ bar, at least lead to an horizontal R_a close to the requirements and are considered to be used in order to produce prototype elements for pushbelt efficiency test. It is unknown how disadvantageous this around 10 mm smaller radius than specified in the requirements is for the obtained efficiency, and the efficiency of the pushbelt might still be improved using these ground elements.

7. Conclusion and recommendations

7.1 Conclusion

The purpose of this research was to investigate the relationship between applied grinding process parameters and achieved curvature and roughness of the pushbelt element saddle surface.
The saddle of the elements should be adjusted with the aid of a newly developed grinding machine such that the friction in the element-ring contact of the operating pushbelt is reduced in order to increase the efficiency of the pushbelt. The specified requirements are that the saddle surface roughness R_a measured across the saddle's x-profile (fig. 4.2), also called horizontal R_a, has to be reduced to $R_a = 0.150$ µm or preferably lower, and a short saddle radius (SSR) r = 28.00 mm (fig. 2.2) should be created.
After preliminary grinding tests with the machine, it was chosen to use a P600 grinding belt at a constant speed of 40 belt revolutions per minute in the final experimental design. Furthermore, the distance between the element saddles in the element holder in the machine was specified to 3.48 mm, since at smaller distances no stable grinding result could be achieved. The measurement data obtained from the performed experiments with the grinding machine, was used to analyze the response variables R_a and r dependent on the factors grinding time t and pressure p of the machine's pneumatic cylinder which generates the tension force in the grinding belt. The goal of the data analysis was to examine the relation between the involved process variables and eventually find feasible process conditions in order to achieve the required grinding result.

It was found that the size of the created SSR is mainly affected by the applied pressure p during grinding. The achievable SSR decreases with increasing pressure p, and an increasing grinding time t only causes relatively small reductions of the size of the SSR. The obtained SSR was consistently smaller than the required 28.00 mm within the experimental factor range with grinding times between 45 s and 135 s and pressures between 1.0 bar and 2.5 bar. Although the element saddles lie on a radius of 28.00 mm in the element holder, the resultant radius across the saddle surface after grinding is apparently smaller. The reason for this is that due to the spacing of the elements in the holder, the grinding belt which is lying across the saddles, takes the shortest path between two subsequent saddles (fig. 4.27) and, therefore, forms a smaller radius across each single element saddle. This effect is apparently intensified with increasing pressure p since the grinding belt lies tighter across the saddle surface, which leads to the relatively small achieved size of the SSR during the experiments.

The required horizontal R_a of 0.150 µm or lower was also not achieved within the experimental factor range. It was found that the horizontal surface roughness R_a is affected by both, the grinding time t and the pressure p, but the grinding time is dominating factor for lowering the roughness. Furthermore, it was observed that an increasing pressure p reduces the variation of achieved R_a values between the sample elements. At higher pressures p, the grinding belt is attached more tight to the saddle surface, which apparently leads to a more consistent grinding result. However, variations between left and right saddles might come from deviations in the texture of the used grinding belts or from possibly differing slip of the grinding belts at the driving axle, which would cause a slightly different amount of grinding revolutions for the left and the right saddle.

In order to be able to estimate machine parameters corresponding to the response variables, an empirical model was created by fitting the experimental data to exponential and also polynomial functions. Both obtained empirical models (5.13, 5.17) show that, in order to achieve a surface roughness R_a and a short saddle radius r approaching the requirements, the grinding time t and the pressure p have be relatively high to obtain the desired R_a, however, the pressure p has to be relatively low to achieve the desired r, which is contradicting and implies that a trade-off has to be made between R_a and r in order to achieve a grinding result as close as possible to the requirements.

Within the experimental data range, the accuracy of the exponential and polynomial models was found to be similar, however beyond that range, the exponential model was considered to represent the actual trends of the response variables better than the polynomial model.
Therefore, the exponential model was used in order to predict the machine parameters corresponding to the required horizontal surface roughness R_a and SSR. The predicted machine parameters are $t = 390$ s and $p = 0.19$ bar, however, the horizontal roughness R_a in the prediction is with 0.152 ± 0.007 µm slightly higher than the desired 0.150 µm. The reason for this is that the exponential model reaches a plateau at this point and the R_a does not significantly decrease from this predicted point on. Nonetheless, the predicted parame-

ters are unfortunately not feasible since the pressure is much too low in order to obtain stable grinding results because the grinding belt is not able to bend sufficiently across the saddle at this low pressure. Therefore, the achievable surface roughness R_a is, considering the estimated error margin, fluctuating around the desired value and the desired size of the SSR can not be achieved with the grinding machine in this configuration.
A feasible machine setting was determined to be $p = 1.3$ bar and $t = 180$ s, which should give, according to the exponential model, a horizontal $R_a = 0.157$ µm $\pm$ 0.007 µm and a short saddle radius $r = 17.77$ mm $\pm$ 0.35 mm. The grinding result of the measured sample element from the validation experiment at the same settings is close to the prediction and has a horizontal $R_a = 0.149$ µm $\pm$ 0.005 µm and a short saddle radius $r = 17.68$ mm $\pm$ 0.34 mm.
Although, the requirements are not fully met, the found machine settings $p = 1.3$ bar and $t = 180$ s are considered to be used for producing prototype elements for pushbelt tests in order to examine the effect of the achieved element saddle adjustments on the efficiency of the pushbelt.

7.2 Recommendations

In order to be able to achieve a SSR according to the requirements, it is recommended to scale up the diameter of the element holder such that the element saddles lie on a larger radius since the current radius of 28 mm is apparently too small to achieve a radius of 28 mm across the element saddle surface.
Additionally, it is recommended to consider using another type of grinding belt with smaller grit size in order to achieve the desired surface roughness according to the requirements. Even more adequate might be the use of so called engineered grinding belts which contain structured abrasives with a controlled shape, size distribution and orientation of the abrasive grains [1], which would decrease variations and improve the predictability of the grinding result.

References

[1] Andres L. Carrano and James B. Taylor. Geometric Modeling of Engineered Abrasive Processes. *Journal of Manufacturing Processes*, 7(1):17–27, 2005.

[2] Dong Chen, Joanna Schmit, and Matt Novak. Real-time scanner error correction in white light interferometry. In *Optical Metrology and Inspection for Industrial Applications III*, volume 9276, page 92760I. International Society for Optics and Photonics, 2014.

[3] Van Doorne's Transmissie and V / Bosch Group. Improving Push Belt CVT Efficiency by Control Strategies Based on New Variator Wear Insight Maaike van der Laan, Mark van Drogen and Arjen Brandsma. Technical report, 2004.

[4] Francis van der Sluis, Erik van der Noll, and Hendrik de Leeuw. Key Technologies of the Pushbelt CVT. *International Journal of Automotive Engineering*, 4(1):1–8, 2013.

[5] E.S. Gadelmawla, M.M. Koura, T.M.A. Maksoud, I.M. Elewa, and H.H. Soliman. Roughness parameters. *Journal of Materials Processing Technology*, 123(1):133–145, apr 2002.

[6] S. Mezghani and M. El Mansori. Abrasiveness properties assessment of coated abrasives for precision belt grinding. *Surface and Coatings Technology*, 203(5-7):786–789, dec 2008.

[7] Douglas C Montgomery and George C Runger. *Applied statistics and probability for engineers*. John Wiley & Sons, 2011.

[8] RK Roy. *A primer on the Taguchi method*. 2010.

[9] Nilabh Srivastava and Imtiaz Haque. A review on belt and chain continuously variable transmissions (CVT): Dynamics and control. *Mechanism and Machine Theory*, 44(1):19–41, jan 2009.

[10] F. Van der Sluis, T. Van Dongen, G. J. Van Spijk, A. Van der Velde, and A. Van Heeswijk. Fuel consumption potential of the pushbelt CVT. *Proceedings of FISITA 2006 World Automotive Congress*, pages 1–12, 2006.

[11] Francis van der Sluis, Tom van Dongen, Gert-Jan van Spijk, Arie Van der velde, and Ad van Heeswijk. Efficiency Optimization of the Pushbelt CVT. *SAE Technical Paper*, 2007.

[12] Wenxi Wang, Ferdinando Salvatore, Joël Rech, and Jianyong Li. Comprehensive investigation on mechanisms of dry belt grinding on AISI52100 hardened steel. *Tribology International*, 121:310–320, may 2018.

[13] C. Zhu, H. Liu, J. Tian, Q. Xiao, and X. Du. Experimental investigation on the efficiency of the pulley-drive CVT. *International Journal of Automotive Technology*, 11(2):257–261, apr 2010.

A. Reference elements

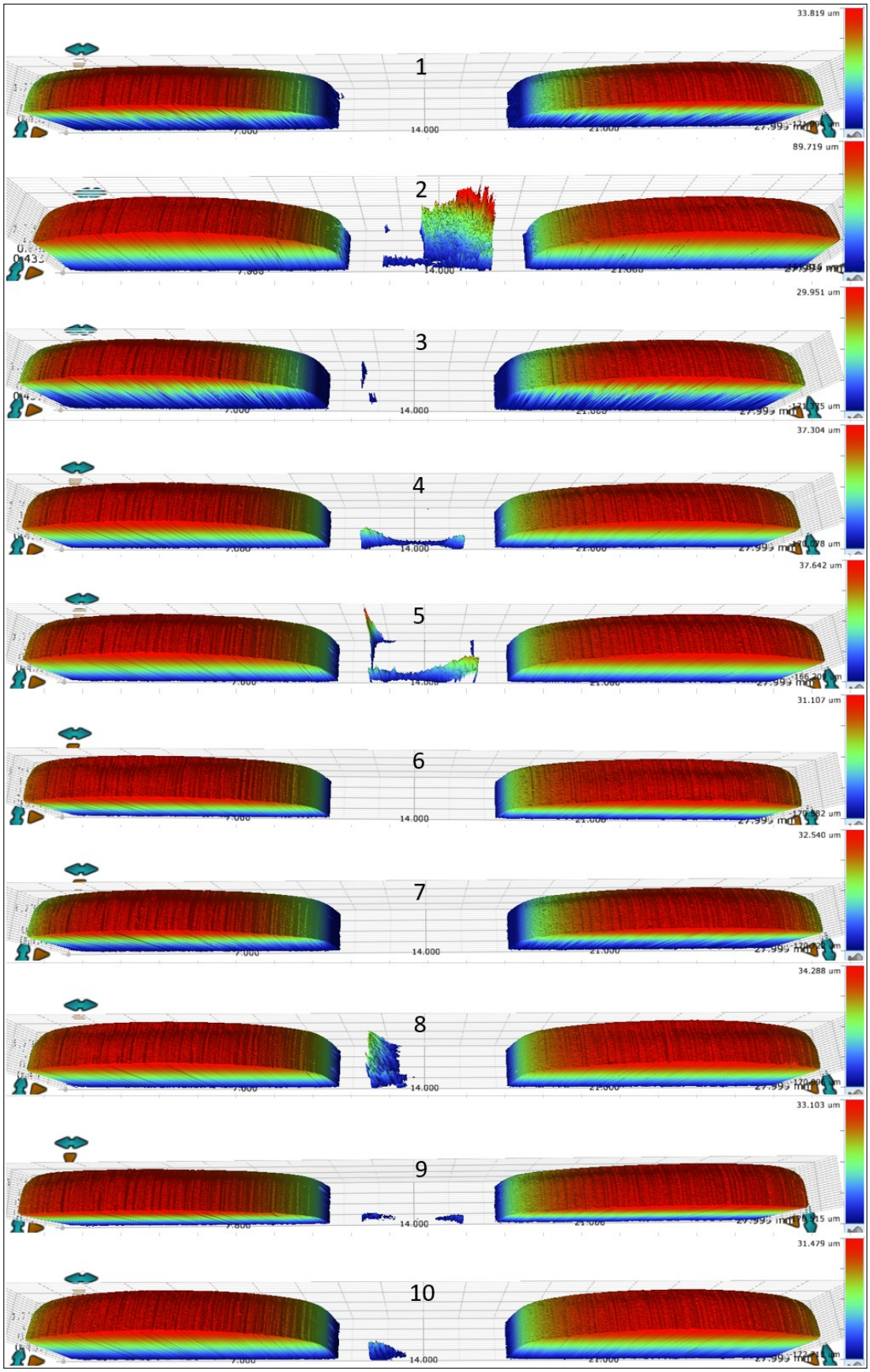

Figure A.1: White light interferometer scans of ten reference elements

B. Reference element analysis

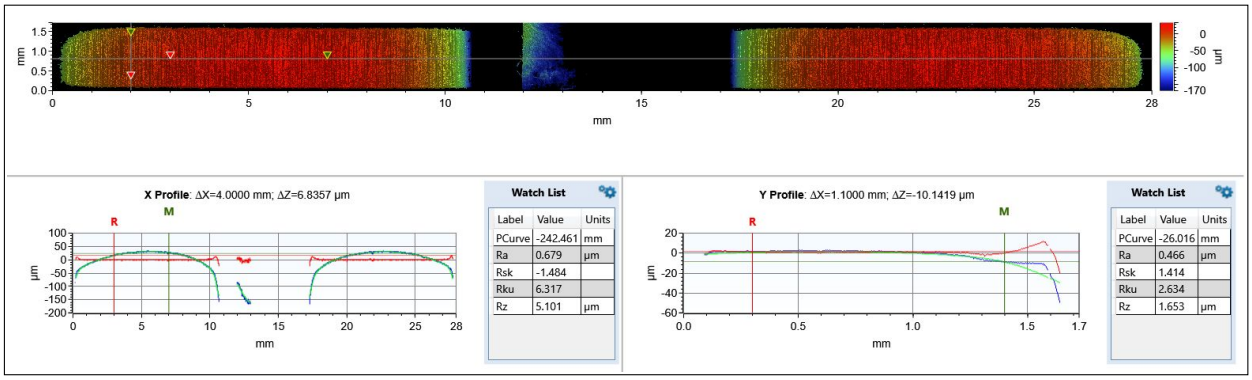

Figure B.1: Analysis position 1 on reference element

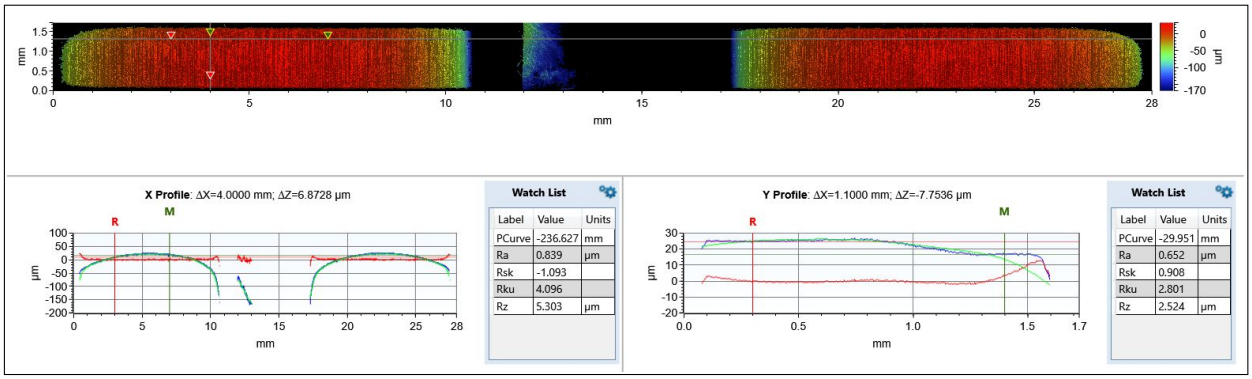

Figure B.2: Analysis position 2 on reference element

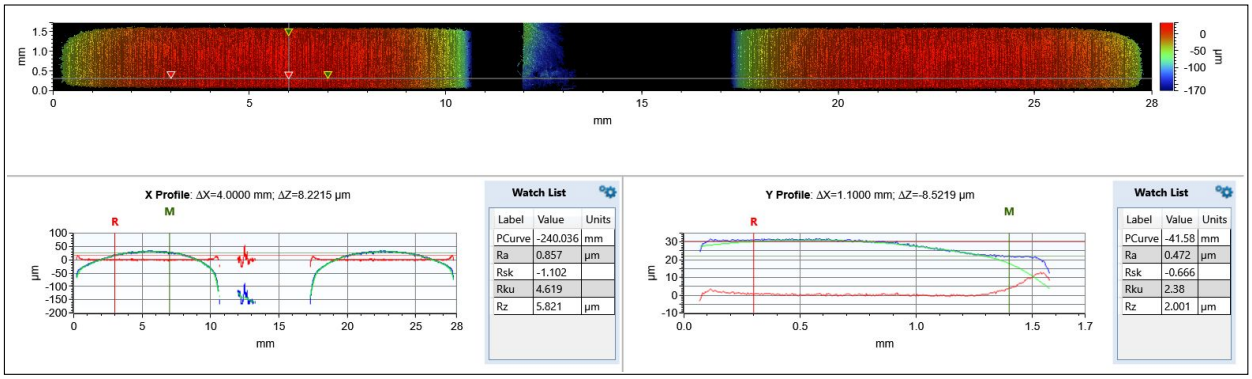

Figure B.3: Analysis position 3 on reference element

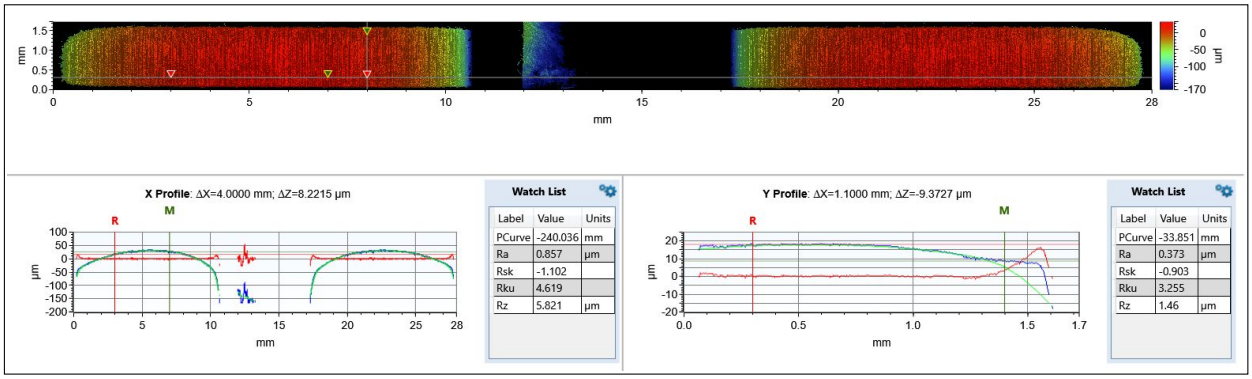

Figure B.4: Analysis position 4 on reference element

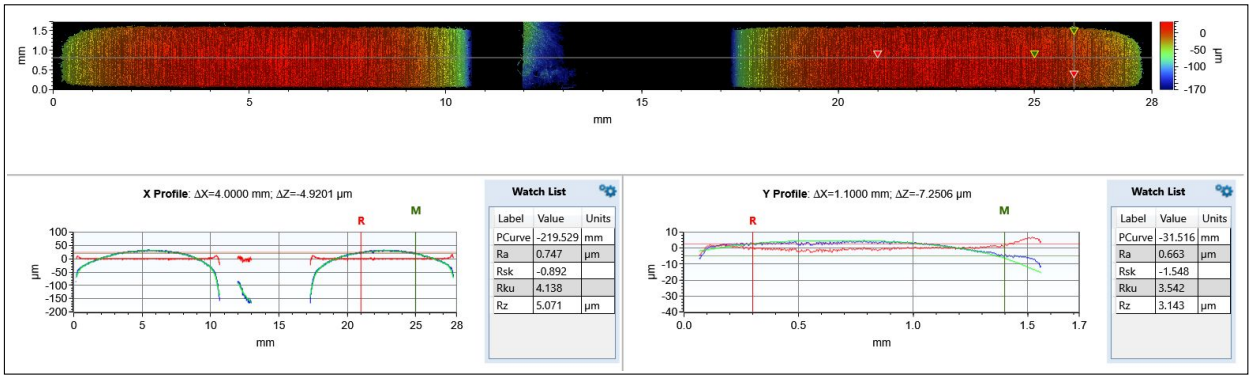

Figure B.5: Analysis position 5 on reference element

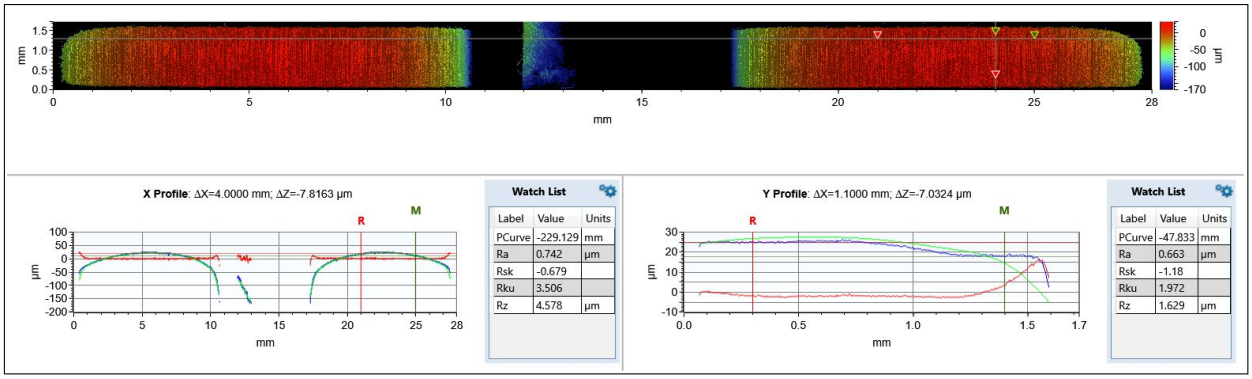

Figure B.6: Analysis position 6 on reference element

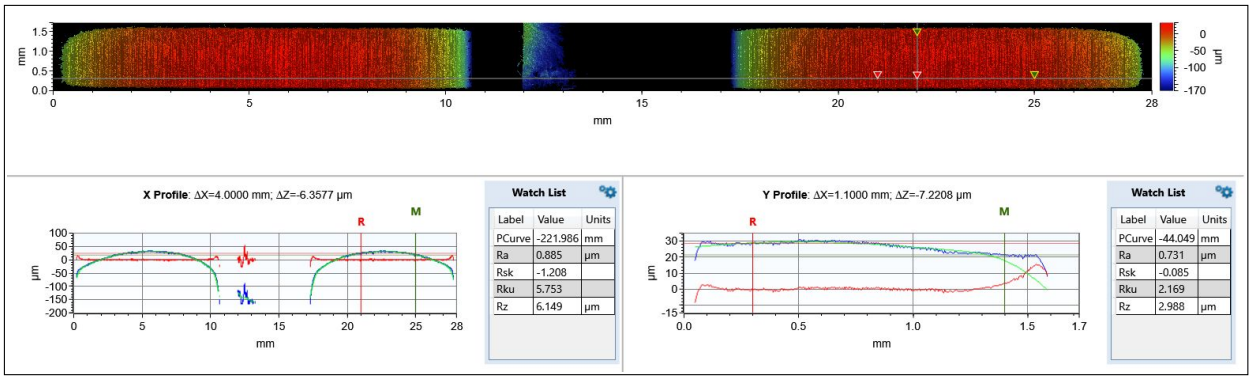

Figure B.7: Analysis position 7 on reference element

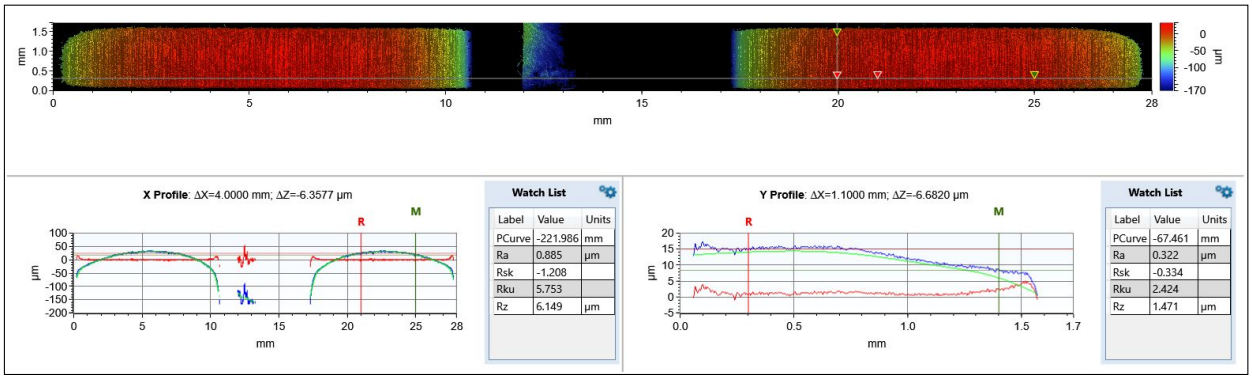

Figure B.8: Analysis position 8 on reference element

C. Full factorial experimental design

Table C.1: Measurement data of 18 experiments in random order

Run	Std.		Factors			Ra (h) [µm]		Ra (v) [µm]		SSR [mm]	
Order	Order	Block	t [s]	p [bar]	Element	Left	Right	Left	Right	Left	Right
1	1	1	45	1.00	7	0.400	0.306	0.278	0.300	14.161	16.127
1	1	1	45	1.00	8	0.307	0.247	0.243	0.278	20.034	24.523
1	1	1	45	1.00	9	0.208	0.198	0.161	0.235	23.216	21.386
2	4	1	90	1.00	7	0.212	0.181	0.226	0.269	20.103	22.020
2	4	1	90	1.00	8	0.215	0.123	0.228	0.209	23.765	20.461
2	4	1	90	1.00	9	0.204	0.150	0.201	0.202	20.389	21.717
3	2	1	45	1.75	7	0.346	0.203	0.395	0.173	17.758	15.915
3	2	1	45	1.75	8	0.244	0.217	0.148	0.320	16.019	18.786
3	2	1	45	1.75	9	0.242	0.210	0.215	0.178	16.452	15.962
4	7	1	135	1.00	7	0.175	0.189	0.212	0.258	19.981	20.488
4	7	1	135	1.00	8	0.191	0.165	0.270	0.208	22.105	21.073
4	7	1	135	1.00	9	0.177	0.171	0.175	0.201	20.972	21.649
5	3	1	45	2.50	7	0.197	0.185	0.155	0.147	12.035	11.564
5	3	1	45	2.50	8	0.206	0.194	0.229	0.195	14.292	15.082
5	3	1	45	2.50	9	0.257	0.198	0.168	0.151	17.247	11.431
6	9	1	135	2.50	7	0.177	0.121	0.126	0.151	13.922	12.344
6	9	1	135	2.50	8	0.174	0.130	0.137	0.110	12.735	13.513
6	9	1	135	2.50	9	0.169	0.122	0.099	0.117	12.183	12.819
7	8	1	135	1.75	7	0.199	0.166	0.138	0.209	16.845	16.071
7	8	1	135	1.75	8	0.184	0.136	0.136	0.163	14.778	16.443
7	8	1	135	1.75	9	0.180	0.139	0.126	0.105	15.936	13.703
8	5	1	90	1.75	7	0.226	0.163	0.109	0.194	16.769	16.633
8	5	1	90	1.75	8	0.183	0.157	0.140	0.163	14.895	16.108
8	5	1	90	1.75	9	0.188	0.160	0.126	0.156	15.279	16.165
9	6	1	90	2.50	7	0.167	0.150	0.113	0.142	13.002	13.611
9	6	1	90	2.50	8	0.167	0.152	0.190	0.172	13.007	12.794
9	6	1	90	2.50	9	0.160	0.148	0.169	0.149	12.973	12.986
10	11	2	45	1.75	7	0.320	0.179	0.304	0.233	16.546	15.885
10	11	2	45	1.75	8	0.210	0.183	0.228	0.194	15.388	15.502
10	11	2	45	1.75	9	0.208	0.177	0.134	0.138	14.188	15.502
11	17	2	135	1.75	7	0.160	0.137	0.113	0.135	14.663	16.168
11	17	2	135	1.75	8	0.145	0.122	0.098	0.129	14.432	14.077
11	17	2	135	1.75	9	0.155	0.120	0.159	0.135	14.303	14.971
12	14	2	90	1.75	7	0.168	0.171	0.113	0.147	15.300	13.229
12	14	2	90	1.75	8	0.176	0.278	0.119	0.239	16.146	15.146
12	14	2	90	1.75	9	0.167	0.163	0.126	0.105	15.690	15.406
13	16	2	135	1.00	7	0.205	0.153	0.207	0.229	20.105	19.493
13	16	2	135	1.00	8	0.200	0.242	0.191	0.287	19.276	16.912
13	16	2	135	1.00	9	0.171	0.163	0.157	0.212	20.845	21.318
14	18	2	135	2.50	7	0.160	0.161	0.162	0.117	13.499	13.497
14	18	2	135	2.50	8	0.160	0.165	0.131	0.146	12.620	12.863
14	18	2	135	2.50	9	0.157	0.165	0.084	0.104	13.784	12.149
15	12	2	45	2.50	7	0.213	0.199	0.137	0.167	13.858	14.322
15	12	2	45	2.50	8	0.223	0.200	0.152	0.145	12.338	13.457
15	12	2	45	2.50	9	0.212	0.194	0.129	0.130	14.110	13.166
16	10	2	45	1.00	7	0.388	0.216	0.272	0.240	17.431	19.830
16	10	2	45	1.00	8	0.277	0.532	0.299	0.349	22.390	22.782
16	10	2	45	1.00	9	0.261	0.215	0.179	0.144	24.290	21.966
17	15	2	90	2.50	7	0.186	0.183	0.149	0.092	14.663	11.854
17	15	2	90	2.50	8	0.178	0.189	0.125	0.144	12.754	15.514
17	15	2	90	2.50	9	0.179	0.191	0.143	0.146	13.542	11.737
18	13	2	90	1.00	7	0.328	0.164	0.174	0.217	21.415	19.572
18	13	2	90	1.00	8	0.210	0.188	0.213	0.270	20.126	22.109
18	13	2	90	1.00	9	0.216	0.164	0.191	0.148	23.919	20.393

D. Two-sample t-test

Table D.1: Two-sample t-test for horizontal R_a of first and replicated experiment

Trial setting		μ_1	μ_2	Hyp.	P-Value	95% CI limits		T-Stat.	DoF	StDev
t [s]	p [bar]					Lower	Upper			
45	1.00	0.278	0.315	0	0.547	-0.095	0.169	0.624	10	0.103
45	1.75	0.244	0.213	0	0.341	-0.100	0.038	-1.000	10	0.054
45	2.50	0.206	0.207	0	0.936	-0.025	0.026	0.083	10	0.020
90	1.00	0.181	0.212	0	0.320	-0.035	0.096	1.047	10	0.051
90	1.75	0.180	0.187	0	0.721	-0.039	0.055	0.367	10	0.036
90	2.50	0.157	0.184	1	0.000	0.018	0.036	6.568	10	0.007
135	1.00	0.178	0.189	0	0.466	-0.021	0.042	0.758	10	0.024
135	1.75	0.167	0.140	0	0.052	-0.055	0.000	-2.209	10	0.021
135	2.50	0.149	0.161	0	0.292	-0.012	0.037	1.113	10	0.019

Table D.2: 2-sample t-test for vertical R_a of first and replicated experiment

Trial setting		μ_1	μ_2	Hyp.	P-Value	95% CI limits		T-Stat.	DoF	StDev
t [s]	p [bar]					Lower	Upper			
45	1.00	0.249	0.247	0	0.958	-0.085	0.081	-0.054	10	0.064
45	1.75	0.238	0.205	0	0.505	-0.139	0.073	-0.692	10	0.083
45	2.50	0.174	0.143	0	0.057	-0.063	0.001	-2.148	10	0.025
90	1.00	0.222	0.202	0	0.334	-0.065	0.024	-1.016	10	0.035
90	1.75	0.148	0.142	0	0.785	-0.060	0.046	-0.280	10	0.041
90	2.50	0.156	0.133	0	0.138	-0.054	0.009	-1.610	10	0.025
135	1.00	0.221	0.214	0	0.772	-0.058	0.045	-0.298	10	0.040
135	1.75	0.146	0.128	0	0.319	-0.056	0.020	-1.048	10	0.029
135	2.50	0.123	0.124	0	0.974	-0.031	0.031	0.034	10	0.024

Table D.3: 2-sample t-test for SSR of first and replicated experiment

Trial setting		μ_1	μ_2	Hyp.	P-Value	95% CI limits		T-Stat.	DoF	StDev
t [s]	p [bar]					Lower	Upper			
45	1.00	19.908	21.448	0	0.443	-2.756	5.837	0.799	10	3.340
45	1.75	16.815	15.502	1	0.047	-2.603	-0.024	-2.269	10	1.003
45	2.50	13.608	13.542	0	0.948	-2.291	2.158	-0.067	10	1.729
90	1.00	21.409	21.255	0	0.862	-2.077	1.771	-0.178	10	1.496
90	1.75	15.975	15.152	0	0.139	-1.960	0.316	-1.609	10	0.885
90	2.50	13.062	13.344	0	0.666	-1.129	1.693	0.445	10	1.097
135	1.00	21.045	19.658	0	0.078	-2.963	0.190	-1.960	10	1.225
135	1.75	15.629	14.769	0	0.161	-2.126	0.405	-1.515	10	0.984
135	2.50	12.919	13.068	0	0.700	-0.689	0.987	0.397	10	0.651

E. Validation experiment

Analysis data of element 9 from validation experiment with the settings p = 1.3 bar and t = 120 s

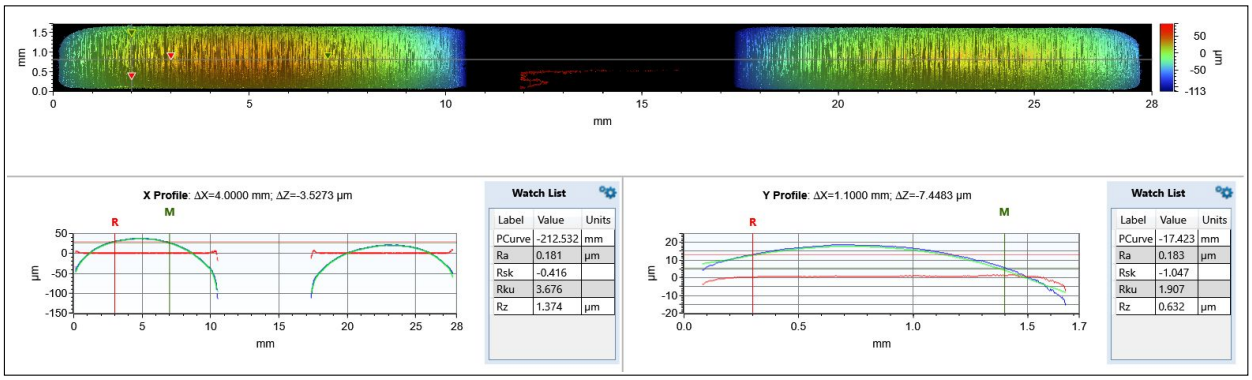

Figure E.1: Analysis position 1 on element 9

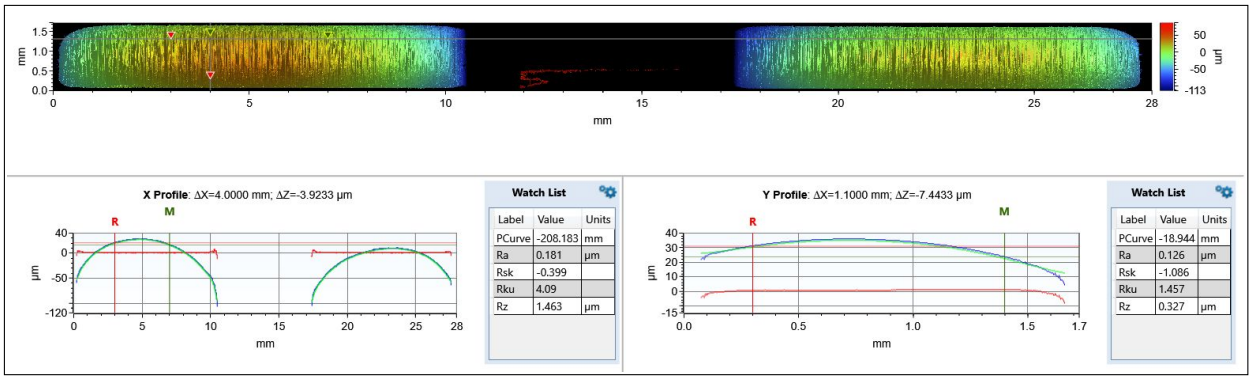

Figure E.2: Analysis position 2 on element 9

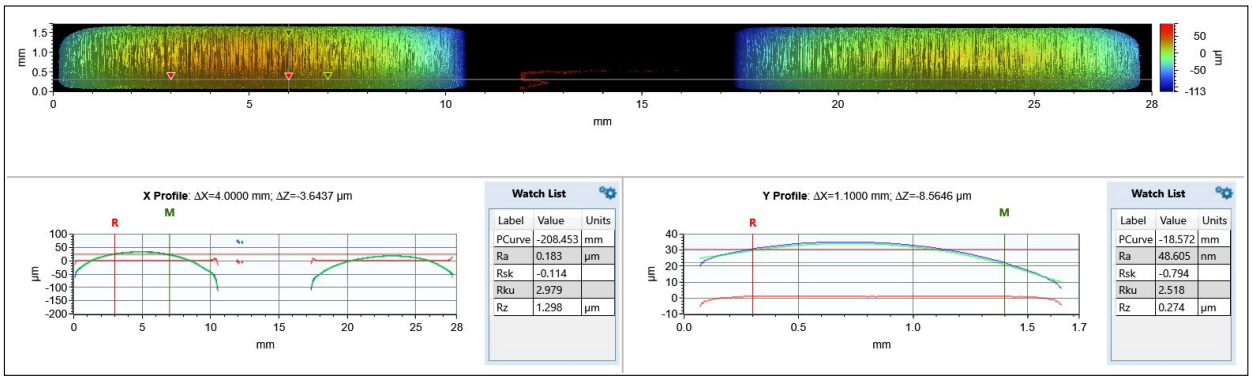

Figure E.3: Analysis position 3 on element 9

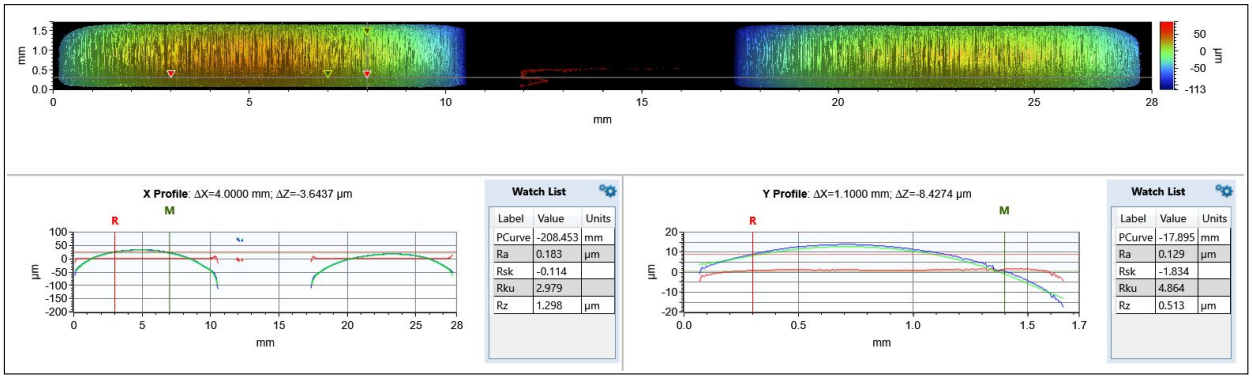

Figure E.4: Analysis position 4 on element 9

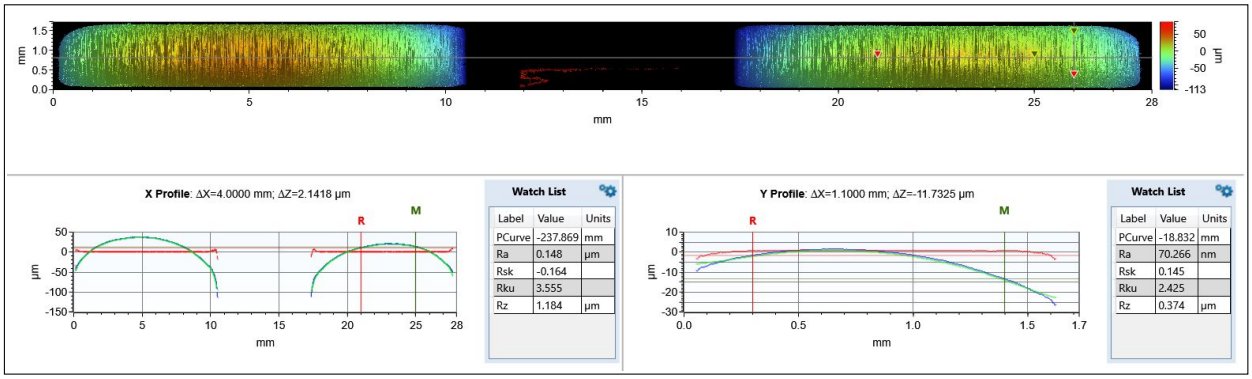

Figure E.5: Analysis position 5 on element 9

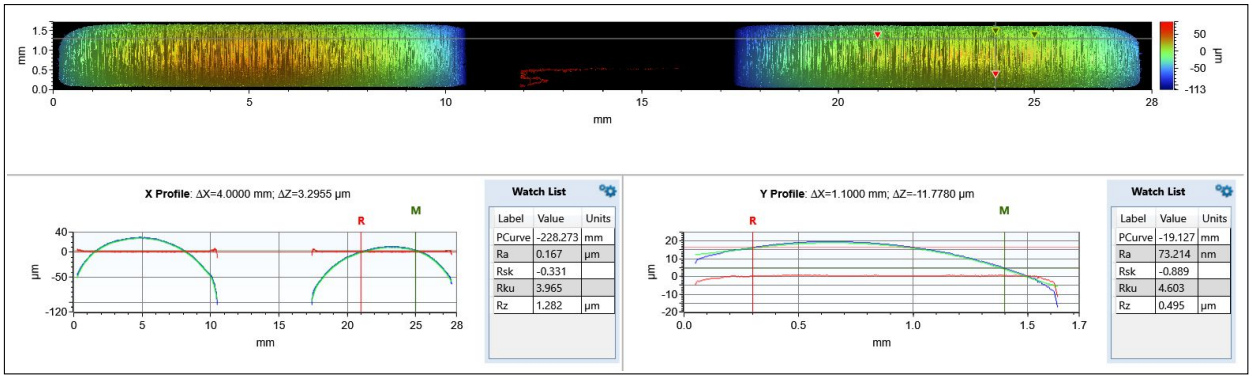

Figure E.6: Analysis position 6 on element 9

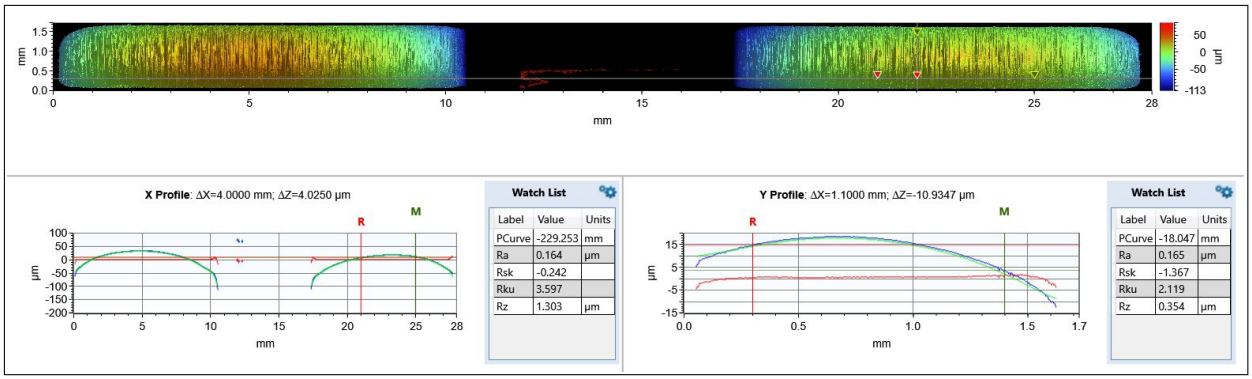

Figure E.7: Analysis position 7 on element 9

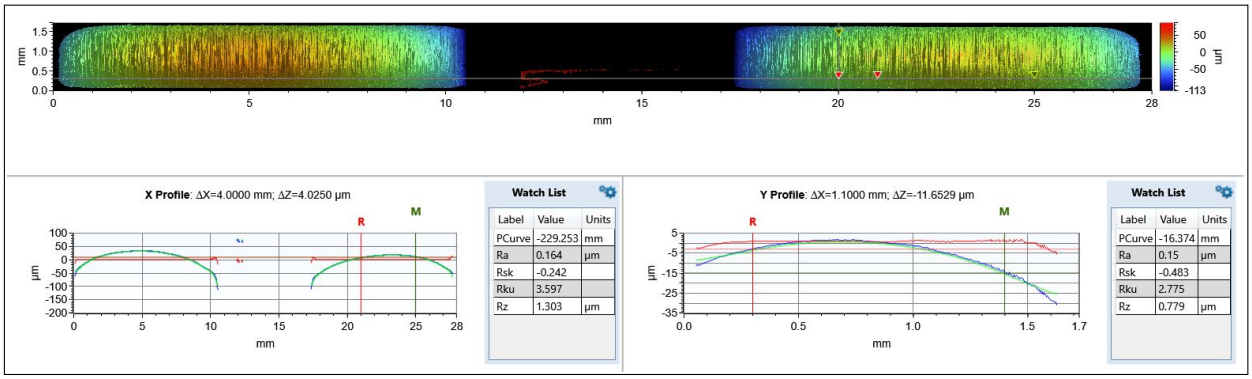

Figure E.8: Analysis position 8 on element 9

F. Contour plots of short saddle radius

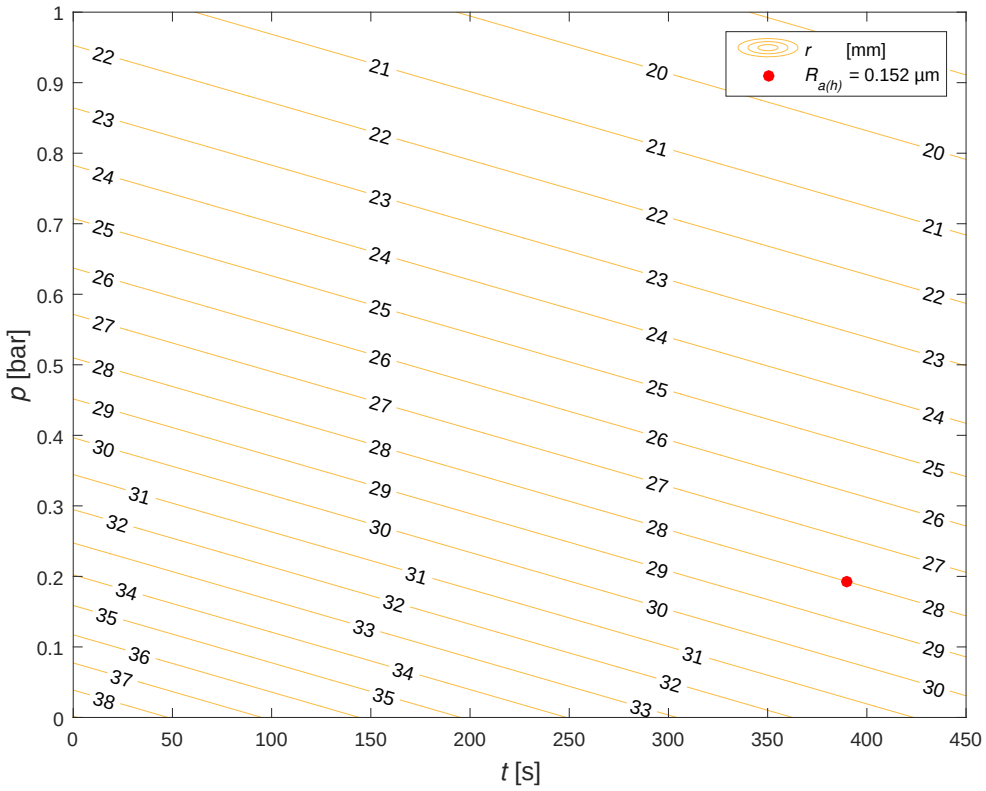

Figure F.1: Contour plot of exponential model for short saddle radius r at pressures below $p = 1$ bar

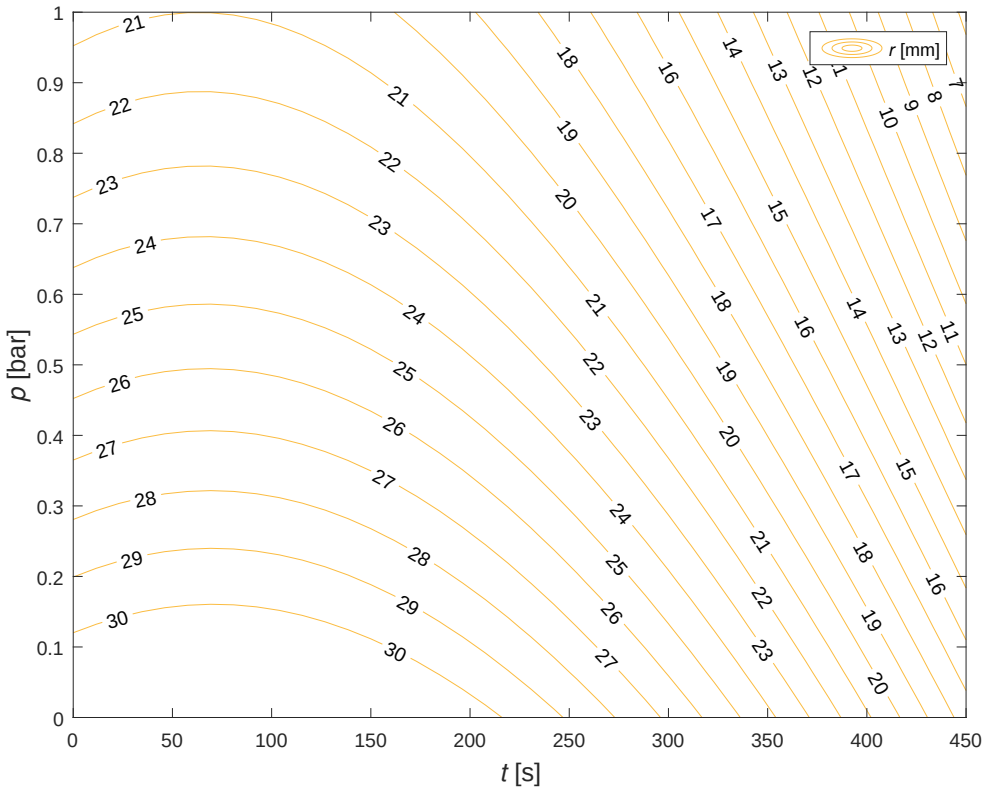

Figure F.2: Contour plot of polynomial model for short saddle radius r at pressures below $p = 1$ bar